



8-1999

Aircraft nose wheel steering : a gyroscopic precession study

Mark A. Werth

Follow this and additional works at: https://trace.tennessee.edu/utk_gradthes

Recommended Citation

Werth, Mark A., "Aircraft nose wheel steering : a gyroscopic precession study. " Master's Thesis, University of Tennessee, 1999.

https://trace.tennessee.edu/utk_gradthes/10045

This Thesis is brought to you for free and open access by the Graduate School at TRACE: Tennessee Research and Creative Exchange. It has been accepted for inclusion in Masters Theses by an authorized administrator of TRACE: Tennessee Research and Creative Exchange. For more information, please contact trace@utk.edu.

To the Graduate Council:

I am submitting herewith a thesis written by Mark A. Werth entitled "Aircraft nose wheel steering : a gyroscopic precession study." I have examined the final electronic copy of this thesis for form and content and recommend that it be accepted in partial fulfillment of the requirements for the degree of Master of Science, with a major in Aviation Systems.

William Lewis, Major Professor

We have read this thesis and recommend its acceptance:

Fred Stellar, W. R. Lawrence

Accepted for the Council:

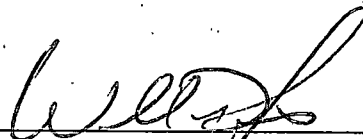
Carolyn R. Hodges

Vice Provost and Dean of the Graduate School

(Original signatures are on file with official student records.)

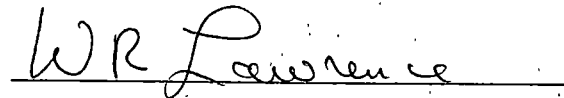
To the Graduate Council:

I am submitting herewith a thesis written by Mark A. Werth entitled "AIRCRAFT NOSE WHEEL STEERING-A GYROSCOPIC PRECESSION STUDY." I have examined the final copy of this thesis for form and content and recommend that it be accepted in partial fulfillment of the requirements for the degree of Master of Science, with a major in Aviation Systems.



William Lewis, Major Professor

We have read this thesis
and recommend its acceptance:



Accepted for the Council:



Associate Vice Chancellor and
Dean of The Graduate School

**AIRCRAFT NOSE WHEEL STEERING-
A GYROSCOPIC PRECESSION STUDY**

A Thesis
Presented for the
Master of Science
Degree
The University of Tennessee, Knoxville

Mark A. Werth
August 1999

Copyright © Mark A. Werth, 1999
All rights reserved

DEDICATION

This thesis is dedicated
to all the men and women
of Naval Aviation who have given
their lives in service
to the United States of America.

Without their unequalled devotion to duty,
this great country might not exist.

It is the freedom of our country
that allows scholars to pursue
their dream and better themselves
as well as those around them.

I am forever indebted to them.

ACKNOWLEDGEMENTS

The list of individuals that have contributed to my education is long and illustrious. Most notable of these persons is my father. Without his unending patience and love for me, I could have never accomplished the feats that I have. Although he is not a teaching professional, his ability to teach me has been unequaled by anyone. He has taught me the importance of perseverance and devotion to duty. There are many times in my life when he provided the guidance I needed to make the right decisions, sometimes against my will. But had he not convinced me that I was wasting my talents if I chose to bypass college, or given me the moral courage to complete officer training for the United States Marine Corps, my dream of becoming a test pilot would have never come true. I thank both him and my mother for the love that they have given me and the opportunities to excel that they have provided.

I would like to extend a special thank you to all the men and women of the AV8B Joint Systems Support Activity who keep our Harriers flying, in particular: Mr. Eric Nelson, Mr. Peter Eiserloh, and Mr. David Allen. These three individuals were able to turn the ones and zeros of the aircraft data into something that resembled a strip chart so that I could read it. Without their help, I could not have completed this project.

ABSTRACT

During flight test of the AV8B nose wheel steering system, gyroscopic precession was inadvertently encountered. Following a touch and go landing with a 180 degree turn to downwind, the spinning nose wheel caused the nose landing gear strut to precess away from a centered condition. The physical properties of nose wheel's angular momentum coupled with the pilot's technique can easily be seen to have caused the precession however, this phenomenon had never been seen during the previous 13 years of the Harrier's existence. To quantify this behavior, a study of gyroscopic precession as it applies to aircraft landing gear is presented. Understanding how the aircraft nose landing gear system works in conjunction with the operational procedures employed is critical to understanding why this precession had not previously been detected in other aircraft either. Accordingly, a discussion is presented. Following that, a data presentation section describes the test aircraft and limitations to data collection during the flight test events. A mathematical model was also developed to show how the flight test results conformed to gyroscopic theory.

Analysis of the test data and the mathematical model provided insight about gyroscopic precession in the AV8B nose landing gear system. The data indicated that gyroscopic precession of the nose strut was a function of several variables. Contributing factors were the nose wheel rotational velocity, the aircraft roll rate, and the aircraft roll acceleration. The gyroscopic precession appeared to be mostly due to high rotational wheel speed velocity at the point of aircraft maneuver however, it was discovered that there was a large dependency on aircraft initial roll rate and roll acceleration. The data also revealed that although precession trends can be predicted, an absolute solution is quite unpredictable. The single most important factor during this study of nose wheel gyroscopic precession was pilot technique since this defined the aircraft roll rate, roll acceleration, and nose wheel rotational velocity that generated the precessional moment on the nose strut. It is highly recommended that landing gear design engineers find a method to inhibit nose landing gear strut precession thereby ensuring that pilots do not have to contend with this dangerous phenomenon.

PREFACE

This thesis is written to help the reader understand how the mechanics of a gyroscope apply to the castering nose strut of an aircraft in flight. The nose strut is typically mounted to the fuselage of an aircraft at or near the top of the strut while the lower half of the strut is able to rotate about the strut's longitudinal axis. The ability of the nose strut to rotate is what allows the aircraft to be controlled directionally during ground operations, but this freedom of movement airborne can result in the spinning nose wheel influencing the strut's angular displacement through gyroscopic precession.

Section 1 is an introduction to the problem and provides background information to understand how this phenomenon manifests itself. For a review of solid mechanics and its application to rotating bodies, section 2 is presented. Design and use of several different nose landing gear/steering systems are discussed to aid in understanding why gyroscopic precession is not seen in all aircraft (section 3), and the specific design of the AV8B Harrier nose landing gear system is presented in section 4. Large differences in pilot technique were noted during analysis of flight test data so these are presented along with the results of the data reduction in sections 5 and 6. To quantify gyroscopic precession and present a tool for analysis of it, the mathematical model of section 7 was developed. This model is intended to give the design engineer an analytical method for use in predicting gyroscopic precession. Section 8 offers some nose wheel steering design recommendations to aid in understanding what type of system will work best given the manner in which an aircraft will be used.

As a conclusion to this thesis, major contributors to gyroscopic precession and recommended techniques to deal with this phenomenon are presented (sections 9 and 10). Finally, several data strip charts and spread sheets have been included for review in the appendices. The strip charts in Appendix A are from the series of flight tests and are the basis for the data reduction contained in section 6. The spread sheet in Appendix B is the supporting data for section 7.

TABLE OF CONTENTS

1	INTRODUCTION	1
2	GYROSCOPIC THEORY	4
2.1	BACKGROUND	4
2.2	CONVENTIONS.....	5
2.3	MOMENTUM.....	5
2.4	EULER'S ANGLES.....	10
2.5	DIRECTION COSINES.....	12
3	NOSE WHEEL STEERING SYSTEMS.....	14
3.1	GENERAL	14
3.2	CASTERING NOSE WHEELS	14
3.3	FULL TIME STEERING.....	15
3.4	CASTER-SELECTABLE NOSE WHEEL STEERING	16
3.5	NOSE STRUT DESIGNS	17
4	AV8B CASTERING NOSE WHEEL DESIGN.....	19
4.1	BICYCLE-OUTRIGGER LANDING GEAR DESIGN	19
4.2	STEERING REQUIREMENT	20
4.3	STEERING SYSTEM DESIGN.....	21
4.4	NOSE WHEEL MASS CONTRIBUTION.....	22
5	PILOTING TECHNIQUES	24
5.1	GENERAL	24
5.2	LIGHT CIVIL LANDING PATTERNS	24
5.3	COMMERCIAL AND MILITARY TRANSPORT	25
5.4	USAF TOUCH AND GO PATTERNS.....	26
5.5	USN/USMC TOUCH AND GO PATTERNS.....	27
6	DATA PRESENTATION	29
6.1	METHOD OF TEST	29
6.1.1	Instrumentation.....	29
6.1.2	Data Collection	29
6.2	DATA REDUCTION.....	31
6.2.1	Sign Convention	31
6.2.2	Data Accuracy	32
6.2.3	Nose Wheel Rotational Velocity Computation	33
6.2.4	Computer Analysis	37
6.3	DATA SUMMARY	39
6.4	CONCLUSION.....	41
7	MATHEMATICAL MODEL ANALYSIS	42
7.1	GENERAL	42
7.2	COORDINATE TRANSFORMATION	42
7.3	PRECESSIONAL TORQUE COMPUTATION	47
7.4	COMPARISON TO FLIGHT TEST RESULTS	51
8	NOSE WHEEL STEERING DESIGN CONSIDERATIONS	53
8.1	STEERING SYSTEMS THAT COMPENSATE FOR CRAB ANGLES AT TOUCHDOWN.....	53
8.2	CASTERING SYSTEMS WITH SELF-CENTERING MECHANISMS.....	53
8.3	CASTER-SELECTABLE NWS SYSTEMS WITH CENTERING INDICATORS	54

9	CONCLUSIONS	56
9.1	GENERAL.....	56
9.2	SPECIFIC.....	56
10	RECOMMENDATIONS	59
10.1	GENERAL.....	59
10.2	SPECIFIC.....	59
	REFERENCES	61
	APPENDICES	63
	APPENDIX A: FLIGHT TEST STRIP CHARTS.....	64
	APPENDIX B: TABULAR COMPUTATION OF GYROSCOPIC TORQUE.....	90
	VITA	102

LIST OF TABLES

Table 4-1: Aircraft Nose Wheel Properties	23
Table 6-1: Flight Test Aircraft Parameters	30
Table 6-2: Flight Test Events Investigated	38
Table 6-3: Strip Chart Parameters	38
Table 6-4: Aircraft Data Summary	40
Table 7-1: Coordinate Transformation Angles	43

LIST OF FIGURES

Figure 2-1: Particle Angular Velocity	6
Figure 2-2: Axes Rotation	11
Figure 4-1: AV8B Landing Gear Arrangement.....	19
Figure 4-2: AV8B Castering Nose Landing Gear Strut	22
Figure 5-1: Typical AV8B Landing Pattern Body Rates	28
Figure 6-1: Aircraft Body Axes.....	32
Figure 6-2: Axle Mounted Wheel	34
Figure 6-3: AV8B Nose Wheel Rate of Decay.....	37
Figure 7-1: Nose Strut Precession Angle	48
Figure 7-2: Precession Torque	49
Figure 7-3: Nose Strut Precession Rate	50

LIST OF EQUATIONS

Equation 2.1: Angular Momentum	6
Equation 2.2: Total Body Angular Momentum	6
Equation 2.3: Scalar Components of \mathbf{H}	7
Equation 2.4: Moments of Inertia	7
Equation 2.5: Products of Inertia	7
Equation 2.6: General Scalar Angular Momentum Equations	8
Equation 2.7: Nose Wheel Scalar Angular Momentum Equations	8
Equation 2.8: Rate of Change of Angular Momentum	9
Equation 2.9: Euler Angle Projections (Direction Cosines)	12
Equation 2.10: Direction Cosine Matrix for Rotating Reference Axes	13
Equation 6.1: Nose Wheel Velocity on Deck	33
Equation 6.2: Newton's Second Law	33
Equation 6.3: Rotational Body Equation of Motion	34
Equation 6.4: Rotational Body Differential Equation of Motion	34
Equation 6.5: Linear Differential Equation for Rotational Motion	35
Equation 6.6: AV8B Nose Wheel Differential Equation of Rotational Motion	36
Equation 7.1: Body Axes to Strut Axes Conversion	43
Equation 7.2: Strut Axes to Nose Wheel Axes Conversion	44
Equation 7.3: Nose Wheel Referenced Body Rates	44
Equation 7.4: Nose Wheel Angular Velocity Rate of Change	45
Equation 7.5: Nose Wheel Torquing Moments	45
Equation 7.6: Nose Wheel Axes to Strut Axes Moment Conversion	46
Equation 7.7: Strut Precessional Torquing Moment	46

LIST OF ACRONYMS

DDAS	Digital Data Acquisition System
KGS	Knots Ground Speed
KIAS	Knots Indicated Airspeed
MIL-STD	Military Standard
MUX	Multiplex Data
PSI	Pounds per Square Inch
V/STOL	Vertical or Short Takeoff & Landing

1 INTRODUCTION

Recent flight test results indicate a propensity for the Harrier's castoring nose landing gear to torque away from a neutral angle during pitching and rolling flight which follows touch and go landings. Never before noticed in the AV8B and fairly uncommon to the landing gear design world, this gyroscopic torquing presents a unique design requirement that must be considered by the design engineer.

The concept of gyroscopic precession in aerodynamic vehicles has been well established throughout this past century. In a vehicle that is free to move throughout six degrees of freedom, any component undergoing a high rate of rotation will exhibit the classic gyro dynamics of a spinning body. The study of jet engine and propeller gyro dynamics receives the most attention, but the body of the aircraft itself too has some gyroscopic tendencies. During departures from controlled flight, the aircraft can couple its pitch, roll, and yaw rates and develop into a steady state spin. This is due to the large moments of inertia of the aircraft and the fact that relatively high roll and yaw rates can be generated.

Of a lesser known degree is the gyroscopic tendency of the aircraft wheels. These items generally have small inertia associated with them in comparison to the entire aircraft or even a jet engine. During flight test of the AV8B nose wheel steering system, gyroscopic precession was inadvertently encountered. The high rate of nose wheel rotation during high-speed liftoffs in the Harrier can generate sufficient angular momentum that may result in the nose wheel exhibiting classic gyroscopic effects.

The properties of the AV8B nose wheel, the nose landing gear strut design, the steering system, and the operational flying techniques used all contributed to the accidental discovery of gyroscopic precession. On a test sortie, the aircraft lifted off at approximately 160 knots ground speed. The test pilot turned the aircraft downwind to set up for landing, using the caster mode of the nose wheel steering system, and found some very undesirable handling characteristics at touchdown. When the aircraft touched down, the nose yawed left and the right wing tip dropped as the aircraft responded to what appeared to be an uncommanded nose wheel steering input. Crosswinds were non-existent and the pilot touched the aircraft down on the runway centerline with no crab angle. The ensuing few seconds on the runway were quite eventful as the test pilot managed to add full power and regain directional control of the aircraft while flying it into the air. Not knowing the extent of his landing gear problem, the pilot performed a vertical landing—an option only available to this type of jet aircraft. Post flight analysis of the landing gear system revealed no anomalies with the castering nose wheel steering system and the test team began to review the flight test data to discover the cause of the uncommanded input.

It is easily recognized that the nose wheel acted as gyro mounted in a strut free to rotate about the aircraft directional body axis. The flight test data revealed that the nose strut precessed out 18 degrees from neutral during the 180 degree left turn to downwind after a high speed touch and go. This angle far exceeds any steering angle that would ever be used on the runway at high speed and was the obvious cause for the side force generation on the aircraft at

touchdown. Even though the wheel castered and aligned with the runway within $\frac{1}{2}$ second of touchdown, significant aircraft dynamics occurred in this very short time. The side force caused the nose to yaw left at 5 degrees per second, but more dramatic was the right wing down roll rate that peaked at 22 degrees per second. This type of excursion is an obvious undesirable ground handling characteristic that must be avoided in all aircraft designs.

To quantify this gyroscopic precession effect that had not been seen in the previous 13 years of the Harrier's existence, some specific flight profiles were planned. A matrix of flight test events that would allow comparison of slow to fast liftoffs using differing turn rates to downwind was developed and executed. The sections that follow define the mathematical theory that predicts such behavior, the design of nose wheel steering systems, and piloting techniques which all affect this gyroscopic tendency. These things help to understand why gyroscopic precession of nose landing gear struts is seldom seen in any light civil, military, or commercial aircraft. Flight test results and supporting data are presented, a mathematical analysis conducted, and the factors affecting nose strut precession in flight are discussed. As a conclusion, piloting technique and design recommendations are offered in an attempt to help minimize the dangers of this phenomenon.

2 GYROSCOPIC THEORY

2.1 BACKGROUND

To understand the mechanical properties of a gyroscope, a brief review of solid mechanics is appropriate. Newton's first law states¹, "Every body persists in its state of rest or of uniform motion in a straight line unless it is compelled to change that state by forces impressed on it." Newton's first law is referring to the momentum of an object and the behavior of the gyroscope is an extension of this law for a rotating body. A gyroscope will maintain its rotational rate and orientation unless acted upon by an external force. Once an aircraft nose wheel is rotating and the aircraft is airborne, there are only a few factors influencing the nose wheel's behavior. It is acted upon by the friction of the bearings, the axle (which is mounted to the nose strut), gravity, and the free air stream. For the purposes of this thesis, air stream and gravity effects will be neglected as they are negligible in comparison with the bearing friction and strut forces.

Bearing friction serves to reduce the angular rate of the nose wheel and is only present in one of the three coordinate directions of the nose wheel. Bearing friction effects are discussed and a mathematical model for this friction is developed in section 6.2.3. It will be shown that the nose wheel general exhibits an exponential decay of its rotational rate.

Aircraft roll rate, pitch rate, and yaw rate are transferred to the wheel axle by the nose strut and will change the nose wheel's angular rate in any or all three axes. The nose strut will impart forces and moments to the nose wheel axle in

¹ Physics: David Halliday and Robert Resnik, John Wiley & Sons 1978

five of the six degrees of motion and hence influence the path of the nose wheel. The sixth degree of motion (torque about the strut longitudinal axis) can not be transmitted to the nose wheel. Hence, the rotating wheel functions as a gyroscope and attempts to retain its initial orientation and plane of motion.

2.2 CONVENTIONS

Throughout this section, both vector and scalar equations will be used. Bold font will be used for vector quantities and italics for scalar quantities. All sign conventions will be in accordance with the "right hand rule" of mathematics.

2.3 MOMENTUM

Linear momentum is defined as the product of the body's mass and velocity. Consider a body composed of n mass elements m each with a discrete velocity vector \mathbf{v} . The linear momentum of each particle is $\mathbf{p} = m\mathbf{v}$ and the total system linear moment is $\mathbf{P} = \sum m\mathbf{v}$. Figure 2-1 shows a particle with mass m , located at point A, and moving with an angular velocity ω about its instantaneous axis of rotation OB. The linear velocity of the particle with respect to point O is defined as $\mathbf{v} = \omega \times \mathbf{r}$ and hence the linear momentum is $m\mathbf{v} = m\omega \times \mathbf{r}$.

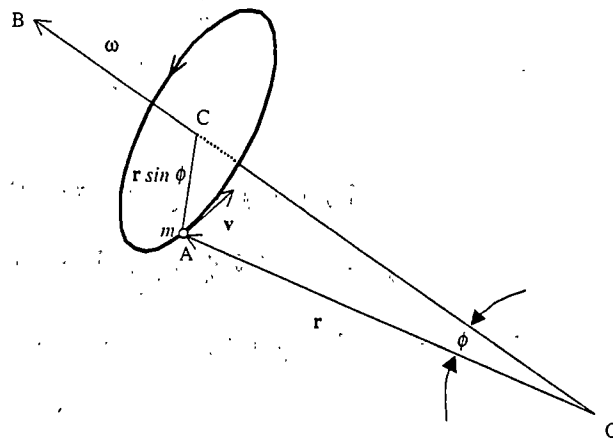


Figure 2-1: Particle Angular Velocity

The moment of momentum \mathbf{h} of this mass about the point O is the product of the orthogonal moment arm with respect to the axis of rotation ($r \sin \phi$) and the linear momentum $m\mathbf{v}$ (Equation 2.1). It is customary and less cumbersome to refer to moment of momentum as angular momentum².

Equation 2.1: Angular Momentum

$$\mathbf{h} = \mathbf{r} \times m\mathbf{v} = m\mathbf{r} \times (\boldsymbol{\omega} \times \mathbf{r})$$

The angular momentum of an entire body of n elements is expressed as the sum of the individual elements and is given in Equation 2.2.

Equation 2.2: Total Body Angular Momentum

$$\mathbf{H} = \sum \mathbf{r} \times m\mathbf{v} = \sum m\mathbf{r} \times (\boldsymbol{\omega} \times \mathbf{r})$$

² The Gyroscope: James B. Scarborough, Interscience Publishers 1958

Computation of the vector triple product reveals $\mathbf{H} = (\Sigma mr^2)\boldsymbol{\omega} - \Sigma m\mathbf{r}(\mathbf{r} \cdot \boldsymbol{\omega})$.

In general, $\mathbf{r} = x\mathbf{i} + y\mathbf{j} + z\mathbf{k}$ and $\boldsymbol{\omega} = \omega_x\mathbf{i} + \omega_y\mathbf{j} + \omega_z\mathbf{k}$. Substituting these vectors into the triple product and solving for \mathbf{H} in the three component directions gives the scalar equations of angular momentum for the rotating body (Equation 2.3).

Equation 2.3: Scalar Components of \mathbf{H}

$$\begin{aligned}H_x &= \omega_x \Sigma m(y^2 + z^2) - \omega_y \Sigma mxy - \omega_z \Sigma mzx \\H_y &= \omega_y \Sigma m(x^2 + z^2) - \omega_z \Sigma myz - \omega_x \Sigma mxy \\H_z &= \omega_z \Sigma m(x^2 + y^2) - \omega_x \Sigma mzx - \omega_y \Sigma myz\end{aligned}$$

The summations that appear in each of the scalar equations are readily identified as the body's moments and products of inertia with respect to the moving frame of reference.

Equation 2.4: Moments of Inertia

$$\begin{aligned}I_{xx} &= \Sigma m(y^2 + z^2) \\I_{yy} &= \Sigma m(x^2 + z^2) \\I_{zz} &= \Sigma m(x^2 + y^2)\end{aligned}$$

Equation 2.5: Products of Inertia

$$\begin{aligned}I_{xy} &= \Sigma mxy \\I_{yz} &= \Sigma myz \\I_{zx} &= \Sigma mzx\end{aligned}$$

Substitution of the moments and products of inertia into Equation 2.3 gives the general solution in scalar form for a three dimensional rotating body (Equation 2.6).

Equation 2.6: General Scalar Angular Momentum Equations

$$H_x = I_{xx}\omega_x - I_{xy}\omega_y - I_{zx}\omega_z$$

$$H_y = I_{yy}\omega_y - I_{yz}\omega_z - I_{xy}\omega_x$$

$$H_z = I_{zz}\omega_z - I_{zx}\omega_x - I_{yz}\omega_y$$

By setting the rotating axes in coincidence with the principle axes of the nose wheel's geometrically symmetric body, all dependency on the products of inertia can be eliminated³ and the total scalar angular momentum equations simplify to those of Equation 2.7.

Equation 2.7: Nose Wheel Scalar Angular Momentum Equations

$$H_x = I_{xx}\omega_x$$

$$H_y = I_{yy}\omega_y$$

$$H_z = I_{zz}\omega_z$$

Of interest is how the change in angular moment of the rotating body produces torquing moments. This torquing moment shows up as nose strut precession in the case of a rolling, pitching, and yawing aircraft. The first time derivative of the total angular momentum vector \mathbf{H} is found to be equal to the moment vector \mathbf{M} by the differentiation shown in Equation 2.8.

Equation 2.8: Rate of Change of Angular Momentum⁴

$$\frac{d\mathbf{H}}{dt} = \frac{d}{dt} \sum (\mathbf{r} \times m\mathbf{v}) = \sum \left(\mathbf{r} \times m \frac{d\mathbf{v}}{dt} + \frac{d\mathbf{r}}{dt} \times m\mathbf{v} \right)$$

where

$$m \frac{d\mathbf{v}}{dt} = m\mathbf{a} = \mathbf{F} \quad \text{and} \quad \frac{d\mathbf{r}}{dt} \times m\mathbf{v} = 0$$

hence

$$\frac{d\mathbf{H}}{dt} = \sum (\mathbf{r} \times \mathbf{F}) = \mathbf{M}$$

Equation 2.8 is the basis for the discussion of gyroscopic precession. One can either study the rate of change of angular momentum given an applied moment or the resultant moment given the applied rate of change of angular momentum. The precessing nose strut example uses both these relationships. Since the strut is confined to maintain position with respect to the aircraft body in two of its three moment directions, aircraft angular rates affect the angular momentum of the nose wheel. Because the strut can not resist a torque in its third moment direction (the castering axis), the rate of change of angular momentum for the nose wheel imparts a precessional torque that is seen as an uncommanded nose wheel steering input.

³ Gyrodynamics: Ronald N. Arnold and Leonard Maunder, Academic Press 1961

⁴ The Gyroscope: James B. Scarborough, Interscience Publishers 1958

To study the interaction of the nose wheel's angular momentum and the strut's precession with respect to the maneuvering aircraft, we must define some coordinate systems. It is desirable to compute angular momentum in a Newtonian based reference frame (inertially fixed). For the purposes of this thesis, the earth can be treated as a Newtonian reference frame since insignificant changes in the earth's rotation angle or aircraft position occur during the 20-30 second time of aircraft maneuver. The aircraft, nose strut, and nose wheel each have their own axes. The changes in angular momentum and torque must be computed taking the aircraft maneuver into account and referring to a common axes system. This is accomplished using Euler angle projections (section 2.4) and direction cosines (section 2.5).

2.4 EULER'S ANGLES.

Because the aircraft, the precessing nose strut, and the nose wheel all have independent frames of reference, a common reference frame must be established. The Newtonian reference frame remains fixed throughout and hence is the ideal base axes system. A vector that is contained within the fixed axes system can be referred to a rotating axes system by a series of angular displacements that, if carried out, would bring the original axes into coincidence with the rotating axes.

Consider the fixed axes system XYZ shown in Figure 2-2 that undergoes a rotation ψ , about its Z -axis within the XY plane to the new position $x_1y_1z_1$. A second rotation, θ , about the y_1 -axis brings the system to $x_2y_2z_2$. A third and final rotation, ϕ , about the x_2 -axis brings the original axes to xyz , the location of the rotating aircraft body axes. The angles ψ , θ , and ϕ are known as Euler's Angles⁵ and correspond to the aircraft yaw angle (heading), pitch angle, and roll angle with respect to the earth (assumed to be a Newtonian axes system).

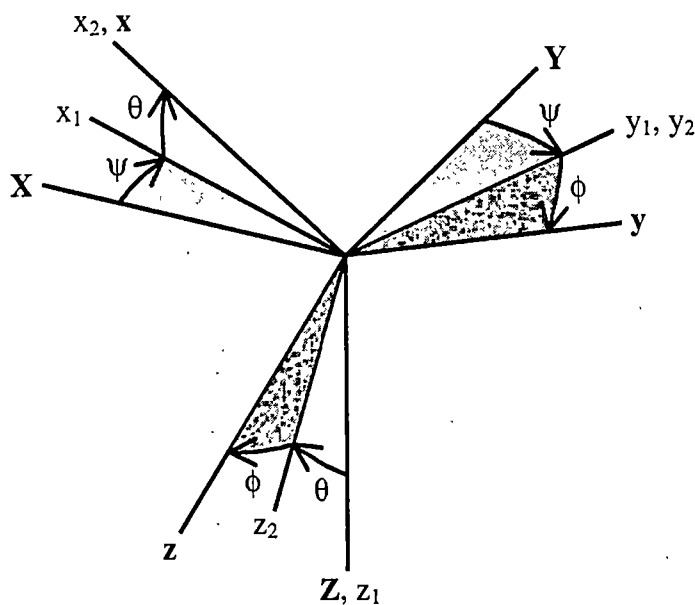


Figure 2-2: Axes Rotation

⁵ Dynamics: Lawrence E. Goodman and William H. Warner, Wadsworth Publishing 1965

The projections of the aircraft body axes onto the earth axes are found by applying these rotations. Section 2.5 describes how these projections can be computed by using direction cosines.

2.5 DIRECTION COSINES

A vector can be defined in the fixed reference frame XYZ and then projected into the rotating axes system xyz (Figure 2-2) noting that the rotation angles of section 2.4 are measured from the fixed axes to the rotating axes. In doing so, a matrix of direction cosines is constructed (Equation 2.9).

Equation 2.9: Euler Angle Projections (Direction Cosines)

$$\begin{bmatrix} x \\ y \\ z \end{bmatrix} = \begin{bmatrix} (\cos\Psi \cos\Theta) & (\sin\Psi \cos\Theta) & (-\sin\Theta) \\ (\cos\Psi \sin\Theta \sin\Phi - \sin\Psi \cos\Phi) & (\sin\Psi \sin\Theta \sin\Phi + \cos\Psi \cos\Phi) & (\cos\Theta \sin\Phi) \\ (\cos\Psi \sin\Theta \cos\Phi + \sin\Psi \sin\Phi) & (\sin\Psi \sin\Theta \cos\Phi - \cos\Psi \sin\Phi) & (\cos\Theta \cos\Phi) \end{bmatrix} \begin{bmatrix} X \\ Y \\ Z \end{bmatrix}$$

If the vector is represented in terms of the rotating axes system, it is found that transposition of the direction cosine matrix will give the solution in terms of the fixed reference frame. The Euler angles of Equation 2.10 are measured from the fixed frame to the rotating frame as in Equation 2.9.

Equation 2.10: Direction Cosine Matrix for Rotating Reference Axes

$$\begin{bmatrix} X \\ Y \\ Z \end{bmatrix} = \begin{bmatrix} (\cos\Psi\cos\Theta) & (\cos\Psi\sin\Theta\sin\Phi - \sin\Psi\cos\Phi) & (\cos\Psi\sin\Theta\cos\Phi + \sin\Psi\sin\Phi) \\ (\sin\Psi\cos\Theta) & (\sin\Psi\sin\Theta\sin\Phi + \cos\Psi\cos\Phi) & (\sin\Psi\sin\Theta\cos\Phi - \cos\Psi\sin\Phi) \\ (-\sin\Theta) & (\cos\Theta\sin\Phi) & (\cos\Theta\cos\Phi) \end{bmatrix} \begin{bmatrix} x \\ y \\ z \end{bmatrix}$$

These direction cosines apply to the scalar components of any vector when referenced from one axes system to another. The importance of maintaining proper signs on the rotation angles is obvious. Direction cosines are used to represent all angular motions of the aircraft, nose strut, and nose wheel systems in one common reference system. Since it is desired to study the magnitude of the torquing moments on the nose strut, these moments must be expressed in terms of the strut axes. In section 7, the change in angular momentum of the nose wheel is demonstrated by mathematical analysis. Before this however, it is important to study steering system designs, look at the various piloting techniques that contribute to gyroscopic precession, and investigate some empirical flight test data

3 NOSE WHEEL STEERING SYSTEMS

3.1 GENERAL

Several nose landing gear and steering systems have been employed since early this century. These systems are employed on aircraft that have tricycle or bicycle-outrigger landing gear systems and they are discussed here to explain why gyroscopic precession does not occur with all aircraft nose wheel steering systems. Steering systems play an important role in whether or not a nose strut can precess.

3.2 CASTERING NOSE WHEELS

While not a nose wheel steering system, the castering nose wheel deserves an explanation of its function in steering an aircraft. The castering nose wheel is free to caster—usually through a full 360 degrees. It is set on a nose strut and usually has a small trail angle to facilitate stability as the aircraft moves forward.

The castering nose wheel provides no means for steering inputs and tracks along with neutral directional stability. It is usually employed with a set of fixed main gear in a tricycle configuration—which provides directional stability. The castering nose wheel's function however, is noticed during landing. In nearly every case, a landing occurs with some amount of aircraft longitudinal axis misalignment with respect to the velocity vector at touchdown. In significant crosswinds, a crab-angle approach can result in as much as 10-15 degrees of heading misalignment. The castering nose wheel will align itself with the velocity vector at touchdown while the main gear provide a stabilizing moment and tend

to align the fuselage with the velocity vector. Without a castering nose wheel, the pilot would have to achieve zero crab angle prior to touchdown or accept a nose gear skid condition.

3.3 FULL TIME STEERING

A full time steering system employs a mechanical or electrical nose wheel steering control mechanism and the associated linkages to command the nose strut angle as a function of the steering controller. The simplest systems, such as employed on the Cessna 172, are full time linkage connections that move the nose strut in response to rudder inputs whenever the strut is not fully extended. More sophisticated systems incorporate fade-in logic that keeps the steering system from engaging during the high-speed landing touchdown phase. In the case of the FA-18 Hornet, the aircraft's mission computer limits the pilot's inputs to the nose wheel as the ground speed of the aircraft increases. At touchdown, the system senses a weight-on-wheels transition and delays pilot inputs, virtually behaving like a castering nose wheel system. As the aircraft slows and the aerodynamic control power of the rudders reduces, the system increases the nose wheel steering authority until full steering control is available. This type of system provides a seamless transition from aerodynamic directional control to nose wheel steering directional control and is an excellent nose wheel steering design.

3.4 CASTER-SELECTABLE NOSE WHEEL STEERING

When budget constraints or reduced system complexity are requirements, a designer will usually opt for a caster-selectable nose wheel steering system. This system is used in a wide range of aircraft such as the A-4, the Learjet, and the C-141. This steering system can be designed without the need for aircraft speed sensors or electronic fly-by-wire control logic. A selectable nose wheel steering system combines the simplicity of a castering nose wheel with the advantages of a steering system. Most often, the nose wheel steering system engages the nose strut with a hydraulic or electric selector valve. The nose strut is then positioned throughout its range of motion (upwards of ± 75 degrees) by hydraulic or mechanical means. The pilot engages or disengages the system through cockpit switches and usually lands the aircraft with the nose wheel steering disengaged. On landing rollout, as the rudder becomes ineffective, the pilot selects steering mode and then limits the control inputs manually. This requires changing the amount of rudder pedal deflection at the moment of steering engagement and can be a significant challenge with a strong crosswind.

Since this type of steering system is used in the majority of aircraft, it must be properly designed. A study of this system in the AV8B Harrier will show that even under normal pilot operations, some unpredictable results can occur. The design engineer must ensure that the potential for undesirable ground handling characteristics is kept to a minimum.

3.5 NOSE STRUT DESIGNS

Nose strut design plays a significant role in gyroscopic precession. Since all nose wheels must be mounted to the nose strut fork, transfer of the gyroscopic precession torque to the strut in two of the three nose wheel body axes occurs. It has been previously stated that this torquing moment is a function of the aircraft roll rate, pitch rate, and yaw rate with respect to the nose wheel's rotational frame of reference and the nose wheel rotational velocity at the point of moment (roll, pitch, yaw) application.

For systems that employ a relatively straight nose strut with a nose wheel mounted directly in line with the strut's axis of rotation, a less significant precession effect will be seen. Even though nose wheel rotational velocities are comparable between the AV8B and the A-4 or T-38, these straight nose strut designs tend to develop less gyroscopic coupling at the nose strut when torquing moments are applied. Figure 4-1 in section 4.1 however, shows how the AV8B nose wheel principle body axes are located aft of the strut centerline axis. Strut design requirements driven by the engine mount location in the Harrier predicate a nose wheel located 0.9 feet aft of the strut axis centerline. This design increases the likelihood of gyroscopic precession since any strut angle other than zero establishes a moment arm in the aircraft pitch axis. This moment arm's length gives the absolute nose wheel velocity vector an increased rate over a conventional strut that remains fixed under the fuselage and increases as a pendulum effect while the aircraft maneuvers. The larger the nose strut steering angle, the more significant this effect becomes. For aircraft designs with a nose

wheel system mounted in-line with the strut centerline, deflection angles do not result in off axis alignment and changes to the strut's moment arm do not occur.

4 AV8B CASTERING NOSE WHEEL DESIGN

4.1 BICYCLE-OUTRIGGER LANDING GEAR DESIGN

Most conventional tactical aircraft have the engine(s) mounted in the nose or tail section of the fuselage. In the case of heavy transport aircraft, the engines are typically mounted in wing nacelles. In each of these designs, significant structural members can be used to absorb the forces of landing and distribute them throughout the fuselage. Additionally, cavities exist for retractable tricycle gear. Since the Harrier airframe is built and balanced around the power plant, a conventional tricycle landing gear system was not used. Instead, a bicycle-outrigger landing gear design with a single, small, stubby main mount was designed and outrigger landing gear positioned at mid-span for lateral stability. Figure 4-1 shows the Harrier landing gear arrangement.

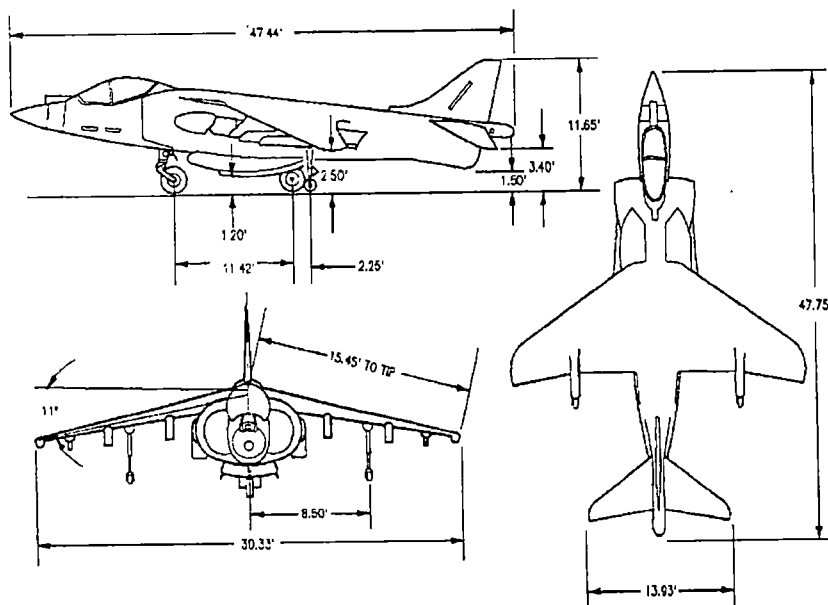


Figure 4-1: AV8B Landing Gear Arrangement⁶

⁶ Photo courtesy of Naval Air Systems Command. Reprinted from A1-AV8BB-NFM-000 NATOPS Manual.

4.2 STEERING REQUIREMENT

The AV8B aircraft was designed for V/STOL operations from prepared sites, grass strips, forward bases, and shipboard environments. To accomplish the close air support mission, the Harrier has to be taxied in close proximity to fixed structures and other general aerodrome hazards that are not encountered by aircraft that operate exclusively from prepared airfields. During operation aboard an aircraft carrier, little more than 100 feet of ship deck width exists for turning the aircraft and taxiing fore or aft. Here, the pilot will taxi under aircraft power and will steer the aircraft with the nose wheel steering system.

At a forward base site constructed along side a strip of asphalt road, the Harrier maneuvers in and out of hide positions using its 10 foot turn radius. Ground support personnel construct expeditionary airfield ramps from aluminum matting, but certainly are incapable of constructing a robust airfield. Taxi around this expeditionary airfield requires precise steering control. During takeoff or landing from a two-lane road, the 17 foot landing gear span only leaves approximately 3-5 feet of clearance from the outrigger landing gear to the edge of the prepared surface. The Harrier pilot is unable to accept any lineup deviations or excursions at touchdown—for the fragile outrigger struts can not withstand the impact of ruts or holes often associated with roadway ditches. For roll-on, landings the aircraft must touch down in the caster steering mode. In a crosswind, the aircraft is flown in a crabbed approach condition. This is done so the landing impact forces are distributed uniformly amongst the two outrigger landing gear and to limit lateral loads on the delicate struts. Any crab angle at

touch down will result in misalignment of the longitudinal axis of the aircraft and the velocity vector. When the main and outrigger wheels come in contact with the ground, their stabilizing effect quickly aligns the fuselage with the aircraft velocity vector so the pilot can maintain a straight track down a narrow runway. As the airplane slows below rudder effectiveness speed (50-60 knots), the pilot must engage the nose wheel steering button on the control stick grip and steer the aircraft as it slows to taxi speed. These operational handling techniques drive the need for a nose wheel steering system that is well behaved at all speeds. Since the Harrier uses a caster—selectable steering system, its design is critical.

4.3 STEERING SYSTEM DESIGN

The aircraft nose strut (see Figure 4-2) incorporates a hydro-electric nose wheel steering control valve solenoid. This solenoid disengages the steering drive motor from the pivoting portion of the strut when electrical power is appropriately applied. The lower half of the strut is free to rotate left or right +/- 179 degrees. When the pilot engages the nose wheel steering system through depression of the nose wheel steering button in the cockpit, the solenoid opens the control valve and allows 3000 PSI hydraulic fluid pressure to act on the steering motor. A steering ratio changer sets the control to either low gain or high gain dependent on pilot switch position. In low gain, full rudder deflection results in a 14 degree steering angle at the nose strut. When high gain is selected, the nose strut can achieve a 45 degree angle, allowing the aircraft to

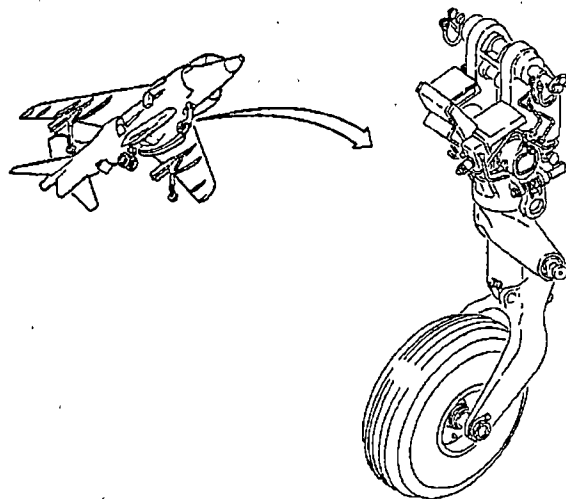


Figure 4-2: AV8B Castering Nose Landing Gear Strut⁷

attain a minimum turn radius. During a typical takeoff or landing, nose strut angle deflections do not exceed approximately 3-5 degrees and this is accomplished with approximately $\frac{1}{4}$ rudder pedal deflection. Since the operator generally does not need more than $\frac{1}{4}$ rudder pedal deflection at high speed, low gain control is satisfactory for runway operations. During ground taxi, the pilot typically selects high gain steering for the required ground operations inherent with forward based, limited space operations.

4.4 NOSE WHEEL MASS CONTRIBUTION

An obvious contributing factor in the science of nose strut precession is the mass moment of inertia of the nose wheel. The gyroscopic theory presented in section 2 highlighted the importance of this inertia. Since the Harrier is

⁷ Photo courtesy of Naval Air Systems Command. Reprinted from A1-AV8BB-130-300 Harrier Maintenance Manual

designed for all-terrain operations, it employs a low pressure, heavy nose tire. Tactical jet aircraft designed for improved runway conditions only, use high pressure rated tires that are inflated to roughly twice the pressure of the AV8B's. As a result, tire size and weight are significantly smaller yet carry the same aircraft load. The F16C, being almost identical in size, weight, and platform design as the AV8B has a much lower inertia nose wheel. Table 4-1 lists the nose wheel properties for each aircraft. Notice that the F16C nose wheel has an inertia value that is 60% lower than the Harrier's. This is largely due to the decreased mass of the high pressure wheel/tire combination but a significant factor as well is the decreased nose wheel radius.

Table 4-1: Aircraft Nose Wheel Properties

Aircraft Type	Avg. Mission Gross Weight (lbs)	Nose Wheel Properties ⁸				
		mass m (slug)	diameter (inches)	width (inches)	pressure (PSI)	moment I_{yy} (slug-in ²)
AV8B	25,000	1.49	26	8.75	150	95
F-16C	25,000	0.36	18	5.7	300	36

⁸ Data courtesy of Boeing St. Louis, Lockheed Ft Worth, AV8B JSSA China Lake, and F-16 CTF Edwards AFB.

5 PILOTING TECHNIQUES

5.1 GENERAL

The single most important factor in the study of nose strut gyroscopic precession is pilot technique. Pilot technique defines the angular rates that appear in the equations of section 2. The roll, pitch, and yaw rates as well as nose wheel rotational velocity and whether or not the landing gear is extended during turning flight after liftoff all contribute to the phenomenon. The following sections illustrate why gyroscopic precession has most likely not been a large factor in aircraft design over the past century. Landing patterns and techniques are generalized into three categories: those of private pilots in light civil aircraft, commercial and military transport, and military tactical jet aviation. Tactical jet aircraft are flown by the United States Air Force, Navy, and Marine Corps. The differences in Air Force and Navy/Marine Corps are so significant that they have each been given separate sections.

5.2 LIGHT CIVIL LANDING PATTERNS

Nose wheel mass properties were discussed in section 4.4 and since the majority of light civil aircraft are in the 3000-8000 lbs gross weight range, their nose wheels are significantly smaller. These wheels have far less mass moment of inertia than a Harrier's nose wheel. More importantly however, is aircraft aerodynamic design which is the number one contributing factor to stall speed—and hence takeoff speed (classically 1.2 times aircraft stall speed). Since the aircraft are light and wing loading is low, takeoff speeds are typically in the range of 60-100 KIAS. This results in a significantly lower nose wheel rotational

velocity at liftoff. Climb performance is usually no greater than a couple thousand feet per minute which implies that the pilot must climb at least 30-60 seconds on a straight flight path prior to turning the aircraft downwind, and roll performance is such that aircraft body axes rates are never substantial. These factors combine very importantly in the equations of section 2 and it can be seen that virtually no gyroscopic moments are generated by these aircraft nose wheels. As a final note, several of these type aircraft employ a full-time steering system in which nose strut precession can not occur.

5.3 COMMERCIAL AND MILITARY TRANSPORT

Commercial aircraft spend a very limited amount of time in touch and go landing patterns because their existence requires sound business judgement. To expend millions of gallons of jet fuel as 777 pilots practice landings is not practical. The air carriers of the world have developed excellent flight simulators that allow their pilots to stay proficient in the takeoff and landing phases of flight. Not always though does a pilot undergo total simulator training, especially during maintenance check flights or new aircraft deliveries. In these cases, an airliner may actually enter a touch and go landing pattern and spend several hours conducting touch and goes. In addition to this, all military transport operational squadrons will likely have their pilots conduct touch and go landings on a routine basis. Since these aircraft are much larger than a tactical jet (with corresponding larger nose wheel moments of inertia) and takeoff with nose wheel rotational velocities as high or higher than the Harrier can experience, why do they not

experience nose strut precession? That answer can again be found after inspection of the transport pilot's technique.

Transport pilots raise the landing gear between takeoff and landing as a matter of routine course. This is to save fuel as well as to develop the strong habit pattern of properly lowering the landing gear and completing the landing checklist before each landing. The process of retracting the nose landing gear includes a method of nose strut centering and usually, disconnection from the controller. This is required so that the nose strut is not activated while inside the wheel well. Because of this, the nose wheel spins down and maintains a centered position. On future extension, the nose strut is centered. As with light civil aircraft, if the pilot of a transport aircraft was to leave the gear down, he could not reasonably generate high enough roll, pitch, and yaw rates and would have to climb straight ahead to ensure wing tip clearance before turning downwind. These two practices also serve to reduce any gyroscopic tendencies and the transport pilot will rarely if ever find the nose strut precessing due to gyroscopic behavior.

5.4 USAF TOUCH AND GO PATTERNS

The Air Force teaches their tactical jet aircrew to raise and lower the landing gear during the process of each touch and go landing. Since the Air Force flies jets in this manner, no amount of roll, pitch, or yaw rate will cause the nose strut to precess. Even the classic Air Force pitch up to downwind; where the pilot executes a full power climb and roll using as high as 15 degrees per

second pitch rate and 180 degrees per second roll rate; can cause an up and locked nose strut to precess.

5.5 USN/USMC TOUCH AND GO PATTERNS

The United States Navy and Marine Corps must operate from aircraft carriers and amphibious landing ships. The carrier environment is very unforgiving and precision landings are an absolute requirement to get aboard. Since the majority of USN/USMC jet aircraft land using a tail hook and hook skips or misses are common place, accepted wisdom within the community is to teach its jet aviators to complete the landing checklist and leave the gear extended once the landing pattern is entered. This drives a touch and go pattern at the field where the landing gear are left extended for each pass. Since Harrier pilots are trained through the Naval Air Training Command, this technique is used and the Harrier is flown with its landing gear extended while in the touch and go pattern.

During a touch and go, the pilot adds full power and begins a climb. Accepted procedures are to climb straight ahead to approximately 300 feet above ground level and then execute a turn to downwind. However, the rate of climb and roll rate used are not specified. Since time to roll, pitch, and yaw application predicates the nose wheel's rotational velocity at the point of torque application and the actual body rates applied define the torque moment, drastically different results can and will be realized.

Figure 5-1 shows the array of roll, pitch, and yaw rates as well as roll acceleration used over the span of 16 touch and go landings with three different pilots. There are drastic differences in pilot technique. The following sections will discuss the effects of these variables and their potential for contribution to the gyroscopic tendency of a nose wheel.

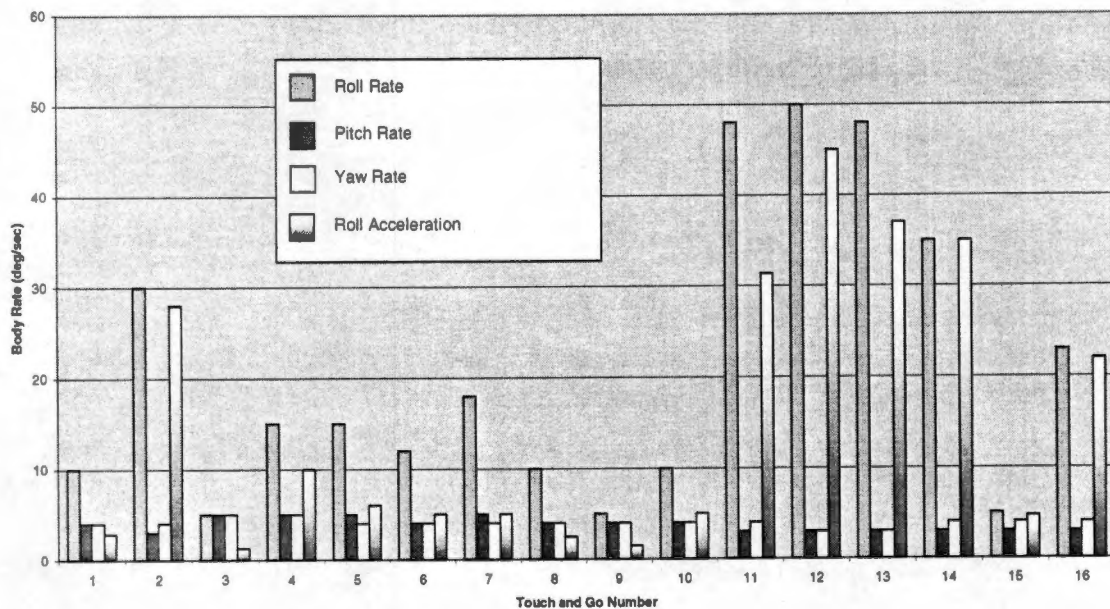


Figure 5-1: Typical AV8B Landing Pattern Body Rates

6 DATA PRESENTATION

6.1 METHOD OF TEST

6.1.1 Instrumentation

Prior to flight test, an AV8B Radar variant aircraft was fully instrumented so that dedicated state parameters could be recorded for post flight analysis of the nose wheel steering control system in support of a flying qualities evaluation. Of particular concern for this test was the relationship of nose strut angle to rudder position with steering control engaged and the behavior of the nose strut during castering operation. The emphasis of flight test was to determine if adequate open and closed-loop control existed with the Harrier nose wheel steering system. The aircraft's MIL-STD 1553 Multiplex Data (MUX) Bus contained significant data parameters in addition to the enhanced Digital Data Acquisition System (DDAS) instrumentation package that was installed specifically for flight test. These parameters were used in the post flight analysis of the data. A list of aircraft parameters is contained in Table 6-1.

6.1.2 Data Collection

Data was collected and analyzed for 9 test sorties. Sorties 1-4 were ground handling and characteristic gathering events that were completed prior to the first flight. Sorties 5-9 were actual airborne sorties with data being collected. Three individual test pilots were used during the tests. The first test pilot flew sorties 5 and 6, the second flew 7 and 8, and the third flew sortie 9.

Table 6-1: Flight Test Aircraft Parameters

Parameter Name	Description (Units)
NZ	Body Axis Normal Acceleration (g)
NY	Body Axis Lateral Acceleration (g)
NX	Body Axis Longitudinal Acceleration (g)
RUDDERPO	Rudder Pedal Position (inches)
NWANGLE	Nose Strut Angle (deg)
AIRSPEED	Indicated Airspeed (KCAS)
PRESSALT	Pressure Altitude (feet MSL)
RADALT	RADAR Altimeter (feet AGL)
LATACCEL	Body Axis Lateral Acceleration (feet/sec ²)
LONACCEL	Body Axis Long Acceleration (feet/sec ²)
NRMACCEL	Body Axis Normal Acceleration (feet/sec ²)
ROLLANGL	Aircraft Roll Angle (deg)
INSHDG	INS Platform Heading (deg, sets alignment axis)
PTCHRATE	Aircraft Pitch Rate (deg/sec)
PTCHANGL	Aircraft Pitch Angle (deg)
ROLLRATE	Aircraft Roll Rate (deg/sec)
TRUEHDG	INS True Heading (deg)
VERTACEL	Earth Axis - Vertical Acceleration (feet/sec ²)
INSXVEL	INS X Velocity (ft/sec, along alignment axis)
YAWRATE	Aircraft Yaw Rate (deg/sec)
INSYVEL	INS Y Velocity (ft/sec)
VERTVEL	INS Z Velocity (ft/sec)
WOW	Weight on Wheels (binary, airborne = 0)
GRNDSPD	Ground Speed (KGS)
FLTTIME	Time since lift off (secs)
OMEGA	Nose Wheel Rotational Velocity (rad/sec)

For each sortie, data was collected using a pulse code modulated telemetry stream of 300 data points per second that was transmitted to a telemetry room where the stream was captured on an analog magnetic tape. From there, the analog tape was read into a computer where the parameters were scaled in the format of Table 6-1 and saved as binary files.

6.2 DATA REDUCTION

6.2.1 Sign Convention

Throughout this section, sign convention will be in accordance with Figure 6-1. Using the right hand rule, this results in positive values for aircraft pitch nose up, aircraft roll right wing down, and aircraft yaw nose right. The aircraft nose wheel was assumed to have its own axes and was initially aligned with the aircraft's axes at liftoff. The parameter OMEGA represents the nose wheel rotational velocity and is a positive value on the strip charts of Appendix A. Because it is desirable to maintain consistency with the aircraft body rates for computation in the equations of section 2, forward motion produces negative spin direction. When body rates and wheel rates are combined in section 7, a negative value for OMEGA is used.

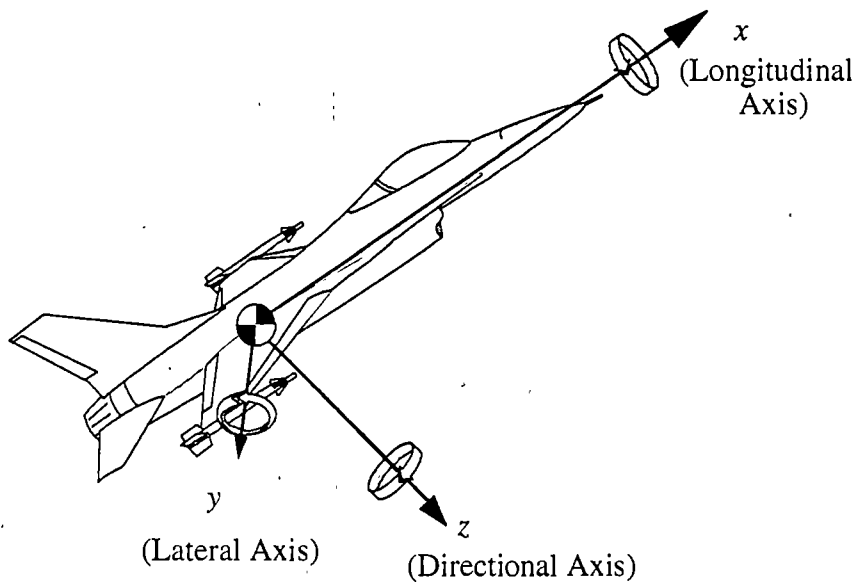


Figure 6-1: Aircraft Body Axes⁹

6.2.2 Data Accuracy

To make the data more manageable during post flight reduction, the stream was reduced to 20 samples per second. Angular measurements taken from the 1553 MUX bus are considered to be very accurate and within 0.1 degree. For the DDAS nose strut angle parameter (NWANGLE), the potentiometer installed on the steering rod proved to be accurate to within approximately 1 degree. Ground speed measurement was also obtained from the MUX bus and was accurate to within 1 knot.

⁹ Reprinted with permission of AIAA from "Introduction to Aeronautics: A Design Perspective."

6.2.3 Nose Wheel Rotational Velocity Computation

Prior to flight test, it was not anticipated that nose wheel rotational velocity would be a required parameter. The purpose of flight test was intended to qualify and quantify the behavior of the nose wheel steering system during takeoff, landing, and ground handling. The discovery of gyroscopic precession highlighted the need for the nose wheel rotational velocity parameter, but it could not be collected or recorded once actual flight test had commenced. In order to analyze gyroscopic precession, an artificial parameter for nose wheel velocity had to be generated. Given the aircraft ground speed v and nose wheel radius r , the rotational velocity ω can be computed as shown in Equation 6.1.

Equation 6.1: Nose Wheel Velocity on Deck

$$\omega = v/r$$

This equation is only valid for the nose wheel when in contact with the ground. Once the aircraft becomes airborne, the nose wheel rotational speed decays to zero. To create a time history trace that represents the nose wheel's characteristics, a mathematical model had to be produced¹⁰. Newton's second law for rotational motion (Equation 6.2) states:

Equation 6.2: Newton's Second Law

$$\sum T = I_{yy} \alpha$$

¹⁰ System Dynamics: Katsuhiko Ogata, Prentice-Hall 1978

Where T is the torque applied to the system, I_{yy} is the polar moment of inertia, and α is the angular acceleration. Applying Newton's second law to a system such as that shown in Figure 6-2 and assuming bearing friction b , yields Equation 6.3.

Equation 6.3: Rotational Body Equation of Motion

$$\sum T = b\omega = -I_{yy}\alpha$$

Since α is the first time differential of ω , Equation 6.3 can be written in the form of Equation 6.4:

Equation 6.4: Rotational Body Differential Equation of Motion

$$I_{yy}\dot{\omega} + b\omega = 0$$

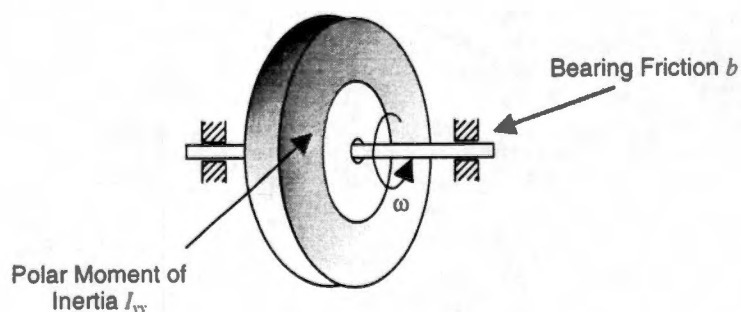


Figure 6-2: Axle Mounted Wheel

Upon inspection, it can be seen that Equation 6.4 is a first order linear differential equation. By setting $\lambda = -b/I_{yy}$, Equation 6.4 can be rewritten and solved as a time history. Equation 6.5 shows a solution for this first order system where $\omega(t)$ is the time dependent variable and ω_0 is the value at time zero. The characteristic root of this first order equation is λ .

Equation 6.5: Linear Differential Equation for Rotational Motion

$$\omega(t) = \omega_0 e^{\lambda t}$$

To verify the validity of this mathematical model, several test runs were accomplished using different size and mass bicycle wheels. A video camera capable of recording 30 frames per second was mounted in a position that allowed video taping the wheel's rotational rate. The wheel was given an initial velocity and allowed to slow down naturally without being influenced by other than the wheel bearings. As the wheel's speed decreased, samples of the angular velocity were recorded.

Inspection of the sample data revealed very well behaved first order linear differential equations for each of the wheels tested. Regression was performed on the data and the characteristic roots for each of the first order systems were found. Since Equation 6.5 is of linear differential form, the initial velocity was of no interest. More importantly, by knowing the characteristic root, the differential equation can be written in the general form.

Due to the excellent results obtained with this test method, it was proven to be a suitable alternative for obtaining a plot of the aircraft nose wheel velocity during the rotational decay phase. An aircraft was placed on jack stands and the nose wheel was given an initial angular rate so that the decaying motion could be recorded. Unfortunately, high values of b/I_{yy} for the aircraft wheel, coupled with the inability to spin the wheel up past approximately 28 rad/sec, did not permit collection of data beyond 3-1/2 seconds. Theory predicts however, that any time slice of data will conform to the exponentially decreasing function. The data was gathered 30 times per second and smoothed by averaging the rotational velocity over each 0.1 second period. Two separate data runs were recorded and are shown in Figure 6-3. Both runs conformed to the first order linear differential equation theory with each data having no more than 3% error from the regressed equation. The average characteristic root for the two separate data runs is approximately $\lambda = -0.18$. The nose wheel differential equation is shown in Equation 6.6.

Equation 6.6: AV8B Nose Wheel Differential Equation of Rotational Motion

$$\omega(t) = \omega_0 e^{-0.18t}$$

This method yielded usable results in a cost effective approach and verified the behavior of the nose wheel as a first order system. Additionally, the author's operational experience while flying next to another Harrier and observing

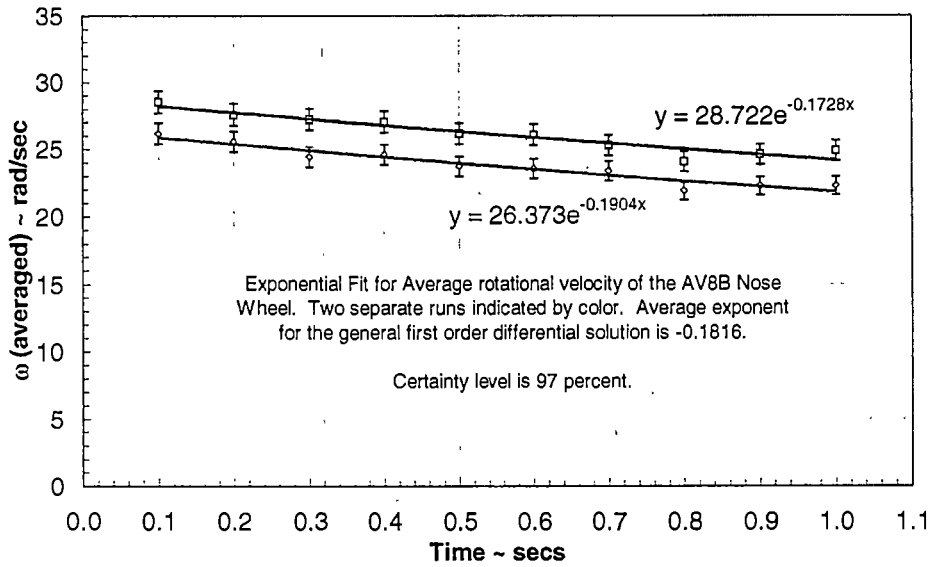


Figure 6-3: AV8B Nose Wheel Rate of Decay

the wheel speed decay indicates that the analytically derived rate is approximately the same as that seen in flight.

6.2.4 Computer Analysis

Post flight data reduction was completed using the United States Navy Test Pilot School Post Flight Data Reduction program version 1.0. Aircraft data was formatted in a time history chart to investigate the takeoff portion of selected flight test events. The data stream was modified during post flight analysis to include the nose wheel rotational velocity parameter (OMEGA) that was created as described in section 6.2.3. Appendix A contains the time history plots for all flight test events investigated.

Low speed, medium speed, and high speed rolling takeoffs were analyzed. Within the five flights, data was selected to investigate particular takeoff evolutions. Table 6-2 is a summary of flight test number and events used during analysis.

Table 6-2: Flight Test Events Investigated

Flight Number	Events Analyzed	Event Numbers
5	1	5.1
6	1	6.1
7	1-3	7.1-7.3
8	1-2	8.1-8.2
9	1-6	9.1-9.6

The post flight data reduction program allowed several parameters to be displayed on each page of strip charts. Two pages per flight event were used so that the necessary parameters could be viewed with respect to a single time reference. Table 6-3 lists the page number, parameter, and charted color.

Table 6-3: Strip Chart Parameters

Page	Parameter	Abbreviation	Color
1	Nose Wheel Angle	NWANGLE	Red
	Nose Wheel Rotational Velocity	OMEGA	Blue
	Weight On Wheels	WOW	Green
	Aircraft Roll Angle	ROLLANGL	Red
	Aircraft Roll Rate	ROLLRATE	Blue
	RADAR Altimeter	RADALT	Green
2	Nose Wheel Angle	NWANGLE	Red
	Rudder Pedal Position	RUDDERPO	Blue
	INS True Heading	TRUEHDG	Green
	Aircraft Pitch Angle	PTCHANGL	Red
	Aircraft Pitch Rate	PTCHRATE	Blue
	Aircraft Yaw Rate	YAWRATE	Green

Detailed analysis of the flight test data indicated that the gyroscopic precession of the nose strut is a function of several variables. Contributing factors are nose wheel rotational velocity, aircraft body rates, aircraft roll acceleration, and total platform heading change (coupled pitch and yaw rate). A summary that compares the influencing parameters to the maximum precession angles follows.

6.3 DATA SUMMARY

The flight test data contained in Appendix A indicates that the nose wheel and strut do not generate motion due to aircraft maneuvering caused by inertial effects when the rotational rate of the nose wheel has significantly decayed. Nor do air stream effects cause the nose strut to weathercock or fair into the relative wind. Once the nose strut attains its maximum precession angle, it maintains that position regardless of aircraft maneuver (for a continuous direction of turn). Theory suggests that the nose strut should continue to precess at a constant rate (see section 2.1) but the existence of air flow as well as minor changes in aircraft body rates apparently cause the strut to stop precessing.

The phenomenon of precession was primarily due to high rotational wheel speed velocity coupled with high aircraft roll rates and it was discovered that pitch rate and yaw rate had a much smaller influence. Because large variations in roll acceleration were noted during post flight analysis, this variable was also analyzed. Table 6-4 summarizes the nose wheel velocity, body rates, roll acceleration, and total precession angle for each event. The data suggests that

for every turn to down wind, magnitudes of pitch rate and yaw rate are nearly equal. Roll rate and roll acceleration are highly dependent on pilot technique. Roll acceleration appears to be the major contributor to precession when nose wheel rotational rates are below approximately 100 radians per second. With rotational rates below approximately 30 radians per second, little to no gyroscopic precession occurs. Events 7.1 and 7.3 represent identical nose wheel energy states. In event 7.1, it is clear that the absence of high roll acceleration and high roll rate allows the nose strut to remain centered. Event 7.3 represents a roll rate that is three times larger and roll acceleration that is six times larger than event 7.1. The result is a precession angle of 10 degrees.

Table 6-4: Aircraft Data Summary

Event	Aircraft Parameters					
	OMEGA (rad/sec)	ROLL RATE (deg/sec)	PITCH RATE (deg/sec)	YAW RATE (deg/sec)	ROLL ACCEL (deg/s/s)	Δ NW ANGLE (deg)
5.1	25	-10	4	-4	-3	-1
6.1	15	-30	3	-4	-28	-2
7.1	50	-5	5	-5	-1	0
7.2	100	-15	5	-5	-10	-16
7.3	50	-15	5	-4	-6	-10
8.1	125	-12	4	-4	-5	-3
8.2	160	-18	5	-4	-5	-15
9.1	113	-48	3	-4	-31	-7
9.2	65	-50	3	-3	-45	-8
9.3	75	-48	3	-3	-37	-7
9.4	75	-35	3	-4	-35	-6
9.5	32	-5	3	-4	-5	0
9.6	68	-23	3	-4	-22	-3

6.4 CONCLUSION

Since the Harrier is a V/STOL aircraft, liftoff speed is highly technique dependent. Slow liftoff or long extensions upwind before turning result in reduced angular velocity for the nose wheel at the point of torque application. If turns are commenced with high nose wheel energy states, lower roll accelerations will result in smaller precession angles. This in part, is due to the fact that the nose wheel velocity is rapidly decaying, and any delay in attaining a maximum aircraft angular rate of change will result in a smaller overall torquing moment. Events 7.2 and 8.1 substantiate that total precession is not just a combined function of aircraft roll rate and nose wheel rotational velocity but that roll acceleration is also a significant factor. The aircraft body rates and nose wheel velocities for these two events are nearly equal, but by doubling the roll acceleration on event 7.2, a resulting precession angle five times as large was attained. This large increase in precession shows that roll acceleration effects are extremely non-linear. This amplifies the uncertainty that exists in trying to predict the outcome of nose strut precession in castering systems and highlights the requirement for a better solution.

7 MATHEMATICAL MODEL ANALYSIS

7.1 GENERAL

To assess the potential for gyroscopic precession in aircraft nose wheel steering systems, a mathematical model was used. Since the nose wheel's angular momentum is the combination of the nose wheel angular velocity and the aircraft angular velocity, computation of total nose wheel angular momentum must first be accomplished. Following that, the nose wheel angular velocity vector (in the nose wheel reference frame) is used to find the angular momentum vector (in the earth based reference frame). The momentum vector will be differentiated to find the moment vector, and then the moment vector will be expressed in terms of the nose strut coordinate system. Reference to the direction cosine matrices (Equation 2.9 and Equation 2.10) is made through out these coordinate transformations.

7.2 COORDINATE TRANSFORMATION

To complete all coordinate transformations from the nose wheel frame of reference, the strut frame of reference, the aircraft body frame of reference, and the earth frame of reference, the angles of rotation listed in Table 7-1 were used. Note that the nose strut is mounted to the aircraft and free to rotate about its z-axis only. As a result, the strut is only free to rotate in the xy_{str} plane, which is coincident with the aircraft xy_{ac} plane. Since the aircraft nose wheel axle is mounted to the strut and coincident with the strut's y-axis, it is convenient to take the axle as the nose wheel's y-axis. Because the nose wheel is mass balanced and geometrically symmetrical about its axle, this also places the nose wheel's y-

axis in coincidence with one of the nose wheel's principle axes. Selecting the nose wheel's x and z axes anywhere on the orthogonal plane that bisects the wheel, keeps the remaining two nose wheel body axes in coincidence with the other principle axes (see section 2.3).

Table 7-1: Coordinate Transformation Angles

Axes System Rotation (positive angle)	Axes Notation	Rotation Angle		
		First	Second	Third
earth to aircraft body	XYZ to $x_{ac}y_{ac}z_{ac}$	ψ	θ	ϕ
aircraft body to strut	$x_{ac}y_{ac}z_{ac}$ to $x_{str}y_{str}z_{str}$	E	none	none
strut to nose wheel	$x_{str}y_{str}z_{str}$ to $x_{nw}y_{nw}z_{nw}$	none	Ω	none

The nose wheel rotational velocity vector is the combination of the nose wheel's spin rate, the aircraft body rates, and the strut precessional rate. For solution of this total vector in the nose wheel reference frame, two direction cosine matrices are applied. Initially, the aircraft body rates (p , q , and r) are operated on by Equation 7.1.

Equation 7.1: Body Axes to Strut Axes Conversion

$$\begin{bmatrix} \mathbf{i} \\ \mathbf{j} \\ \mathbf{k} \end{bmatrix}_{str} = \begin{bmatrix} (\cos E) & (\sin E) & (0) \\ (-\sin E) & (\cos E) & (0) \\ (0) & (0) & (1) \end{bmatrix} \begin{bmatrix} \mathbf{i} \\ \mathbf{j} \\ \mathbf{k} \end{bmatrix}_{ac}$$

The body rates referenced to the strut axes system are then operated on by Equation 7.2.

Equation 7.2: Strut Axes to Nose Wheel Axes Conversion

$$\begin{bmatrix} \mathbf{i} \\ \mathbf{j} \\ \mathbf{k} \end{bmatrix}_{nw} = \begin{bmatrix} (\cos \Omega) & (0) & (\sin \Omega) \\ (0) & (1) & (0) \\ (-\sin \Omega) & (0) & (\cos \Omega) \end{bmatrix} \begin{bmatrix} \mathbf{i} \\ \mathbf{j} \\ \mathbf{k} \end{bmatrix}_{str}$$

The solution for the two coordinate transformations can be directly computed by substituting Equation 7.1 into Equation 7.2. If the unit vectors are replaced with the scalar values for the aircraft body rates and the matrix algebra carried, Equation 7.3 is obtained.

Equation 7.3: Nose Wheel Referenced Body Rates

$$\begin{bmatrix} p \\ q \\ r \end{bmatrix}_{nw} = \begin{bmatrix} (\cos \Omega \cos E) & (\cos \Omega \sin E) & (\sin \Omega) \\ (-\sin E) & (\cos E) & (0) \\ (-\sin \Omega \cos E) & (-\sin \Omega \sin E) & (\cos \Omega) \end{bmatrix} \begin{bmatrix} p \\ q \\ r \end{bmatrix}_{ac}$$

The nose wheel angular velocity vector measured with respect to the nose wheel reference frame is only free to rotate about the nose wheel y-axis. This rotational rate can be represented by the variable ω_{nw} . The variable ω_{nw} is the time dependent value from Equation 6.6 and is the major contributor to the

angular momentum of the nose wheel. The absolute nose wheel rotational velocity vector can then be defined as $\omega = p_{nw}\mathbf{i}_{nw} + (q_{nw} + \omega_{nw})\mathbf{j}_{nw} + (r_{nw} + \dot{E}_{str})\mathbf{k}_{nw}$ and represents the rotational rate of the nose wheel's trihedral reference frame in relation to the earth fixed axes system. Noting that ω is of the form $\omega = \omega_x\mathbf{i}_{nw} + \omega_y\mathbf{j}_{nw} + \omega_z\mathbf{k}_{nw}$ and recalling Equation 2.7, the total angular momentum vector \mathbf{H} , which is referenced to the earth fixed axes system, is defined. Differentiation of \mathbf{H} , noting that the unit vectors in the nose wheel frame are not constant with respect to the earth fixed frame, produces Equation 7.4.

Equation 7.4: Nose Wheel Angular Velocity Rate of Change

$$\frac{d\mathbf{H}}{dt} = \left(\frac{dH_x}{dt} - H_y\omega_z + H_z\omega_y \right) \mathbf{i}_{nw} + \left(\frac{dH_y}{dt} + H_x\omega_z - H_z\omega_x \right) \mathbf{j}_{nw} + \left(\frac{dH_z}{dt} - H_x\omega_y + H_y\omega_x \right) \mathbf{k}_{nw}$$

Recalling Equation 2.8, the scalar values of the moment produced through the change in angular momentum of the nose wheel can be written (Equation 7.5).

Equation 7.5: Nose Wheel Torquing Moments

$$\begin{aligned} M_x &= \frac{dH_x}{dt} - H_y\omega_z + H_z\omega_y = I_{xx} \frac{d\omega_x}{dt} - (I_{yy} - I_{zz})\omega_y\omega_z \\ M_y &= \frac{dH_y}{dt} + H_x\omega_z - H_z\omega_x = I_{yy} \frac{d\omega_y}{dt} + (I_{xx} - I_{zz})\omega_x\omega_z \\ M_z &= \frac{dH_z}{dt} - H_x\omega_y + H_y\omega_x = I_{zz} \frac{d\omega_z}{dt} - (I_{xx} - I_{yy})\omega_x\omega_y \end{aligned}$$

The remaining step required to express the moment vector in terms of the strut axes system is trivial and can be achieved by one more direction cosine matrix operation. Equation 7.6 defines the strut referenced torque produced by the nose wheel.

Equation 7.6: Nose Wheel Axes to Strut Axes Moment Conversion

$$\begin{bmatrix} M_x \\ M_y \\ M_z \end{bmatrix}_{\text{str}} = \begin{bmatrix} \cos\Omega & 0 & -\sin\Omega \\ 0 & 1 & 0 \\ \sin\Omega & 0 & \cos\Omega \end{bmatrix} \begin{bmatrix} M_x \\ M_y \\ M_z \end{bmatrix}_{\text{nw}}$$

The only torquing moment of interest in the strut axes reference system is M_z . M_y has previously been identified as the torque of the nose wheel bearings and M_x is opposed by the nose wheel axle to strut mount. Equation 7.7 describes the moment produced on the strut by the nose wheel. It is a complex time dependent non-linear differential equation whose solution is not trivial.

Equation 7.7: Strut Precessional Torquing Moment

$$M_{z_{\text{str}}} = M_{x_{\text{nw}}} \sin\Omega + M_{z_{\text{nw}}} \cos\Omega$$

7.3 PRECESSIONAL TORQUE COMPUTATION

Appendix B contains an Excel generated spread sheet for tabular investigation of the previous mathematics discussion. Solution of the time dependent gyroscopic torquing equation requires an iterative process that is beyond the scope of this thesis due to the requirement for simultaneous iteration on four variables. To compute the nose wheel rotational velocity vector requires knowledge of the steering angle (E), but knowledge of the steering angle's time dependent non-linear behavior requires solution of the moment equation. To allow analysis, some parameters from flight event 9.2 were used. The initial aircraft maneuver at the point of gyroscopic torquing was analyzed over a 20 second time period to observe the build up of torquing moment in relationship to the aircraft maneuver and strut precession. Included in Appendix B is the first 11.5 seconds of this time history. Only the first 11.5 seconds are included since no moment or precession dynamics occurred beyond that time.

Since the iterative process could not be used, a stepped algorithm was developed. Initially, the moment (Mz_{str}) was computed given an initial strut position (E_0) and the aircraft roll rate (p_{ac}), pitch rate (q_{ac}), and yaw rate (r_{ac}) from flight test data. This was accomplished by transforming the flight test aircraft body rates (Body Axes Referenced p, q, r) into the nose wheel frame of reference (Nose Wheel Axes Referenced p, q, r) by application of Equation 7.3. The body rates were then added to the nose wheel rate (ω_{nw}) and strut rate (\dot{E}_{str}) to define the absolute nose wheel rotational velocity vector (ω). This vector was tabulated in scalar form, creating the variables ω_x , ω_y , and ω_z . These scalar variables were

then differentiated and entered into Equation 7.5 which allowed computation of $M_{z_{str}}$ directly from Equation 7.6 and Equation 7.7. Knowledge of the moment vector then produced a predicted precession rate (\dot{F}). This precession rate was integrated and a new value for the computed nose strut angle (F) obtained.

Figure 7-1 depicts the flight test strut precession angle (E) over the 20 second time period as well as the computed angle (F) derived by the stepped algorithm.

The sharp edges of the computed angle plot in Figure 7-1 were generated by the inclusion of strut breakout moments which were evident from the flight test data. The plot of actual strut precession shows smoothed corners and this is most likely due to the inertia of the strut and nose wheel system which tends not

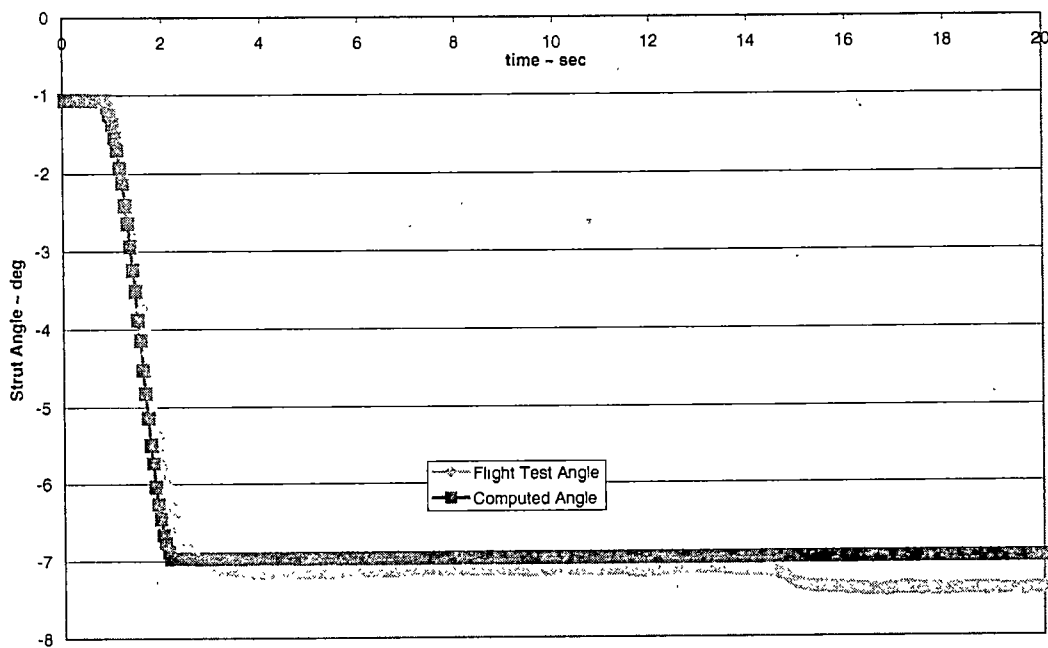


Figure 7-1: Nose Strut Precession Angle

to comply with such simplifications. Results using this method were highly dependent on analysis of the flight test data. The actual precession rates for several data runs were found to correlate directly with the computed moments. In several cases, the strut precession rate and moment exhibited parabolic shaped curves. These curves represented the initial acceleration of the strut to its maximum precession rate followed by deceleration to zero precession rate. Figure 7-2 and Figure 7-3 indicate the relationship between precession torque and precession rate for event 9.2.

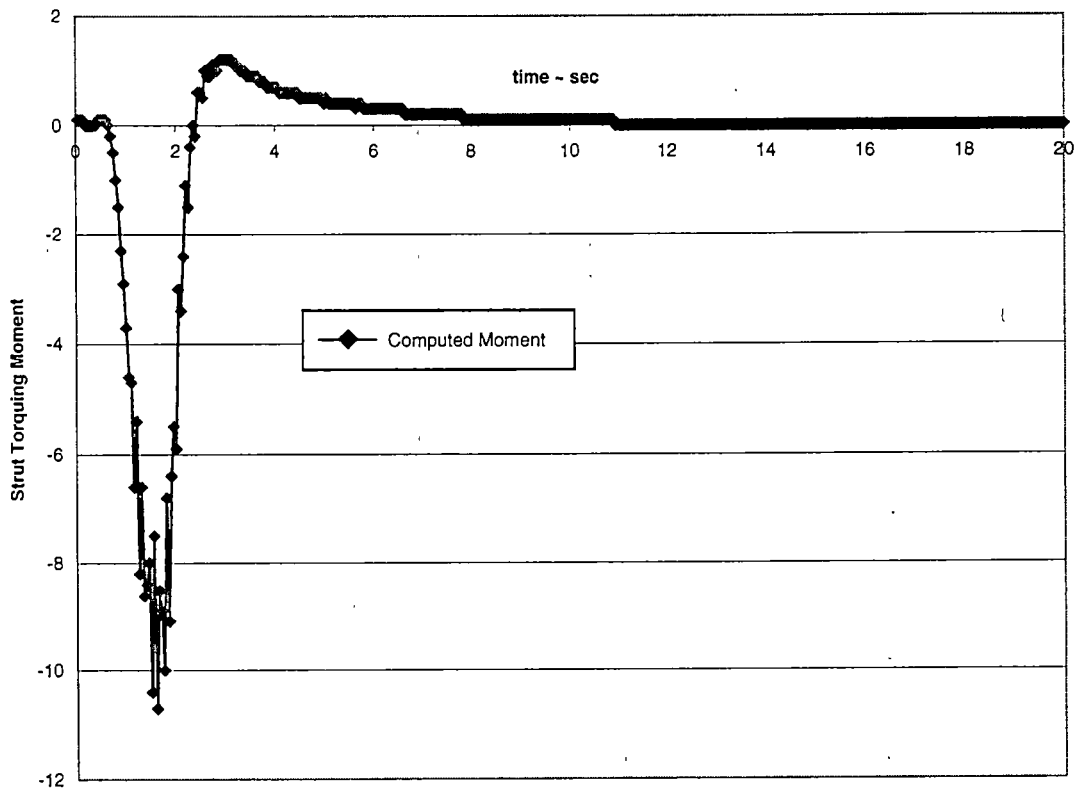


Figure 7-2: Precession Torque

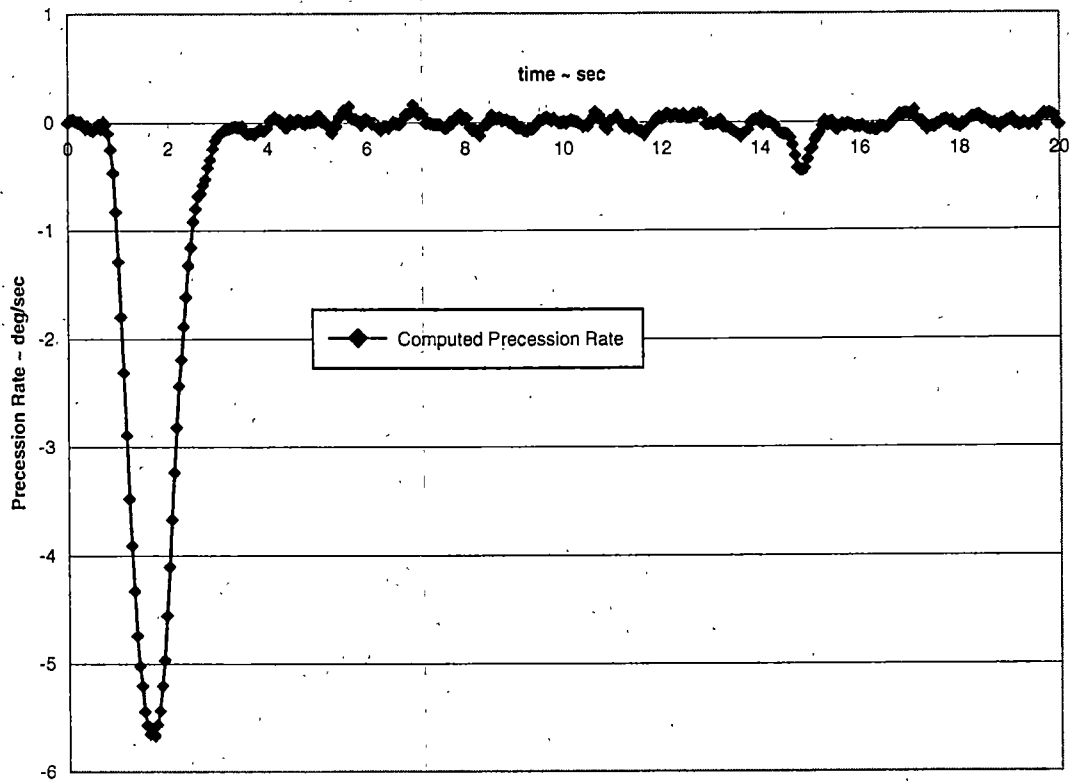


Figure 7-3: Nose Strut Precession Rate

Although the event analyzed here shows a precession angle that only builds to approximately 7 degrees and other events were much more dramatic (out to 18 degrees), this flight test event provided the smoothest aircraft maneuver for analysis. Several events had data drop outs that occurred within the region of data desired for analysis. This is evident in the plots of Appendix A by several flat line segments in the data. Even though this data was filtered to smooth the drop outs, they could not be completely removed.

7.4 COMPARISON TO FLIGHT TEST RESULTS

The mathematical solution of the torquing moment and the resultant prediction of the nose strut precession angle produced results that are consistent with the behavior identified in flight test. Unfortunately, no two flight events are the same which makes it difficult to separate the contributors of gyroscopic precession for independent study. Adding to the uncertainty within this analysis is the fact that the nose wheel rotational velocity was approximated and not actually measured in flight test. Additionally, the mathematical model developed does not account for the nose wheel being mounted approximately 0.9 feet aft of the strut centerline and slightly displaced from the aircraft center of rotation. Even though these simplifying assumptions were made, this study has identified a few key points. The most obvious point to be taken from this thesis is that the faster the nose wheel rotational velocity at the point of aircraft roll, coupled with large magnitudes of initial roll response, the larger the resultant strut precession angle will be. This is readily predicted by Equation 7.5.

Roll rate and roll acceleration provide the first change in angular momentum for the nose wheel, and there is a high dependency on pilot technique with this parameter. The pitch rate and yaw rate parameters are small and nearly equal for each turn to downwind regardless of nose wheel velocity or roll rate since the aircraft is flown in a common configuration at near equal airspeeds for each landing pattern evolution. Hence, pitch rate and yaw rate tend to have a smaller influence in relation to the others. Of significant note is that wheel rotational velocities that occur with takeoff speeds less than

approximately 100 knots generate less than 1-2 degrees of nose strut precession regardless of aircraft maneuver performed.

Because the aircraft operates in this dynamic environment, nose wheel steering designs must appropriately account for gyroscopic behavior. Pilot procedures can be implemented to reduce this effect and it is highly recommended that 180 degree turns to downwind be performed with a minimum amount of energy present in the nose wheel. Since the objective of good system design is to alleviate pilot compensation, several design ideas follow. They are intended to help the landing gear design engineer understand what systems provide a pilot the capability to avoid precession or deal with it when it occurs. Ultimately, the nose wheel must be centered prior to touchdown and the pilot must be assured that this condition exists.

8 NOSE WHEEL STEERING DESIGN CONSIDERATIONS

8.1 STEERING SYSTEMS THAT COMPENSATE FOR CRAB ANGLES AT TOUCHDOWN

In section 3.3, full time steering systems were discussed. With this type of system, the nose strut is continuously controlled and not free to precess. This solves the gyroscopic torquing problem, but current full time steering systems can be improved. With the use of the onboard computers and inertial navigation systems that exist in all but the smallest of general aviation aircraft, a design engineer can create a system that is intelligent enough to compensate for crab angle at touchdown. By calculating the aircraft side slip, the designer can predict the nose wheel angle required to create no side force on landing. As the aircraft fuselage is aligned with the ground track, the nose strut can be commanded to center. Ultimately, the pilot will slow the aircraft, and to maintain directional control, both nose wheel steering and aerodynamic controls should be used. A sophisticated fade in logic that limits nose wheel steering gain as a function of ground speed can provide the smooth transition a pilot desires. Obviously, this type of system is very expensive to design and implement. A comparison of cost, complexity, and reliability must be done to ensure the airframe is worthy of such a design. If not, a simpler approach is required.

8.2 CASTERING SYSTEMS WITH SELF-CENTERING MECHANISMS

Most every retractable landing gear system has a centering mechanism that prevents retraction of a nose strut when it is out of alignment. This is a necessity since little fuselage area exists for storage. A mechanism such as this could be designed so that when the aircraft is not in contact with the ground, the

nose strut is commanded to center. Unfortunately, this type of system has a very undesirable failure mode. Indication of an airborne state usually comes from a weight-on-wheels contact switch. If this switch fails on the deck the nose strut will be commanded to center, and the pilot will not have directional control of the aircraft. System safety could be greatly enhanced with some control logic that looks for weight-on-wheels transition and nose wheel rotational velocity. Also, the pilot could be given a control in the cockpit that allows him to command the strut to center. In the case of a caster-selectable nose wheel steering system, this can be accomplished with a short engagement of the nose wheel steering button while airborne. That however, requires the pilot to be able to assess the centering of the directional controller (rudder pedals or wheel). Such a system is a design of its own.

8.3 CASTER-SELECTABLE NWS SYSTEMS WITH CENTERING INDICATORS

A centering mechanism can be simple or complex, but in either case it will give the pilot knowledge of his steering angle. The most basic centering indicator will likely be an indicator light or digital readout that is energized when the nose strut is within some acceptable range of center. For aircraft landing with a castering nose landing gear, that number tends to be around +/- 2 degrees of center. Beyond that, the pilot will definitely notice a side force at touchdown and the larger the centering error, the larger the undesired side force.

An indicator that shows the entire range of motion of the nose gear provides the pilot with far more information. In the case of the current AV8B

nose wheel steering system, a centered rudder pedal condition does not necessarily mean a centered nose landing gear strut—even with nose wheel steering engaged. An excellent solution to this problem is a small linear scale located near the bottom of the Heads Up Display. It could show actual strut position in relation to the center indicator. This would allow the pilot to engage nose wheel steering and drive the strut to center without regard for pedal position. Once the strut has been centered, the nose wheel steering button can then be released and the rudder pedals returned to a center position. Regardless of the method used, the centering indicator must be good enough to provide a centered indication with minimum hysteresis.

9 CONCLUSIONS

9.1 GENERAL

Ground handling of aircraft continues to be a critical requirement as congestion and space at tactical ground facilities is limited. For the majority of flying machines designed today, a nose wheel steering system is employed along with some version of a statically and dynamically stable landing gear design. To create systems that do not provide stability requires pilot compensation, and pilot compensation implies a poor design. With the requirement for easy ground handling comes the requirement to design out all potential systems failures that may be caused by physical world properties or potential human error.

The potential for an uncommanded nose wheel steering input on touchdown has been proven to exist. Gyroscopic precession is not a well-known problem within the Harrier community but certainly is a significant problem that must be addressed. Since most aircraft that pilots operate are beyond the design phase, the pilot must learn how to minimize the chances of something such as an uncommanded steering input occurring. The subject of this thesis has been to identify the theory and explain the mechanics of gyroscopic precession in an aircraft nose strut. Specific conclusions that support the phenomenon of nose strut precession follow.

9.2 SPECIFIC

a) The theory presented in sections 2.3 and 7.3 predict that nose strut precession will occur. The magnitude of the precession angle can be estimated

with some degree of accuracy given an aircraft maneuver and nose wheel energy state.

b) Pilot technique plays a significant role in the phenomenon of gyroscopic precession. The landing pattern techniques used by transport pilots, light civil pilots, and U.S. Air Force tactical jet pilots lend themselves to inhibiting nose strut precession since the landing gear are raised and then lowered in between each landing. For U.S. Navy trained tactical jet pilots, this is not so. Operational requirements dictate that touch and go landings be performed with the landing gear extended at all times. Differences are noticed in the application of aircraft roll rates and accelerations which greatly influence the nose strut precession rate and the resultant precession angle.

c) V/STOL aircraft operations allow the pilot to takeoff with nose wheel velocities ranging from very low to very high. This directly affects the total energy on the nose wheel when the aircraft is maneuvered and subsequently can inhibit precession from occurring or cause large precession angles with the same aircraft maneuver.

d) The largest contributors to the phenomenon of gyroscopic precession are the nose wheel rotational velocity, aircraft roll rate, and roll acceleration. Pitch rate and yaw rate tend to have a lessor influence and for this test were similar on each flight event since the turn to downwind was conducted at roughly the same speed and configuration.

e) Roll acceleration effects are extremely non-linear. On two nearly identical flight test events (7.2 and 8.1), the roll acceleration was doubled but the nose strut precession angle increased by a factor of five.

f) The simplifying assumptions used within this thesis most likely created small errors in the computation of the torquing moment, but the trends remained the same across the spectrum of flight test events analyzed. Therefore, the simplifying assumptions are considered to be valid for this analysis.

10 RECOMMENDATIONS

10.1 GENERAL

The specific recommendations that follow are designed to help the operator compensate for nose strut gyroscopic precession experienced in the AV8B and assist the engineer while he improves the design. Knowledge of how the pilot will use a system can be the difference between developing a useful, safe system and one that is prone to create mishaps. In light of this, the designer should consider all the recommended procedures outlined first and determine ways to alleviate the pilot of these tasks. Regardless of the system design, the pilot must be aware of the capabilities of the craft, understand the cause and effect of gyroscopic precession, and operate within the design envelope of the aircraft.

10.2 SPECIFIC

a) The most obvious recommendation is to delay any aircraft maneuvering until the nose wheel's rotational rate has sufficiently decayed. This may not be practical though if landing patterns are to be kept small. If turning is required with nose wheel energy present, the pilot should use slow rolls. This will allow the nose wheel more time to reduce its rotational rate prior to excessive gyroscopic torquing occurring and reduce the effect of gyroscopic precession.

b) Another solution is to raise the landing gear between successive touch and go landings—if the aircraft is so equipped. This action will cause the nose strut to center and it will maintain that position while the rotational velocity decays.

c) The Harrier pilot can use the following rule of thumb to predict when nose wheel rotational velocity has sufficiently decayed (less than approximately 25 rad/sec) so that gyroscopic precession will not occur: Maintain wings level upwind prior to turning for a length of time (in seconds) equal to 10% of the takeoff ground speed (in knots). For example, takeoff at 150 KGS, delay for 15 seconds; takeoff at 50 KGS, delay for 5 seconds.

d) The designer should provide the pilot with an indicating system that accurately reports the nose strut steering angle. This will allow the pilot to ensure the nose wheel is centered prior to touchdown.

e) A well designed self-centering mechanism will achieve the same effect as raising the landing gear between landings. It will force the nose strut to center while the nose wheel velocity decays. Care must be taken to ensure landing dynamics do not force the nose strut to remain centered during landing rollout.

f) A full time steering design will inhibit any gyroscopic precession potential. This system will not only alleviate potential for nose strut misalignment during landing, but will also make the pilot's task of tracking centerline during crosswind landings much easier since a transition from aerodynamic controls to ground steering controls will not be required.

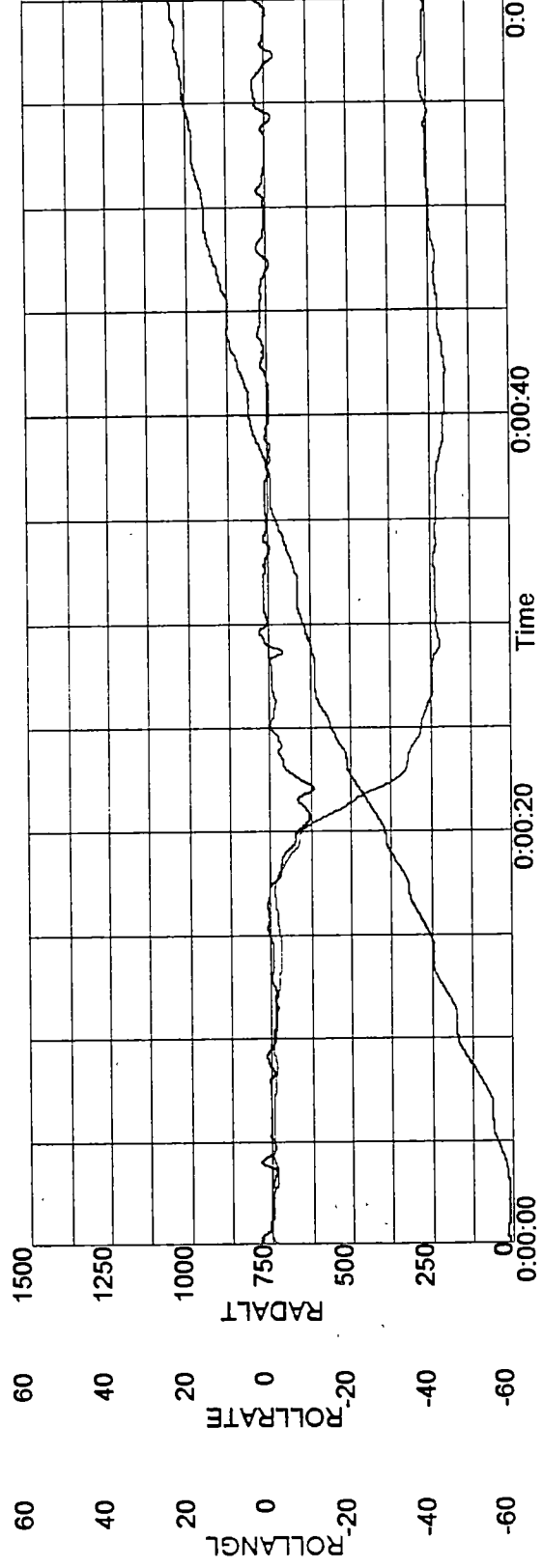
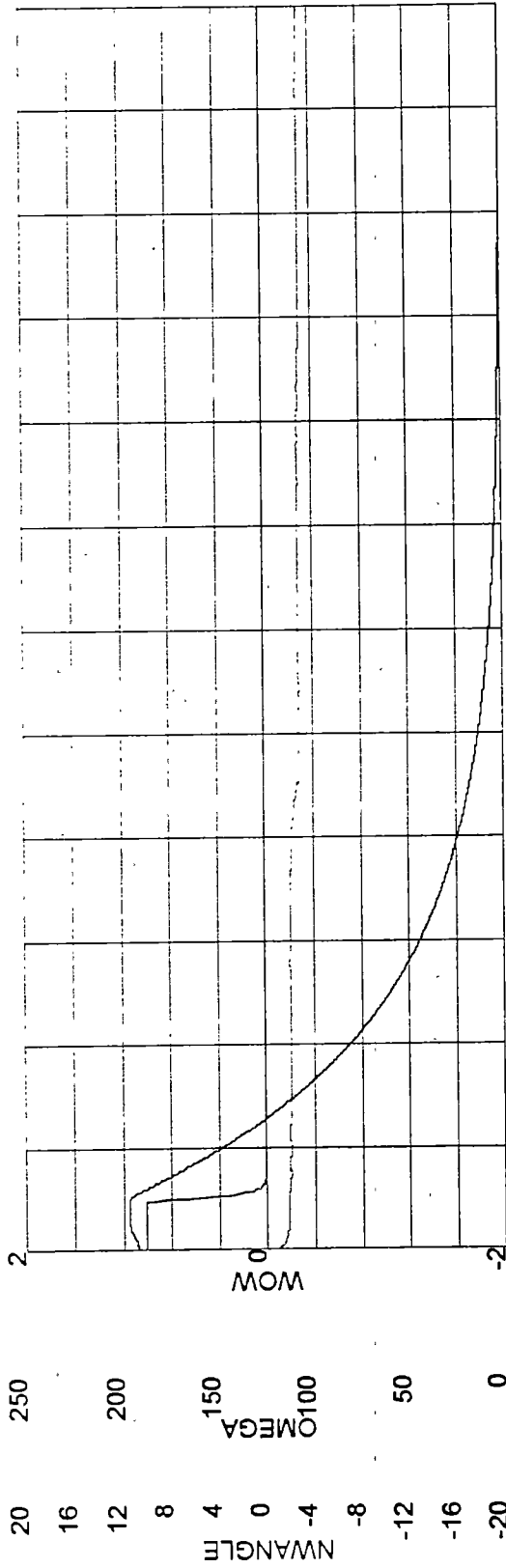
REFERENCES

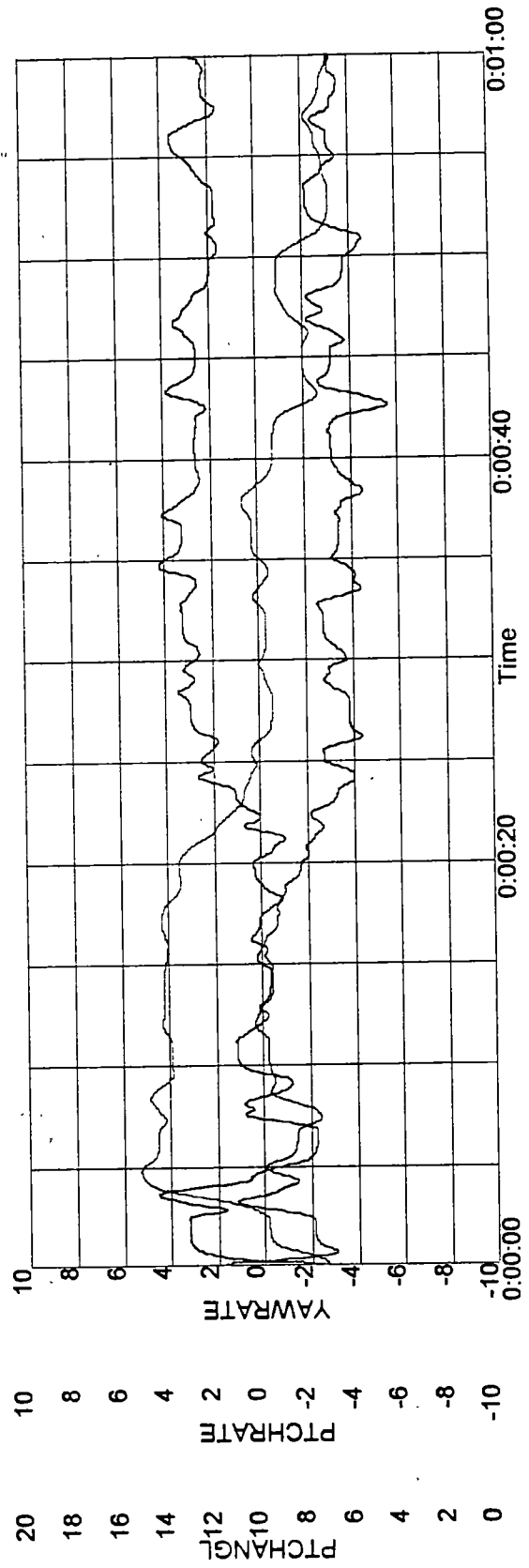
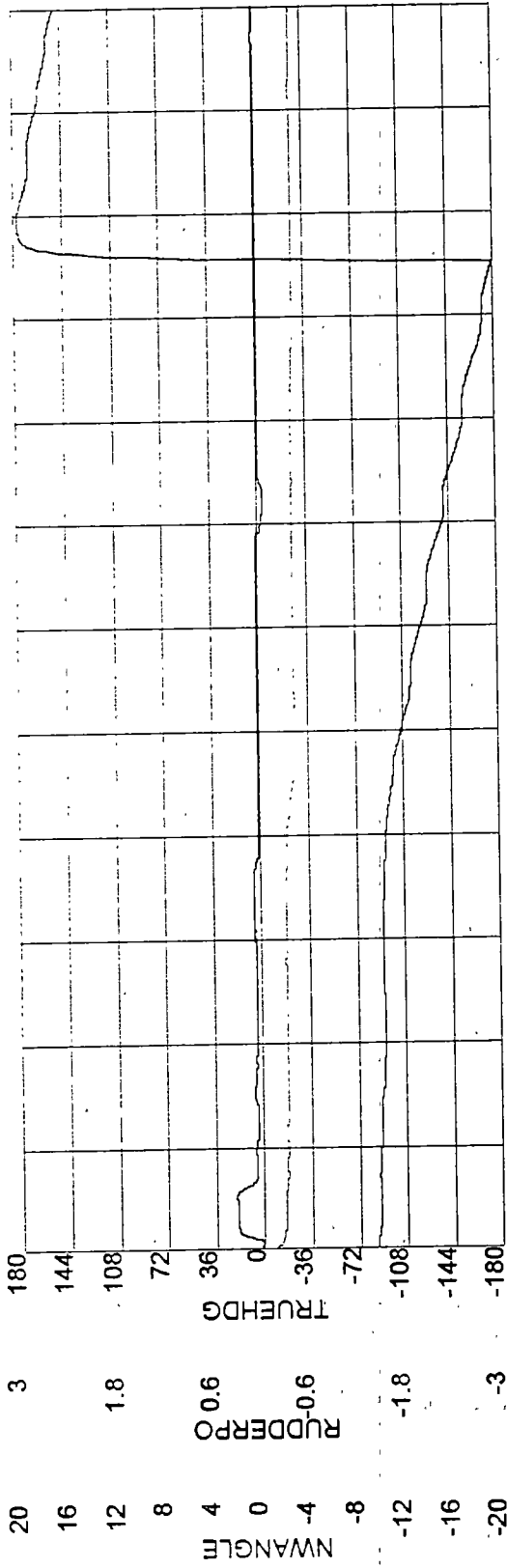
REFERENCES

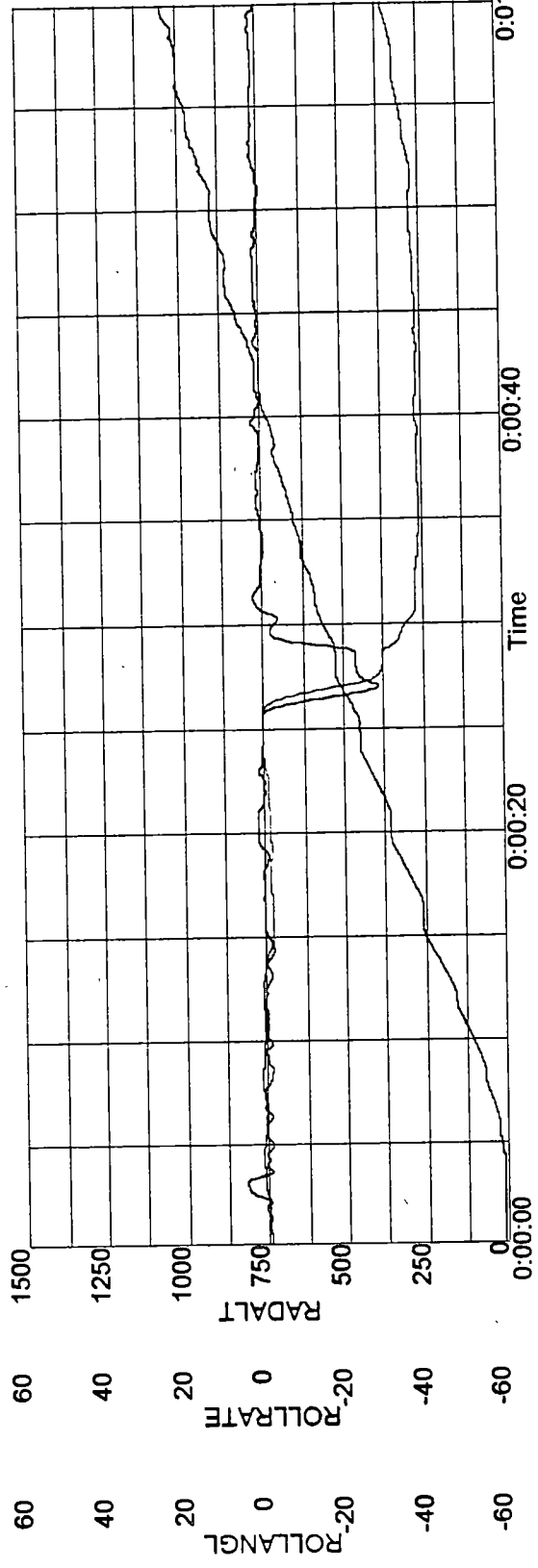
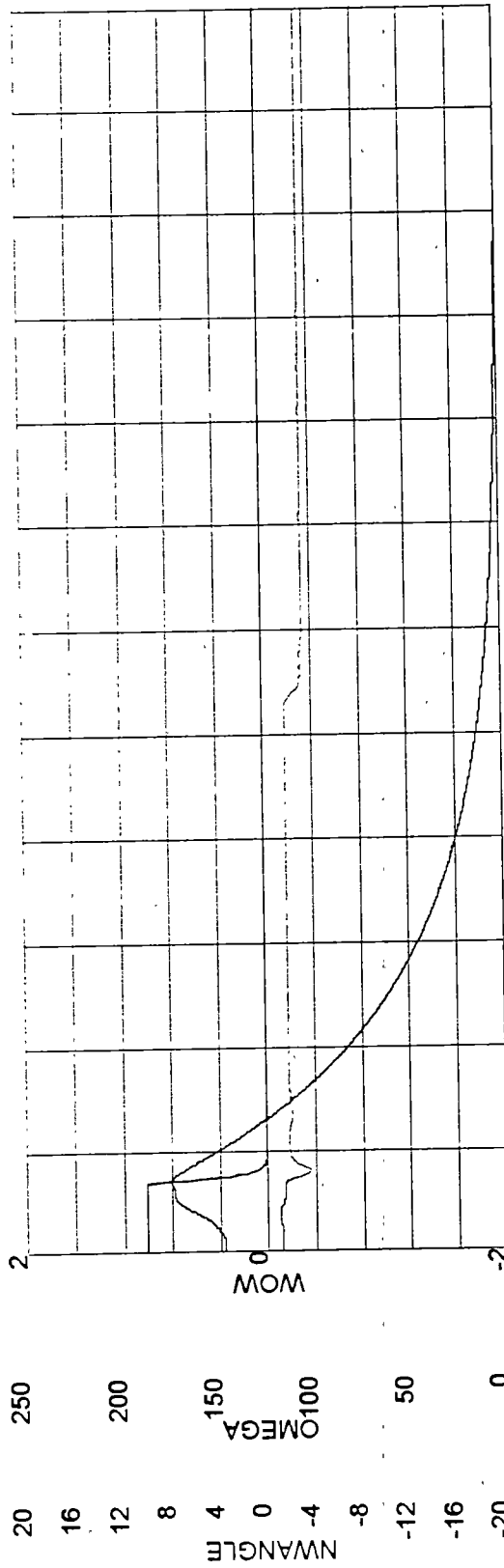
- 1) *THE GYROSCOPE-THEORY AND APPLICATIONS*, James B. Scarborough, Interscience Publishers Inc., New York; 1958.
- 2) *GYRODYNAMICS AND ITS ENGINEERING APPLICATIONS*, Ronald N. Arnold and Leonard Maunder, Academic Press, New York, 1961.
- 3) *DYNAMICS OF FLIGHT-STABILITY AND CONTROL 2nd edition*, Bernard Etkin, John Wiley and Sons, New York, 1982.
- 4) *DYNAMICS*, Lawrence E. Goodman and William H. Warner, Wadsworth Publishing Company Inc., California, 1965.
- 5) *SYSTEM DYNAMICS*, Katsuhiko Ogata, Prentice-Hall Inc., New Jersey, 1978.
- 6) *PHYSICS 3rd edition*, David Halliday and Robert Resnick, John Wiley and Sons, New York, 1978.
- 7) *ENGINEERING MECHANICS-STATICS AND DYNAMICS 3rd edition*, R.C. Hibbeler, Macmillan Publishing Co. Inc., New York, 1983.
- 8) *AV8B ECP-251R1 Nose Wheel Steering Evaluation*, NAVAIRWARCENWPNDIV, 1997.

APPENDICES

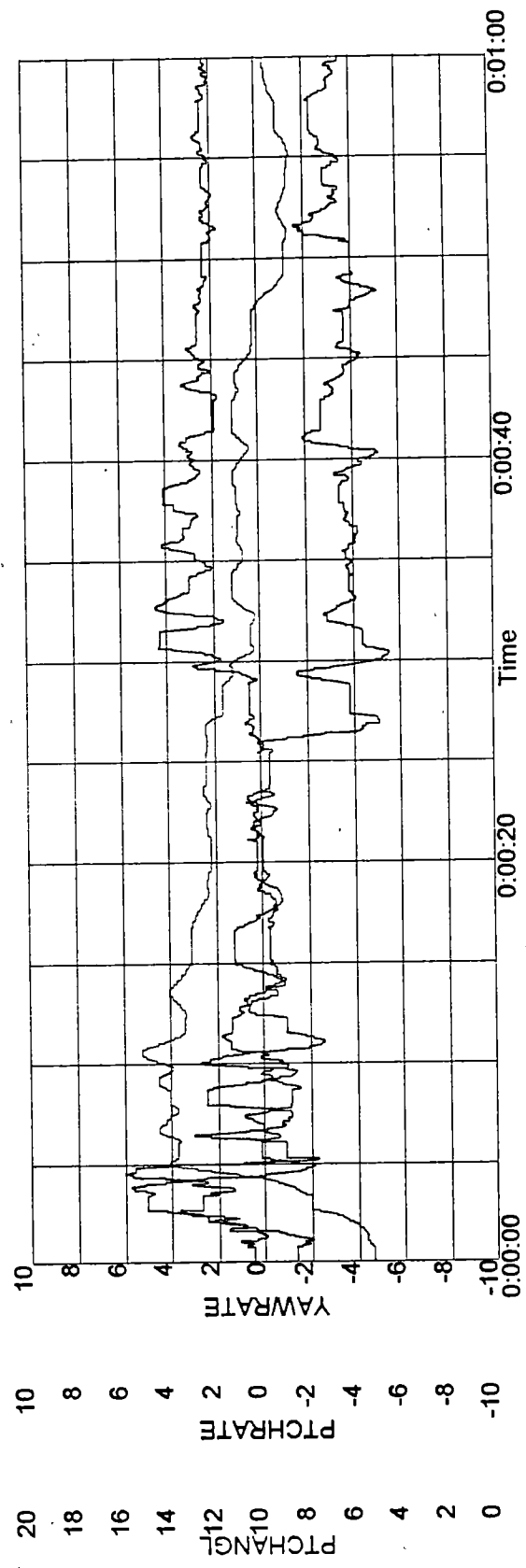
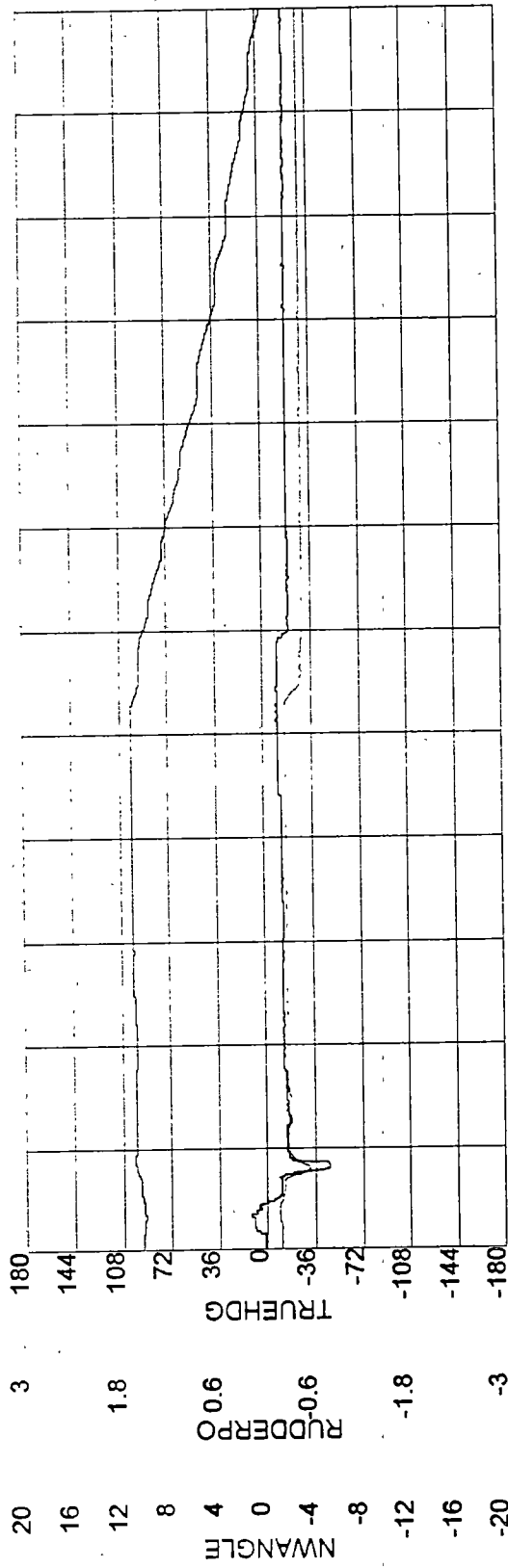
Flight 5 Event 1
page 1 of 2



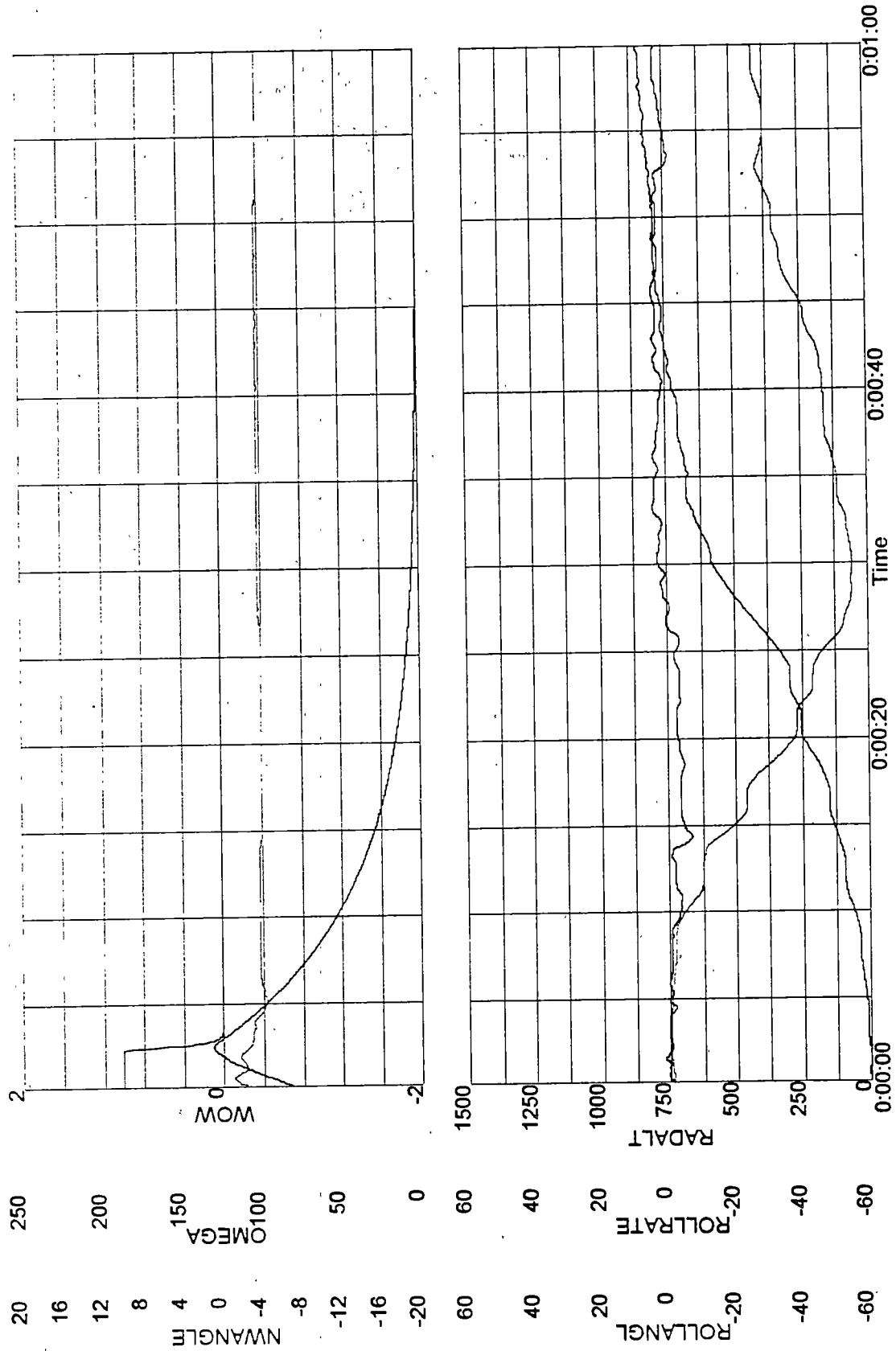




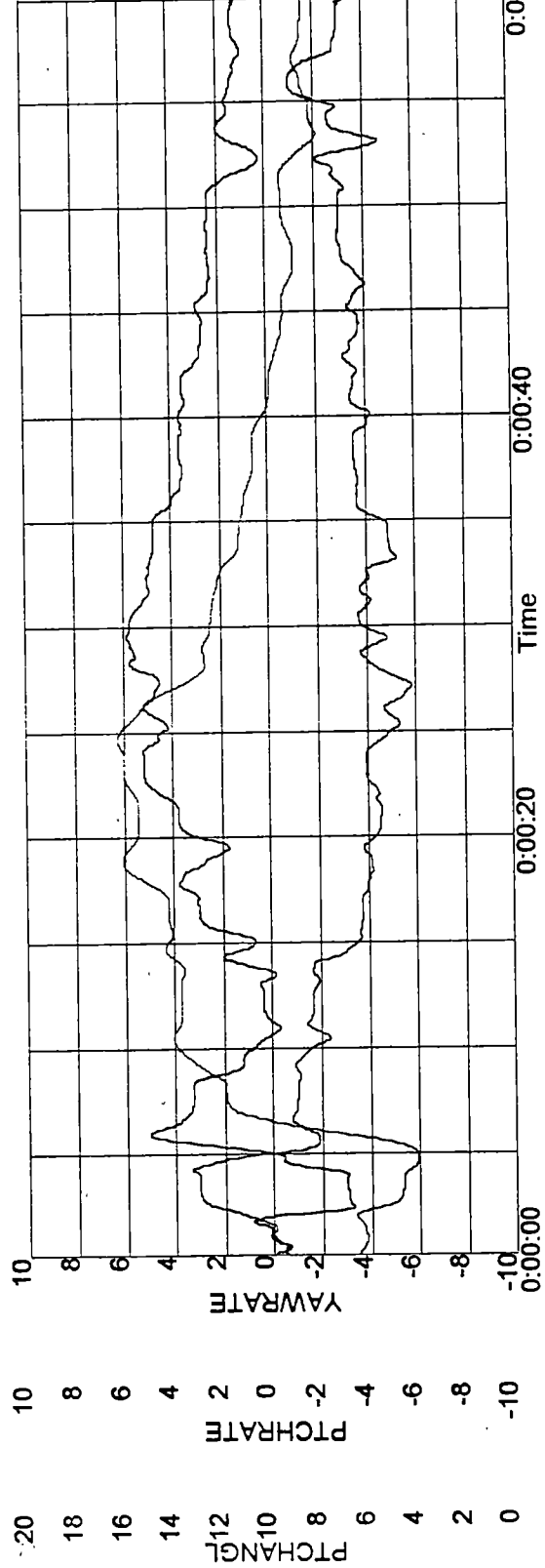
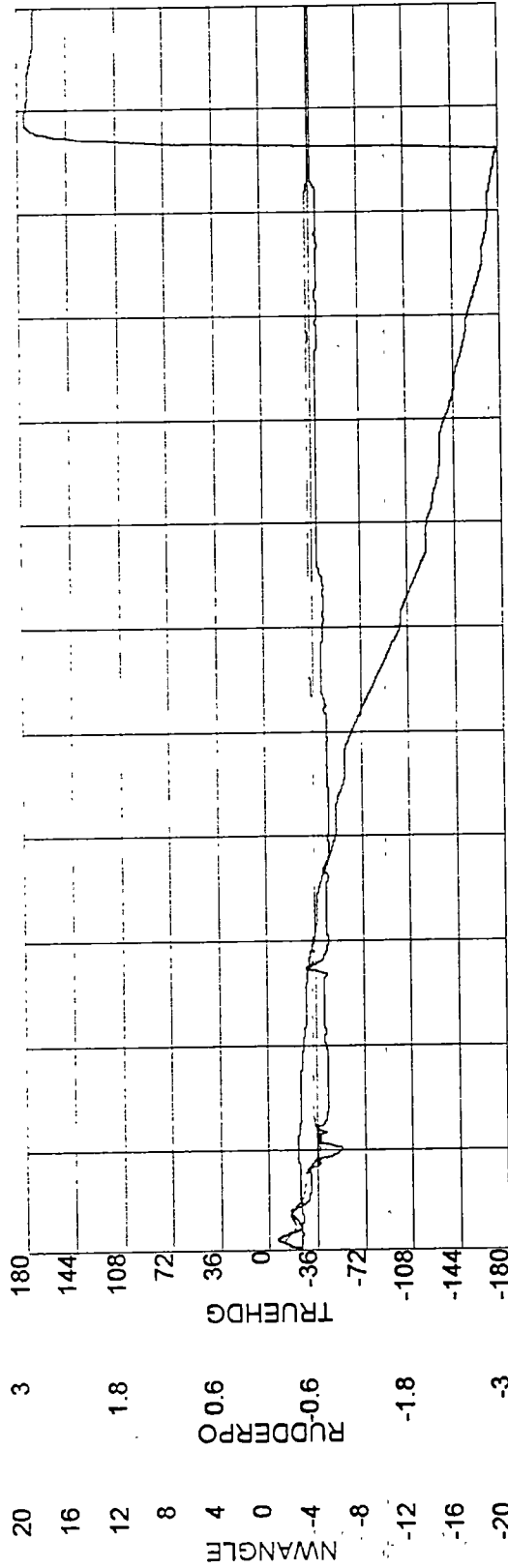
Flight 6 Event 1
page 2 of 2

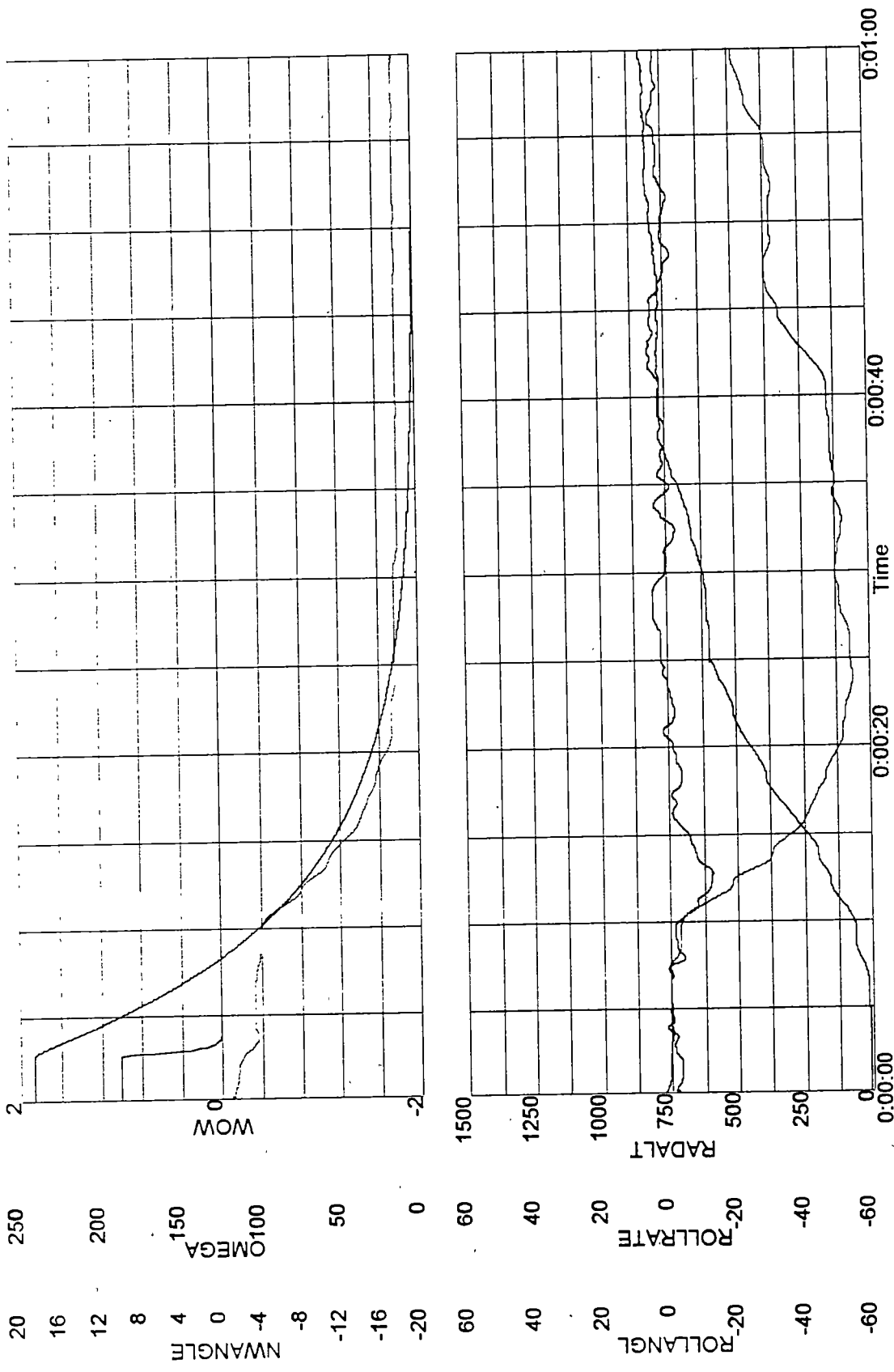


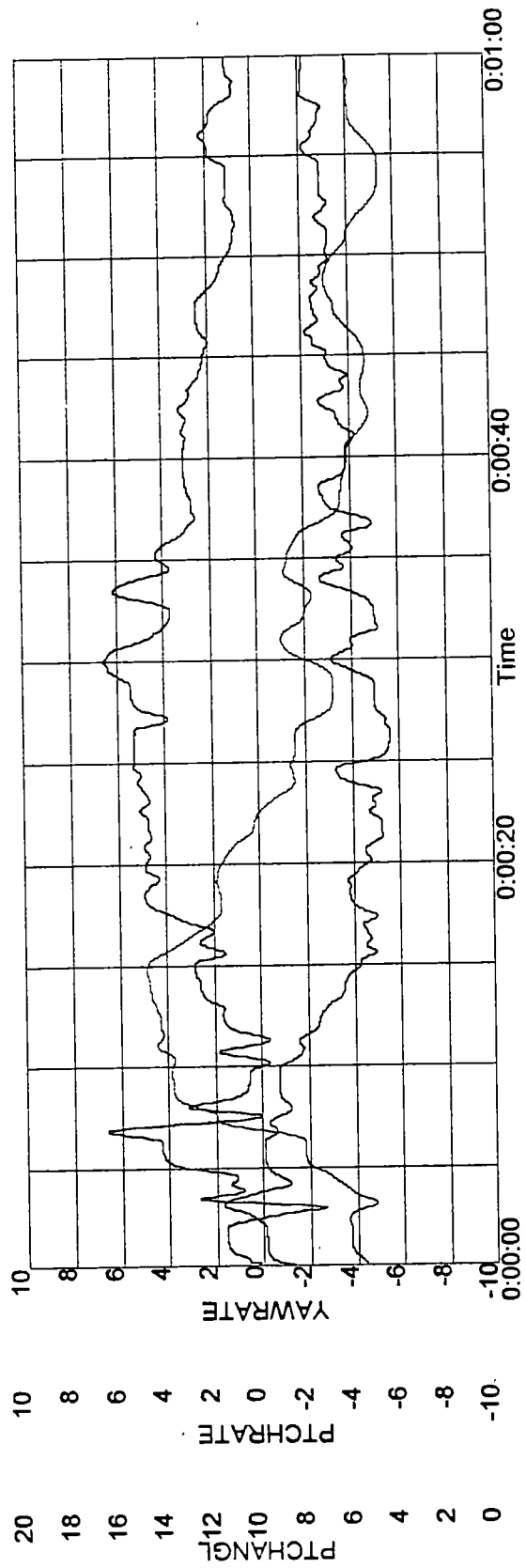
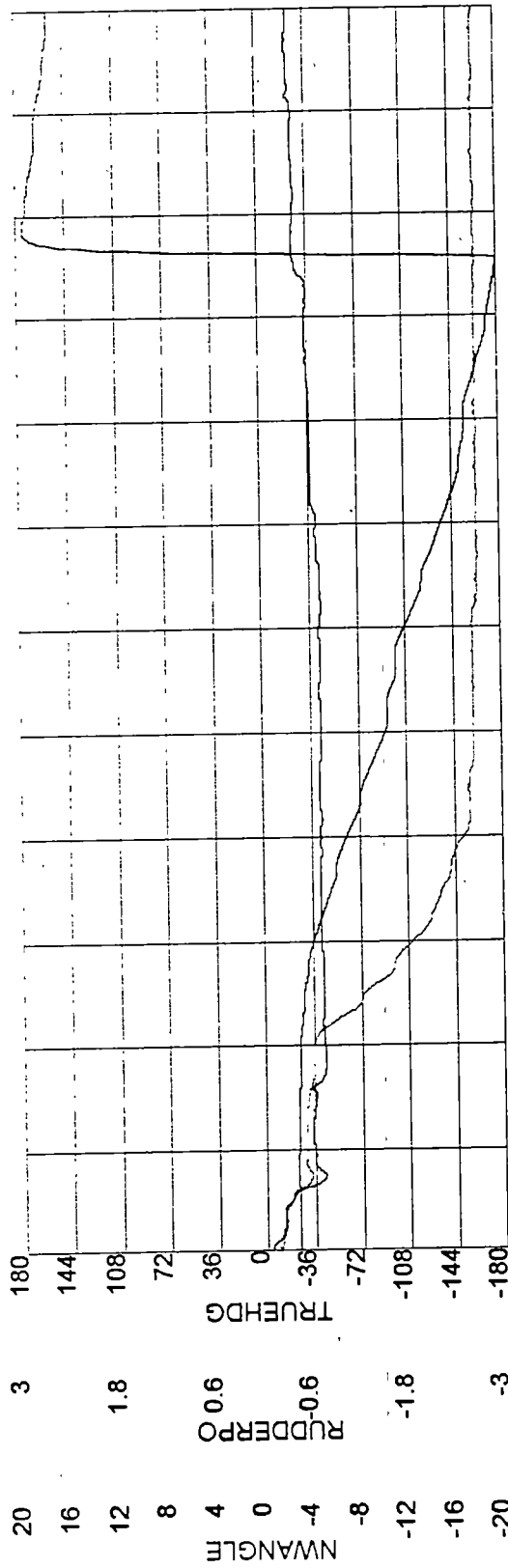
Flight 7 Event 1
page 1 of 2



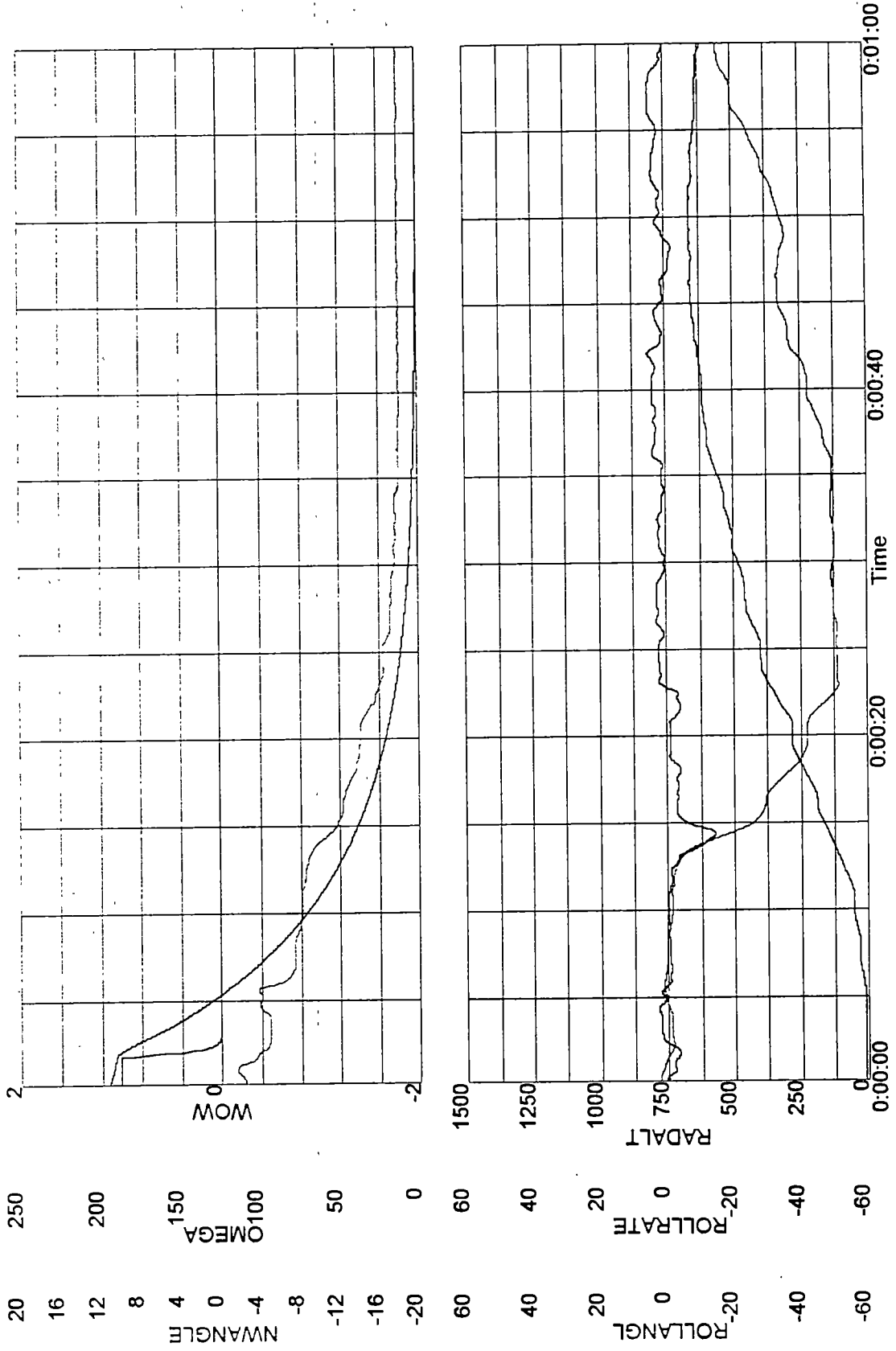
Flight 7 Event 1
page 2 of 2



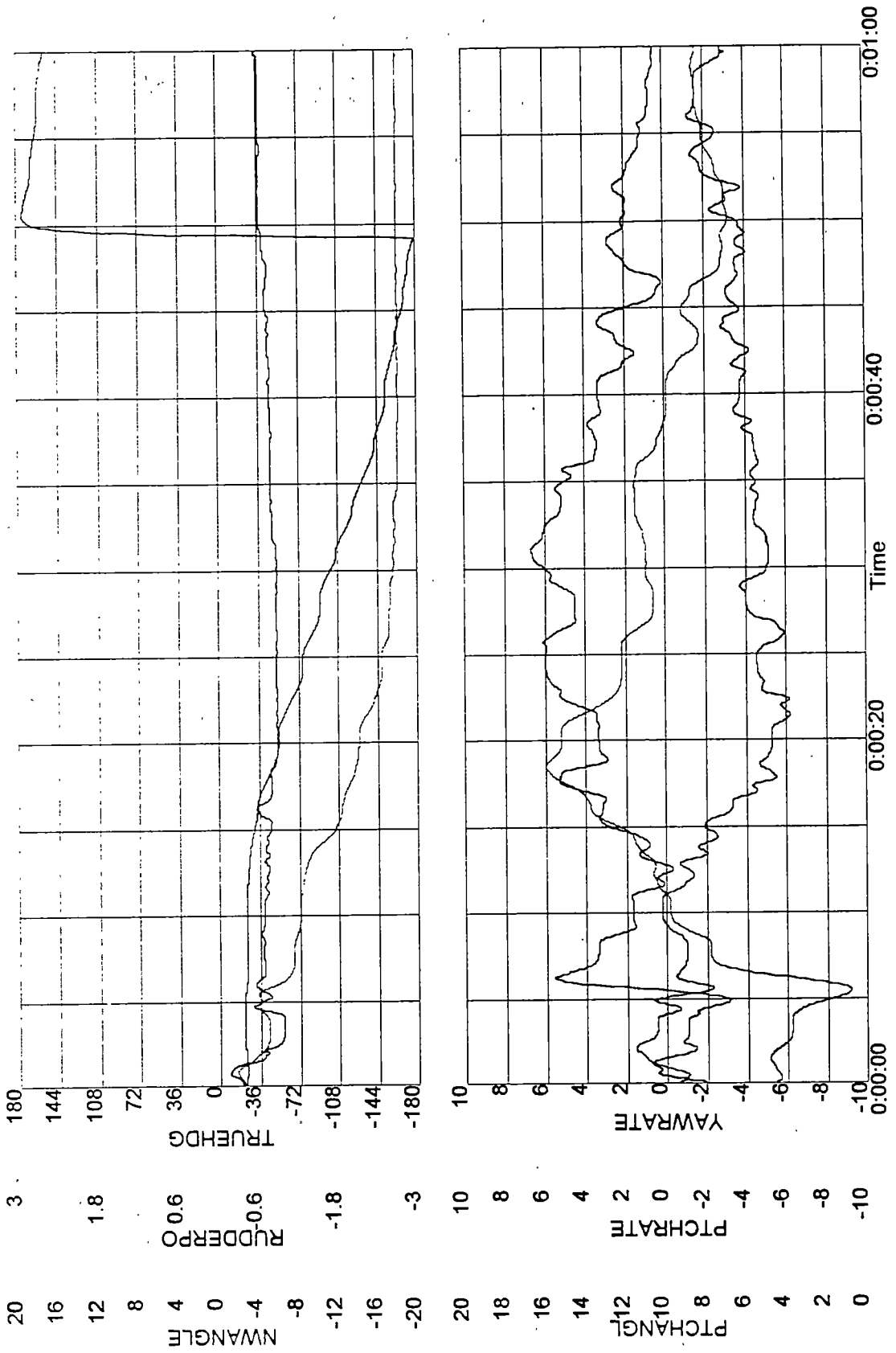




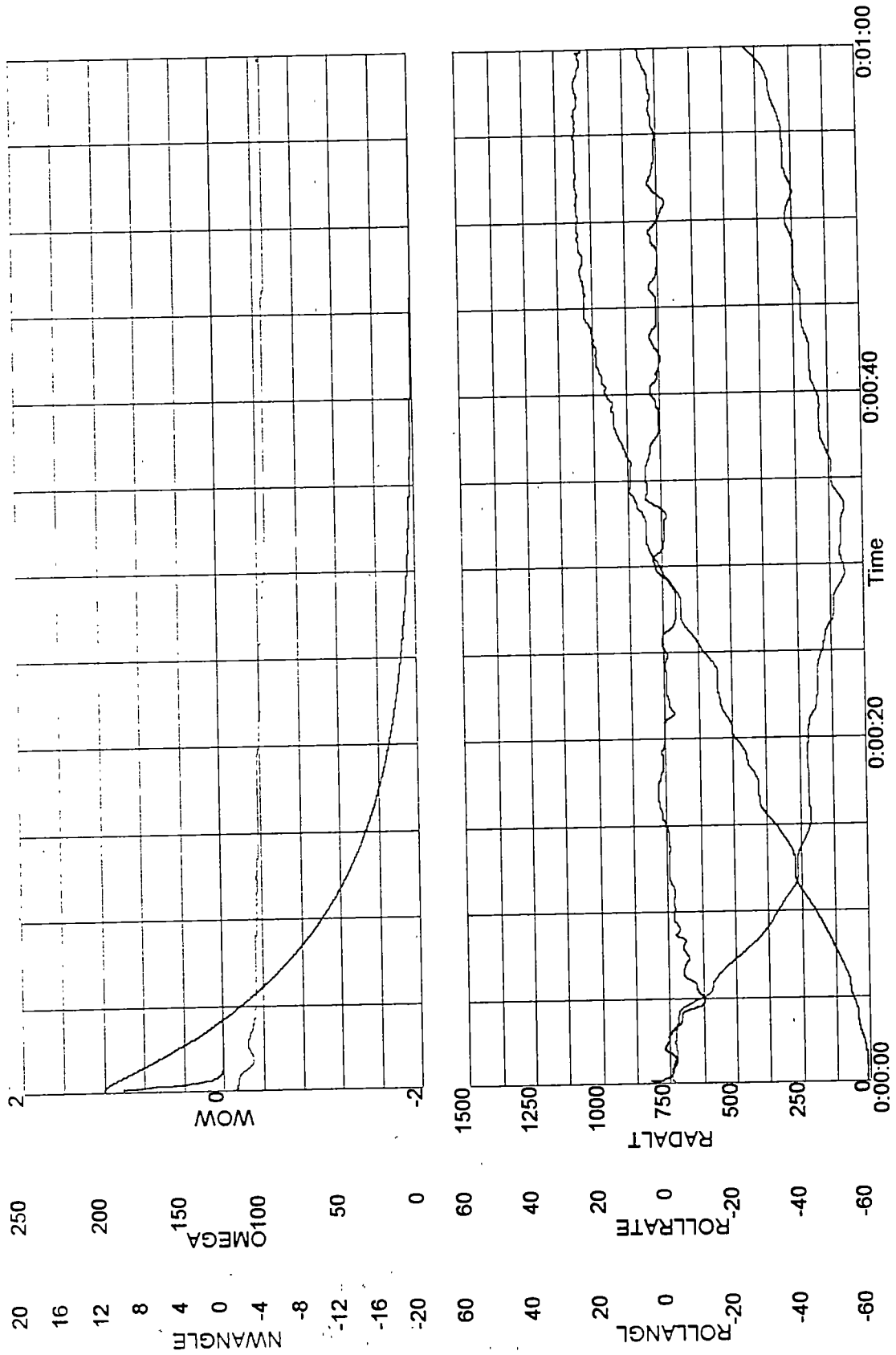
Flight 7 Event 3
page 1 of 2



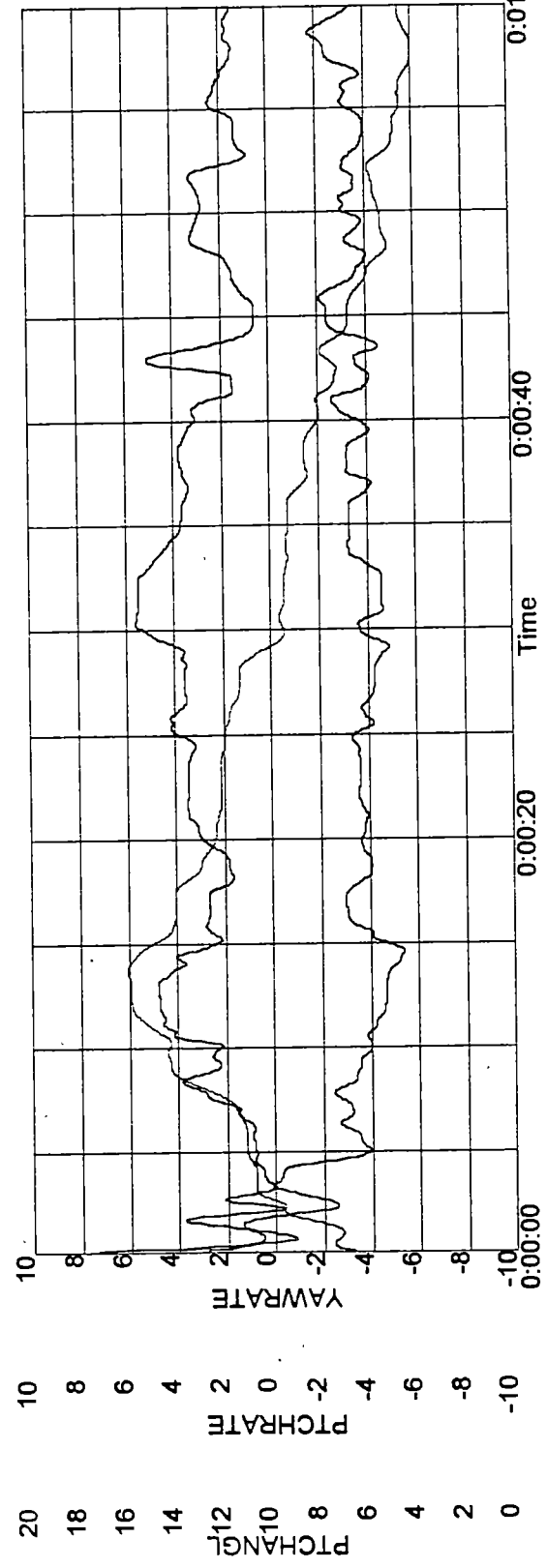
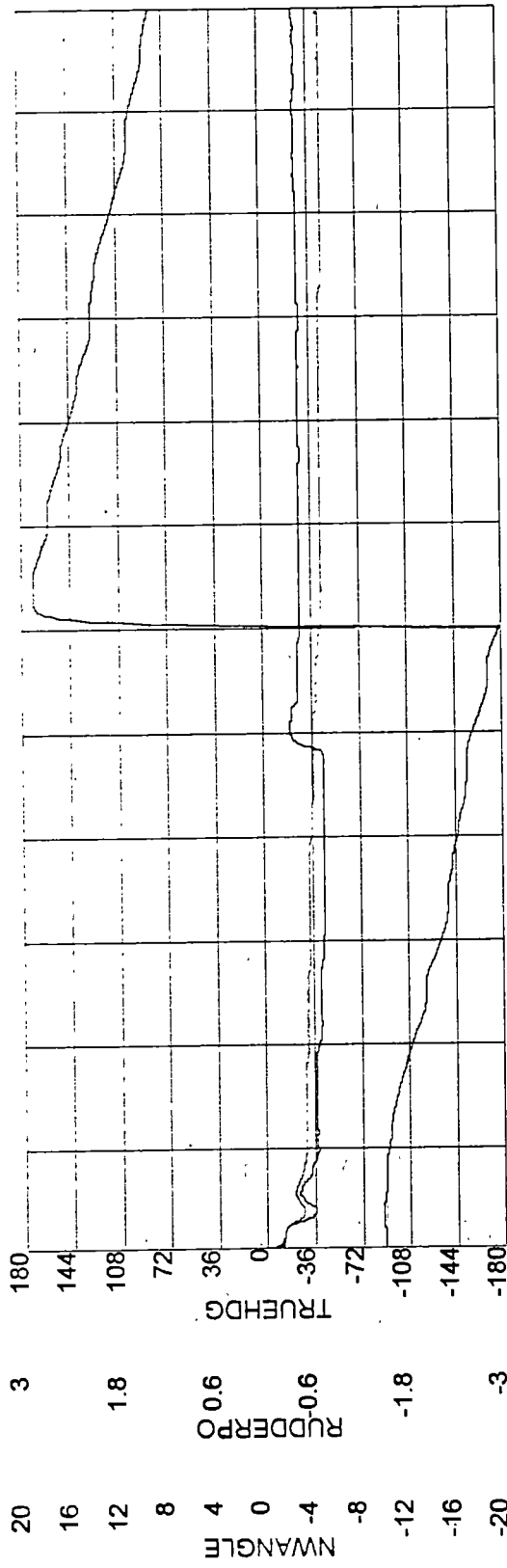
Flight 7 Event 3
page 2 of 2

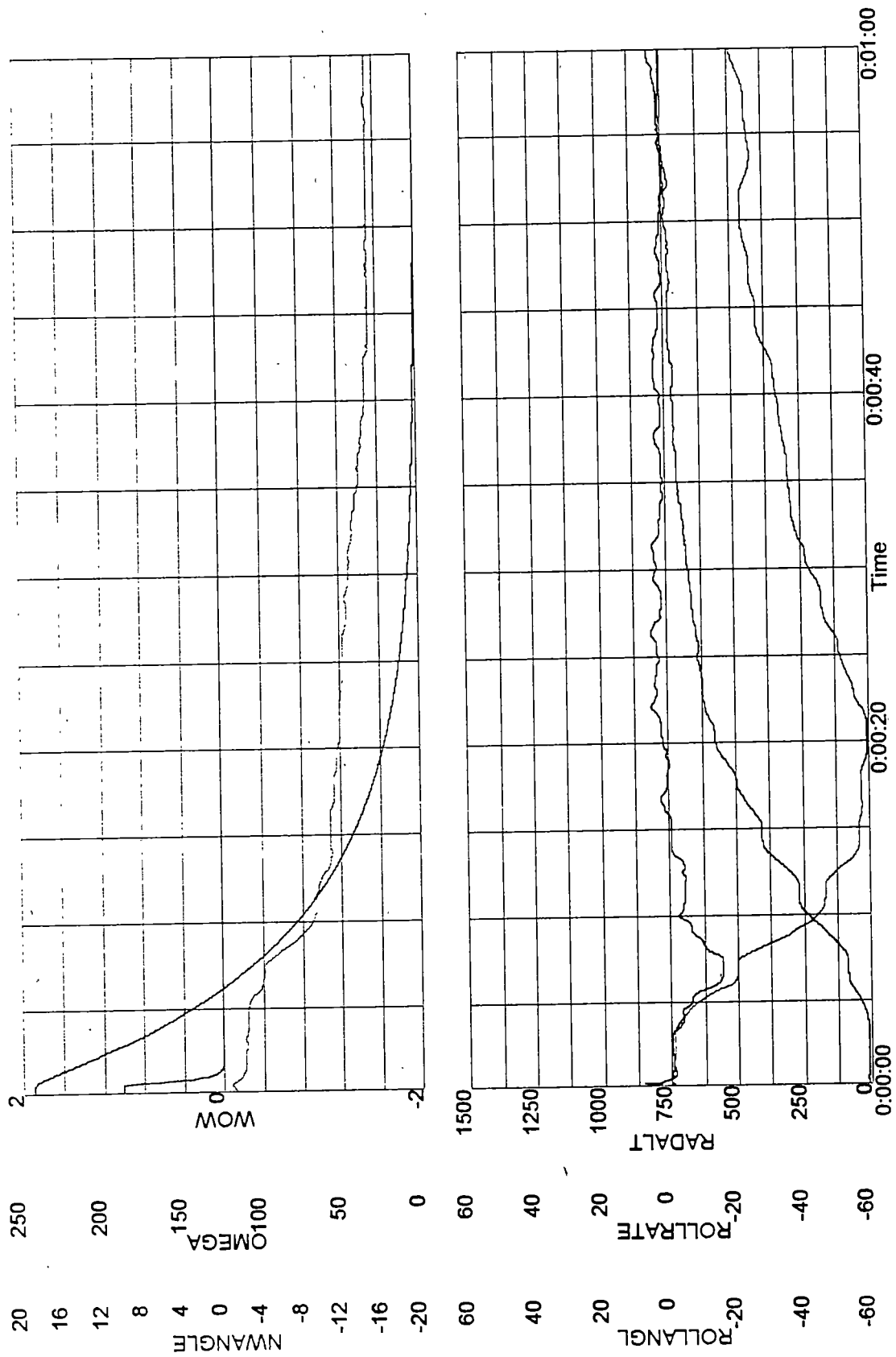


Flight 8 Event 1
page 1 of 2

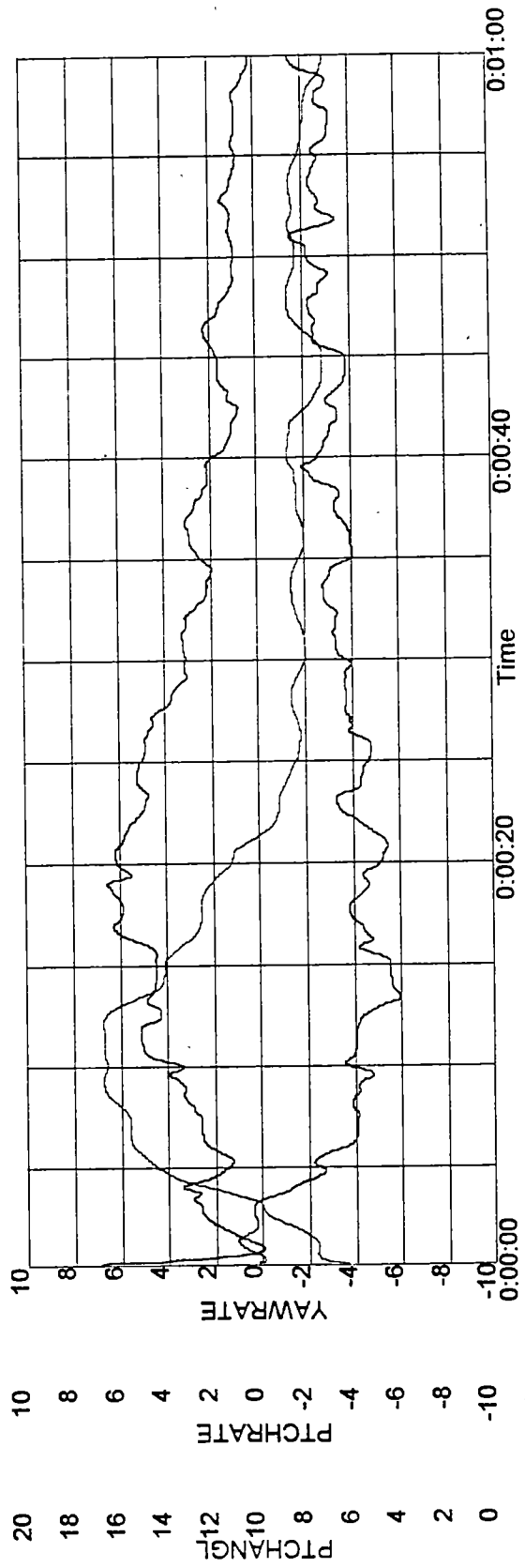
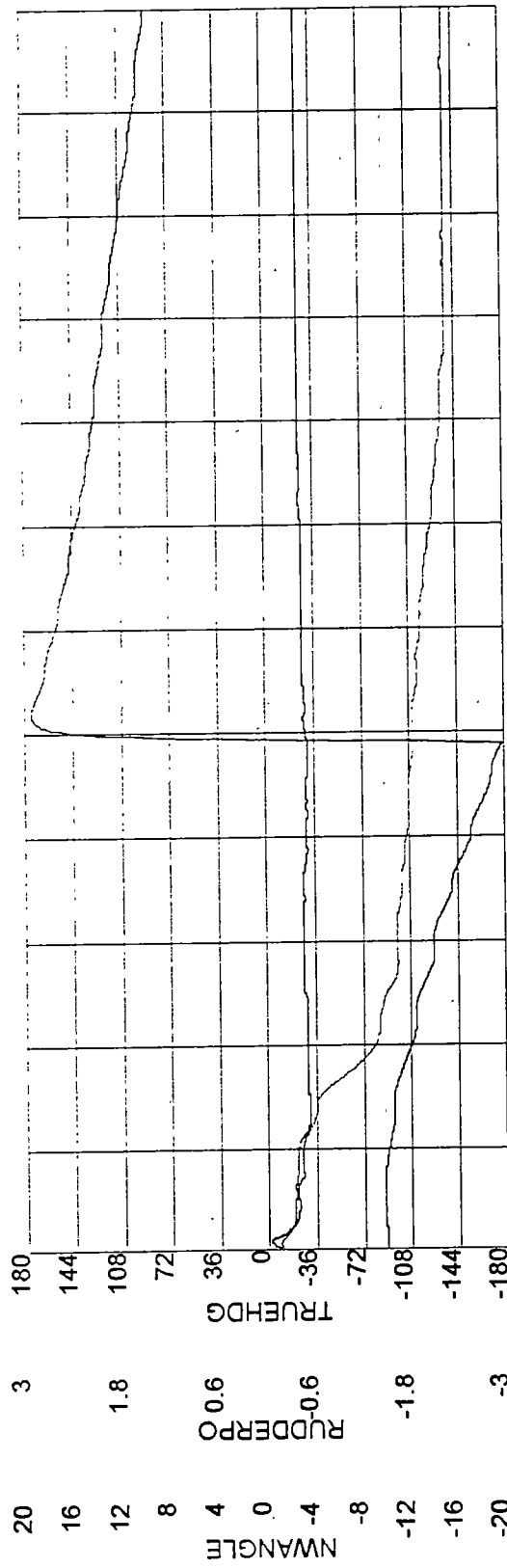


Flight 8 Event 1
page 2 of 2

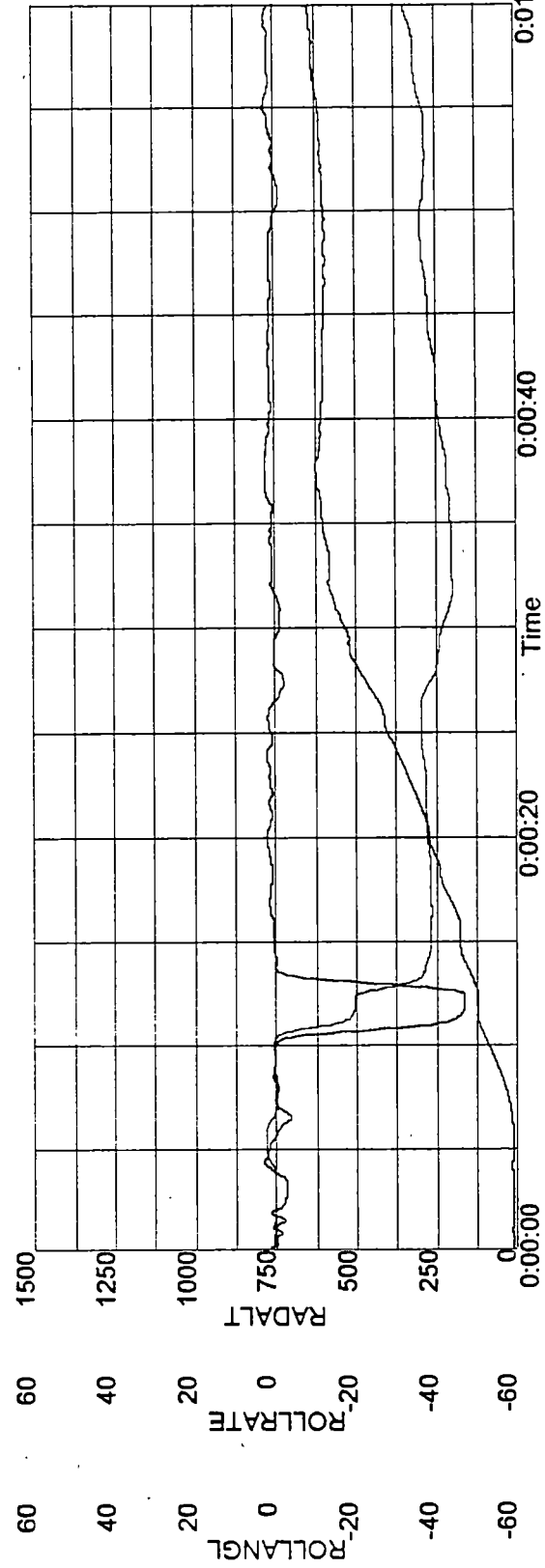
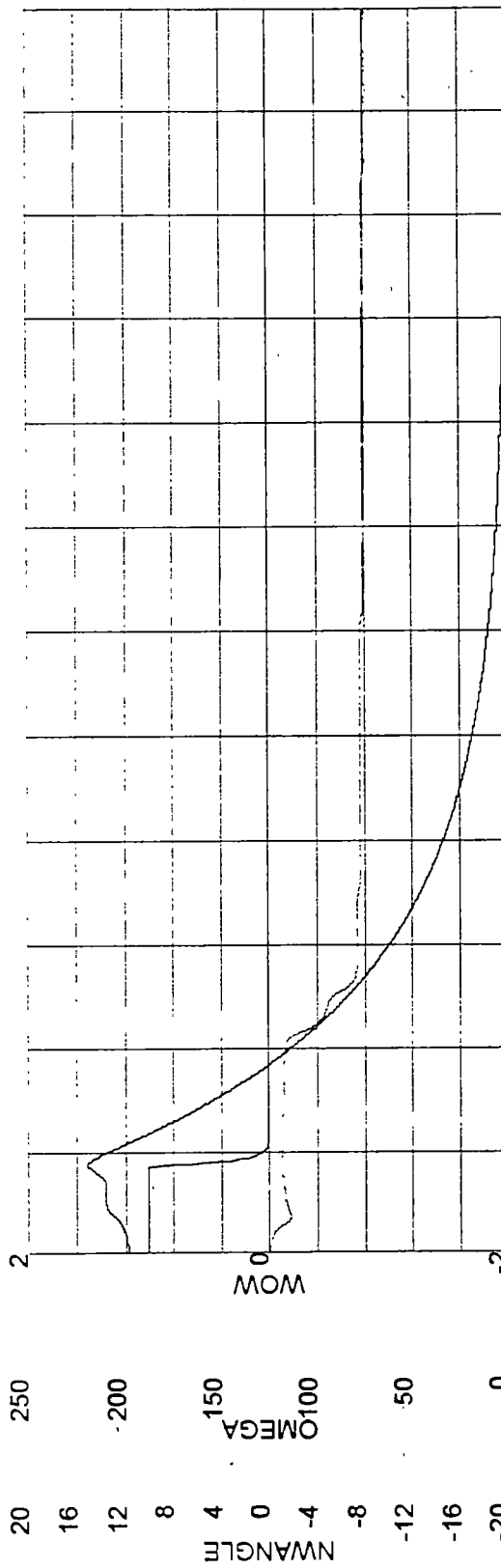




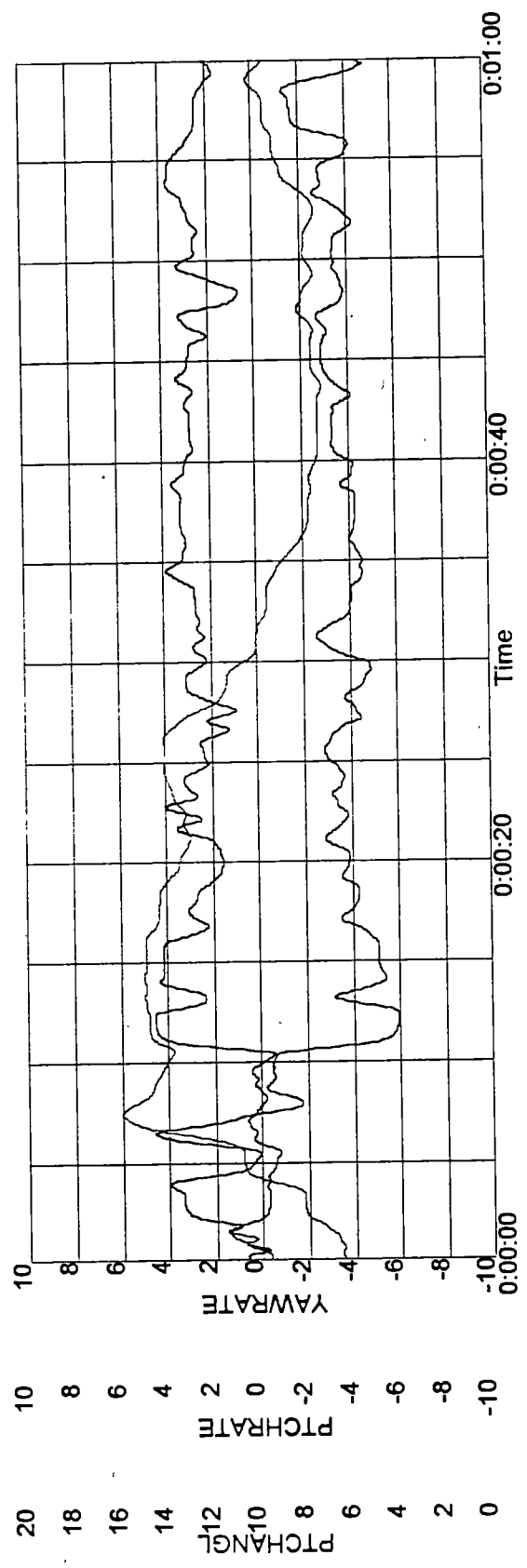
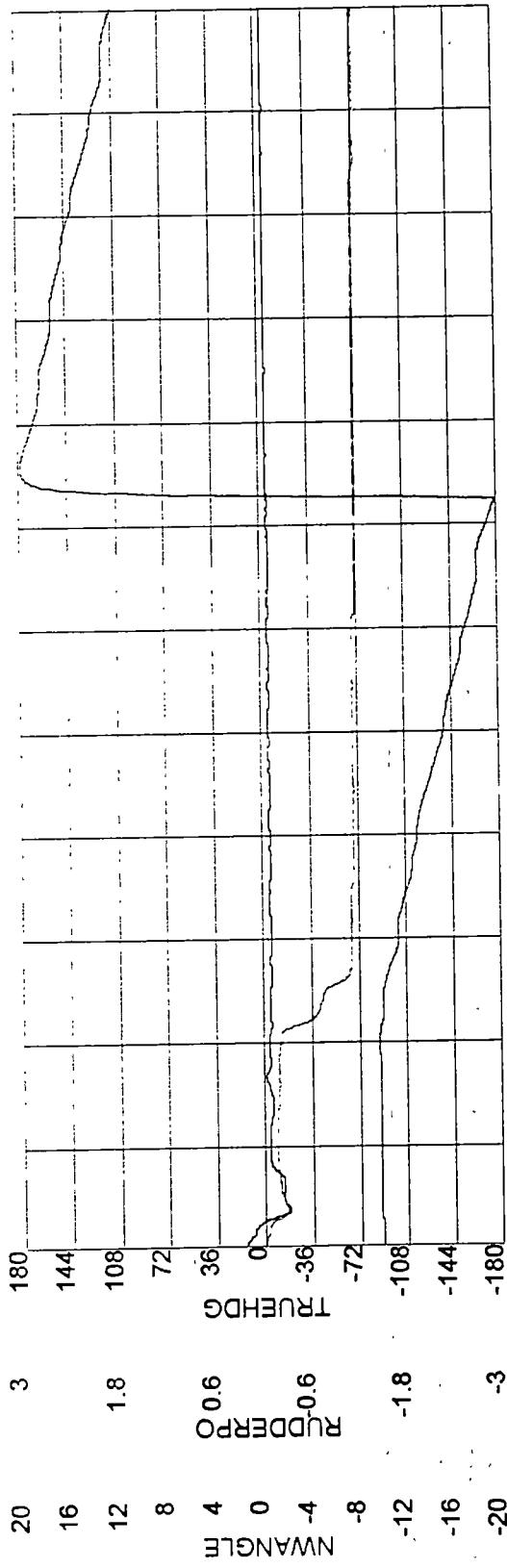
Flight 8 Event 2
page 2 of 2



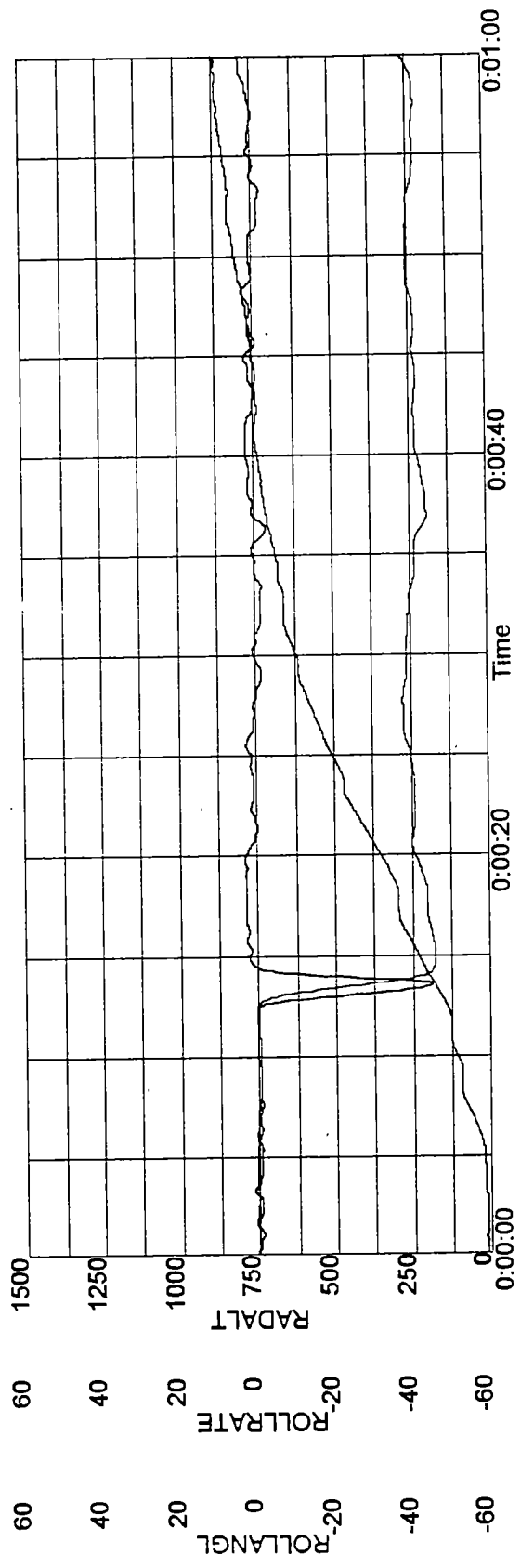
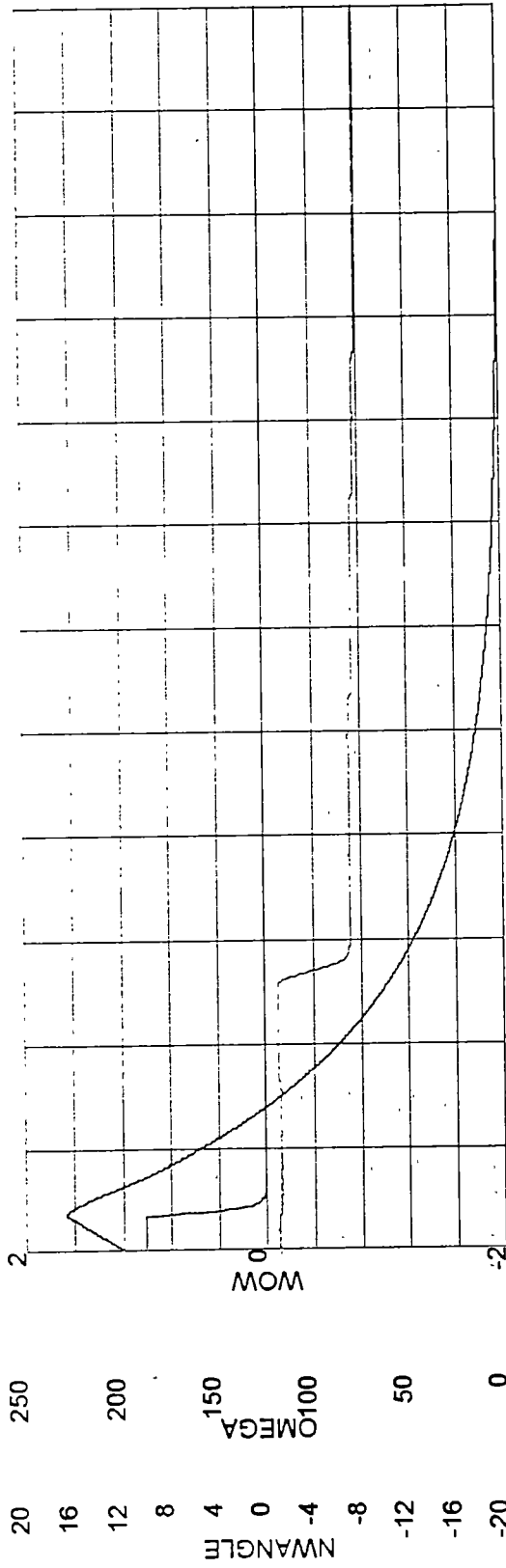
Flight 9 Event 1
page 1 of 2



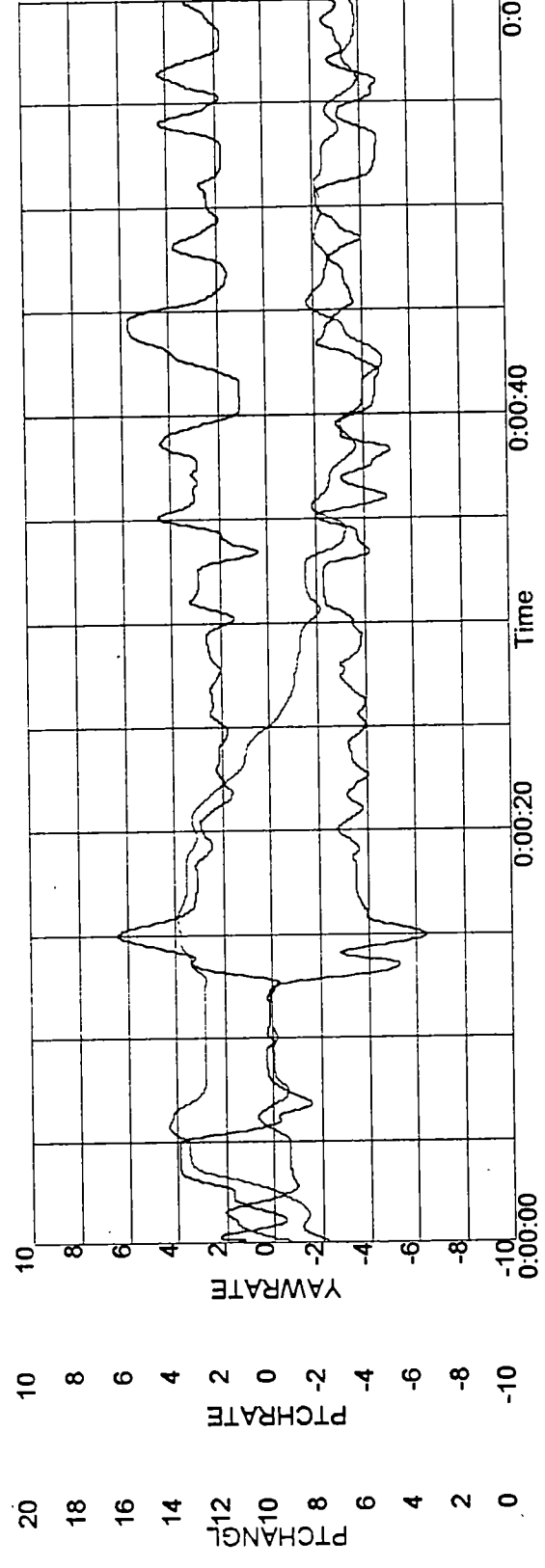
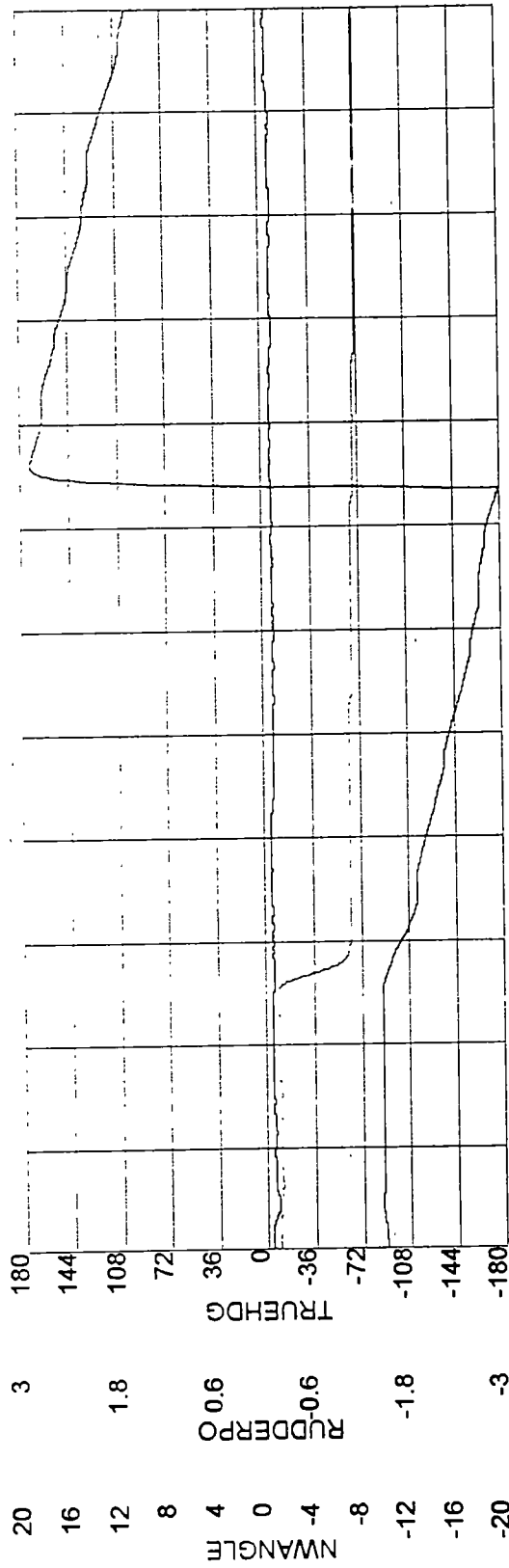
Flight 9 Event 1
page 2 of 2



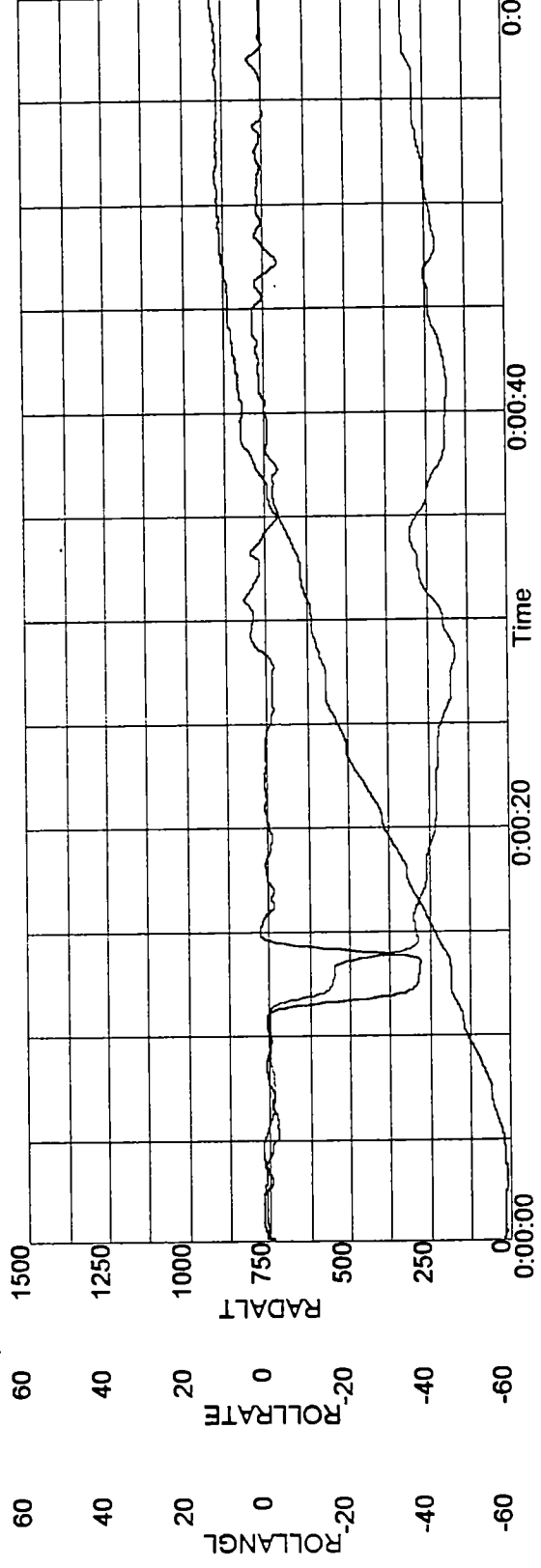
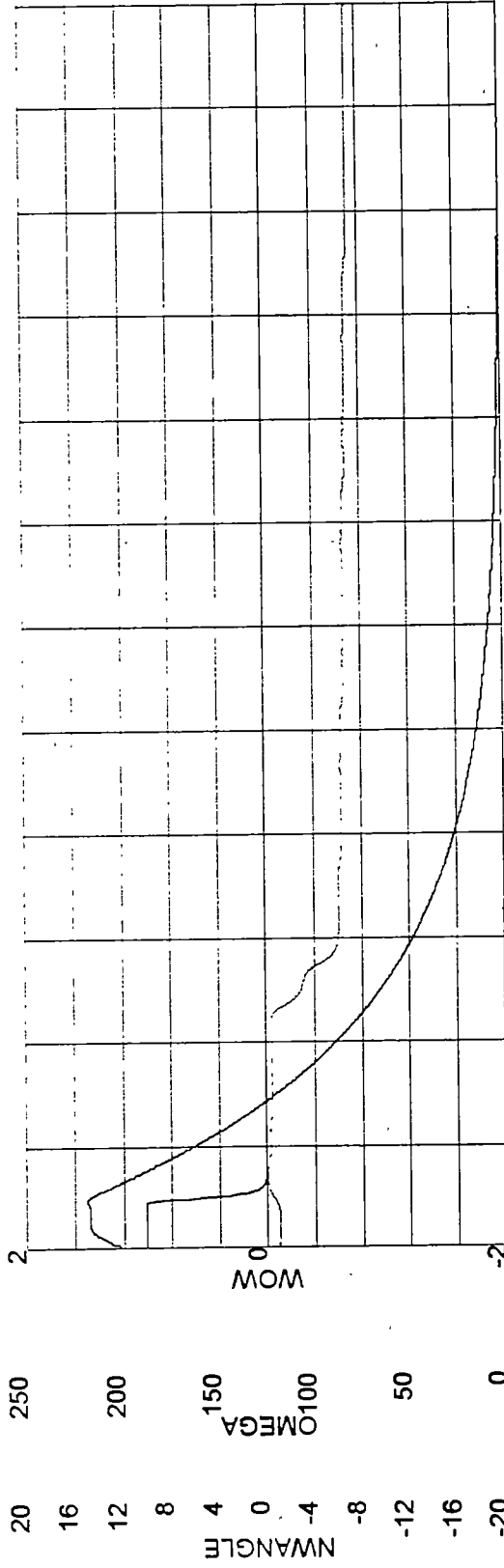
Flight 9 Event 2
page 1 of 2



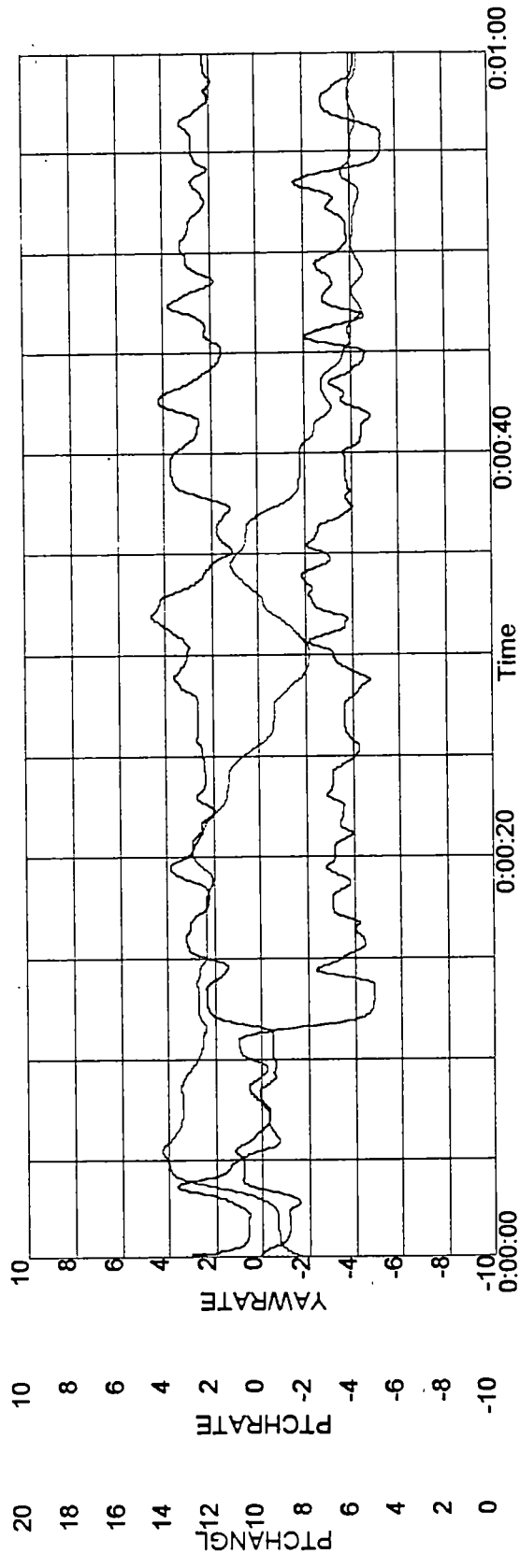
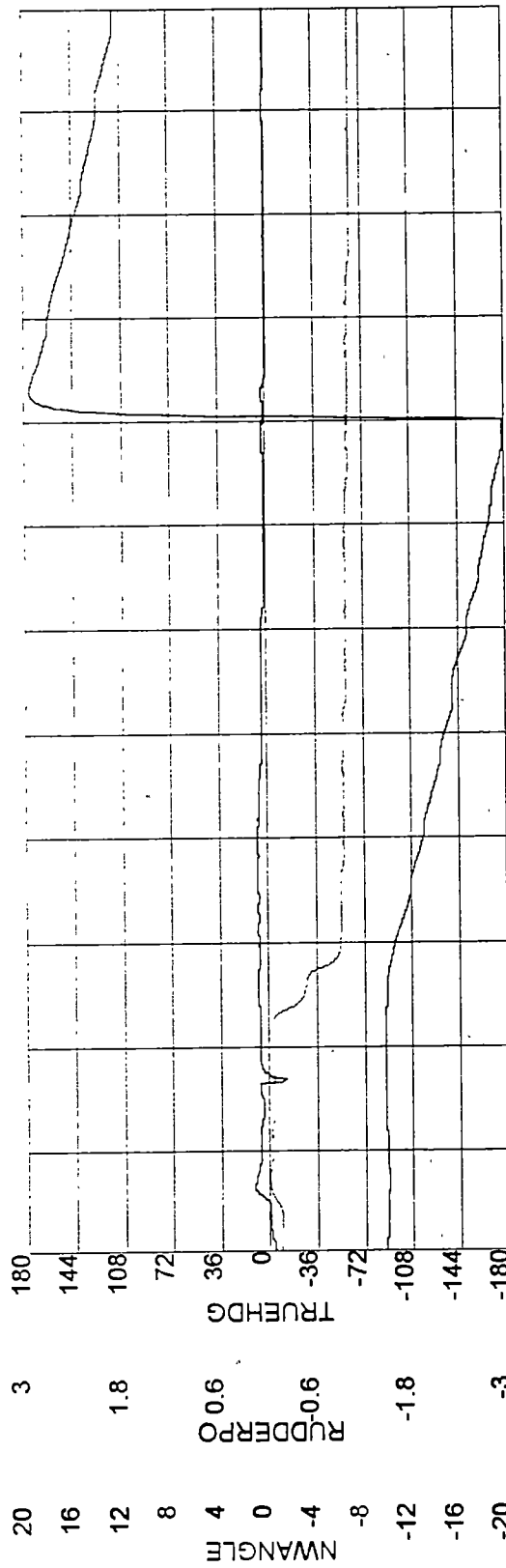
Flight 9 Event 2
page 2 of 2



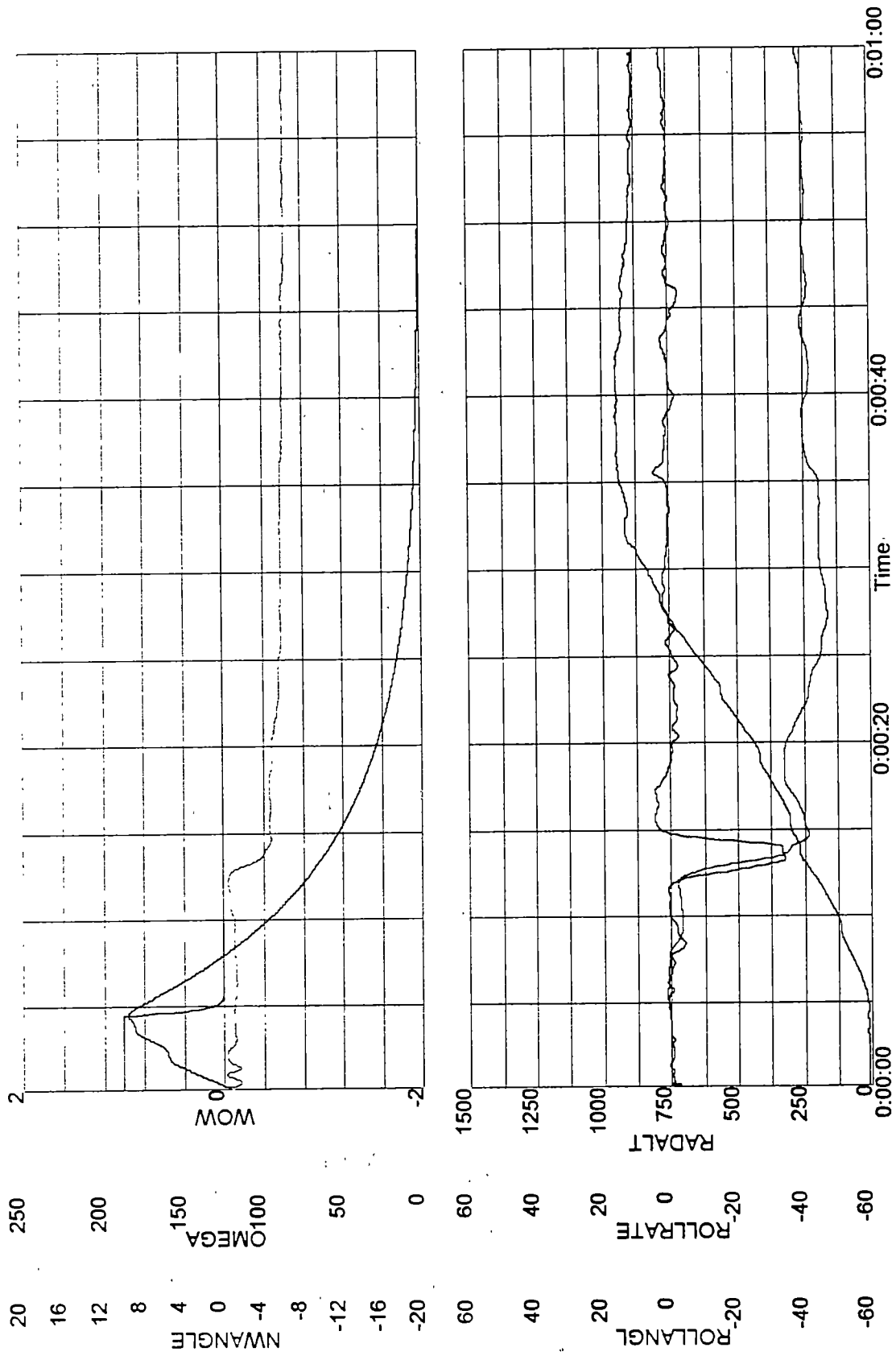
Flight 9 Event 3
page 1 of 2



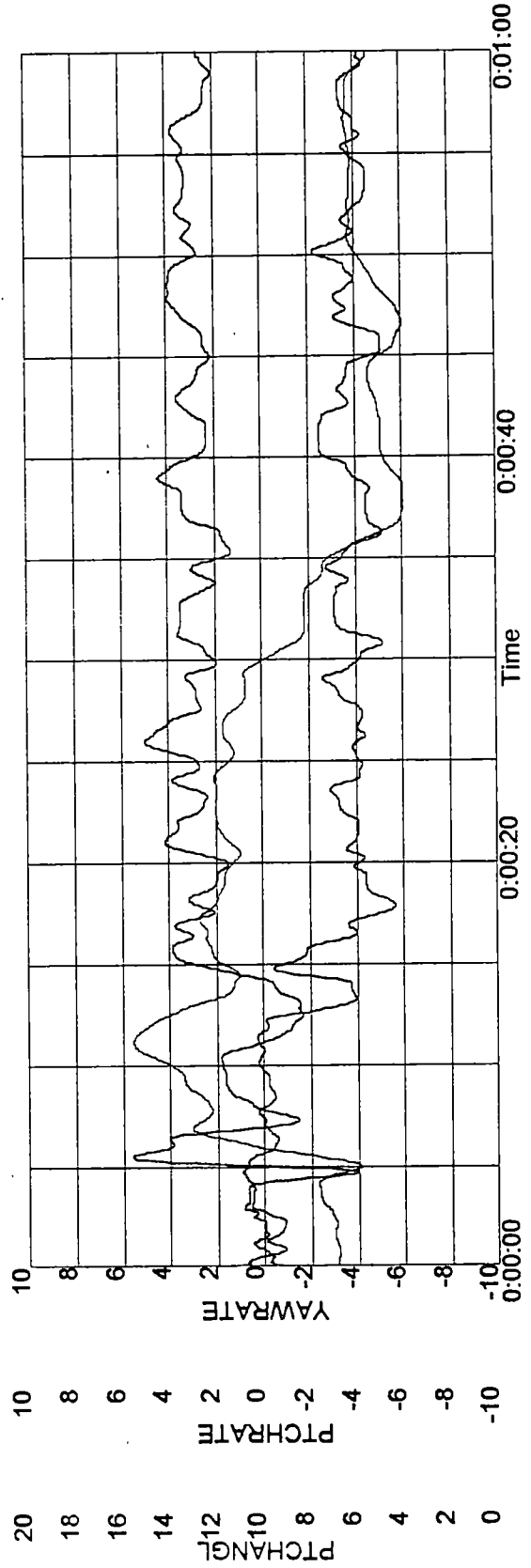
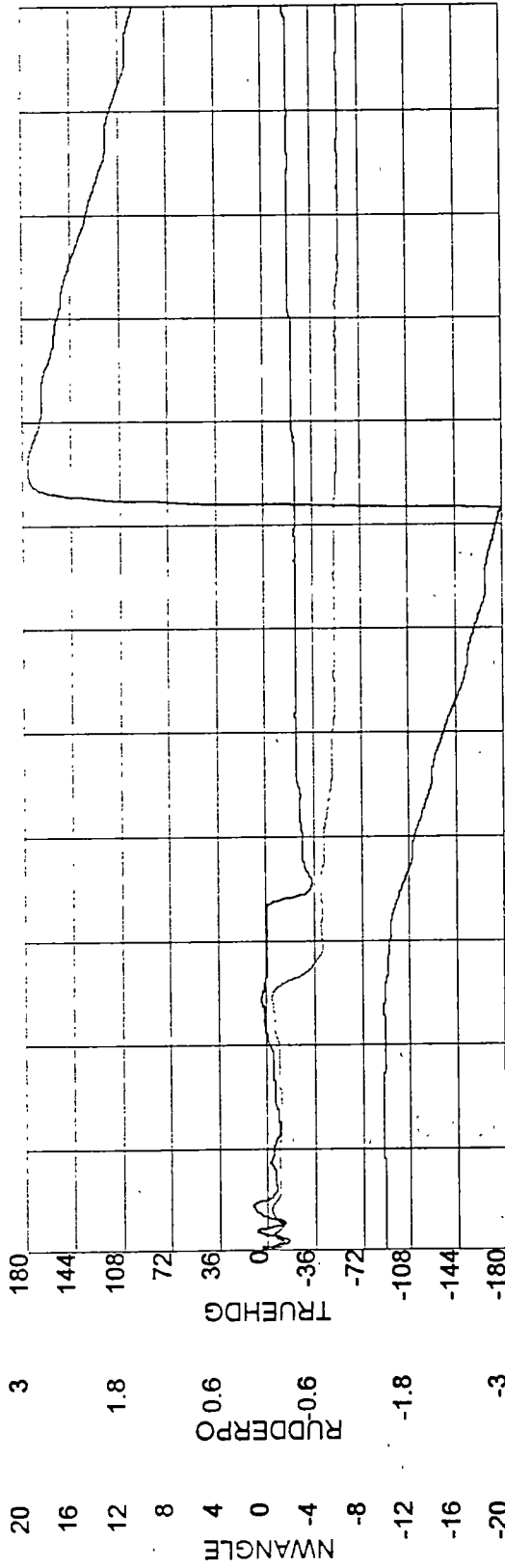
Flight 9 Event 3
page 2 of 2

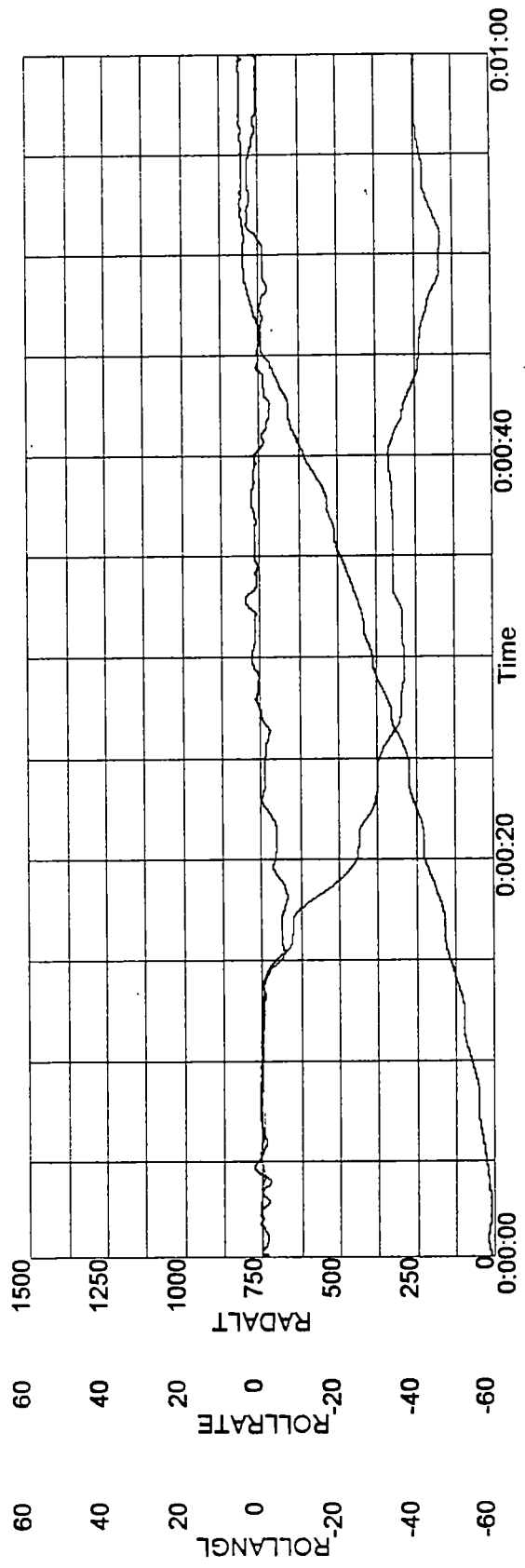
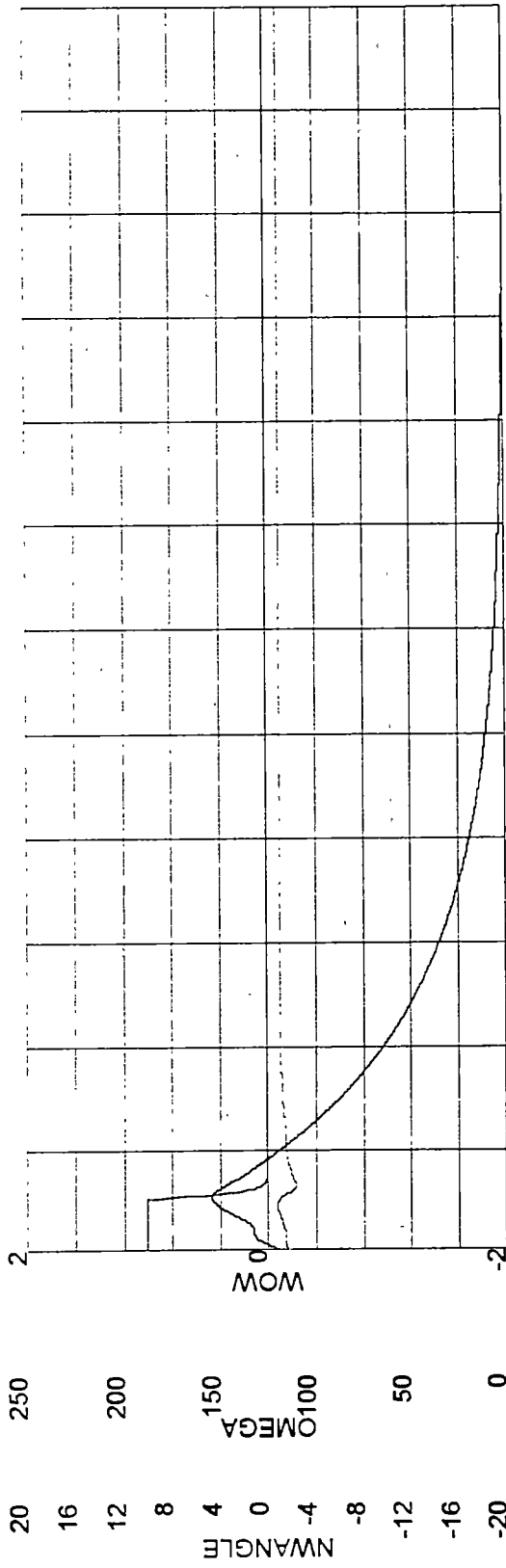


Flight 9 Event 4
page 1 of 2

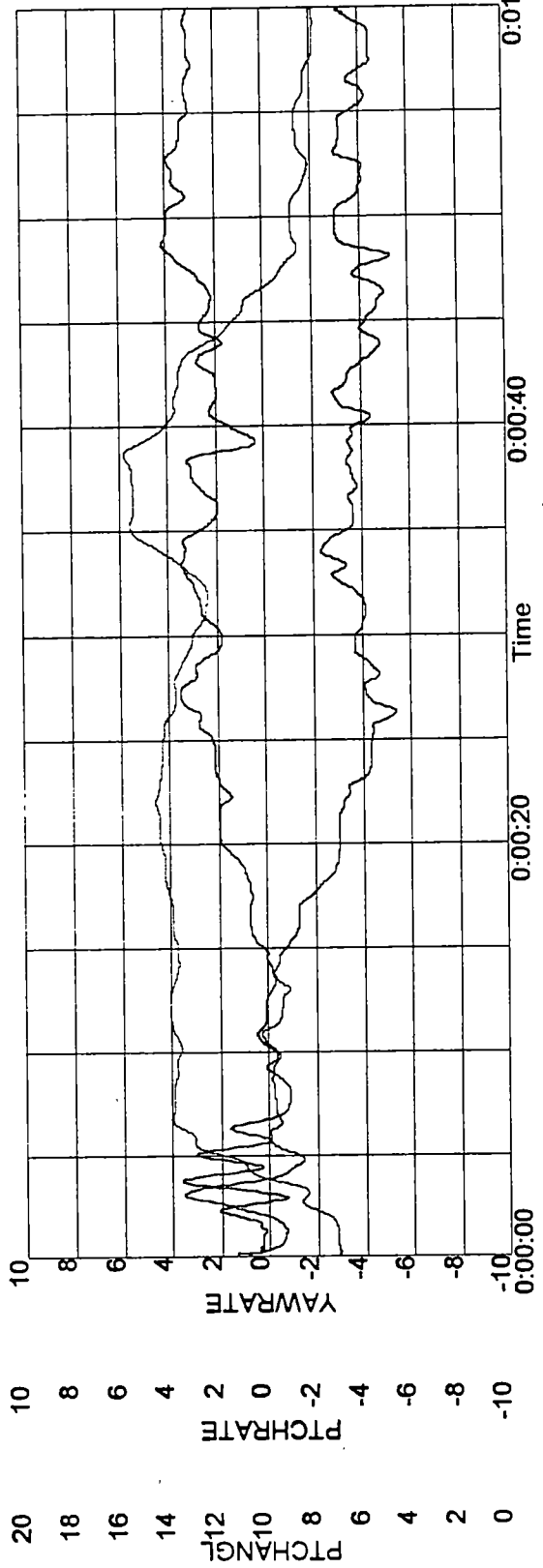
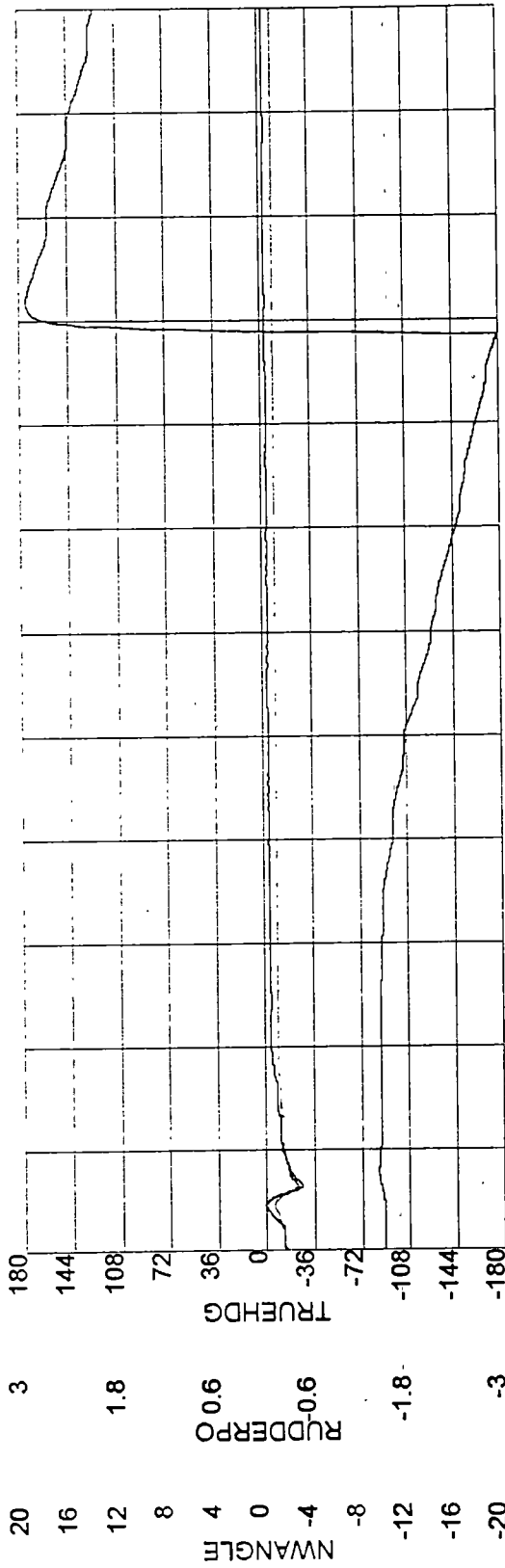


Flight 9 Event 4
page 2 of 2

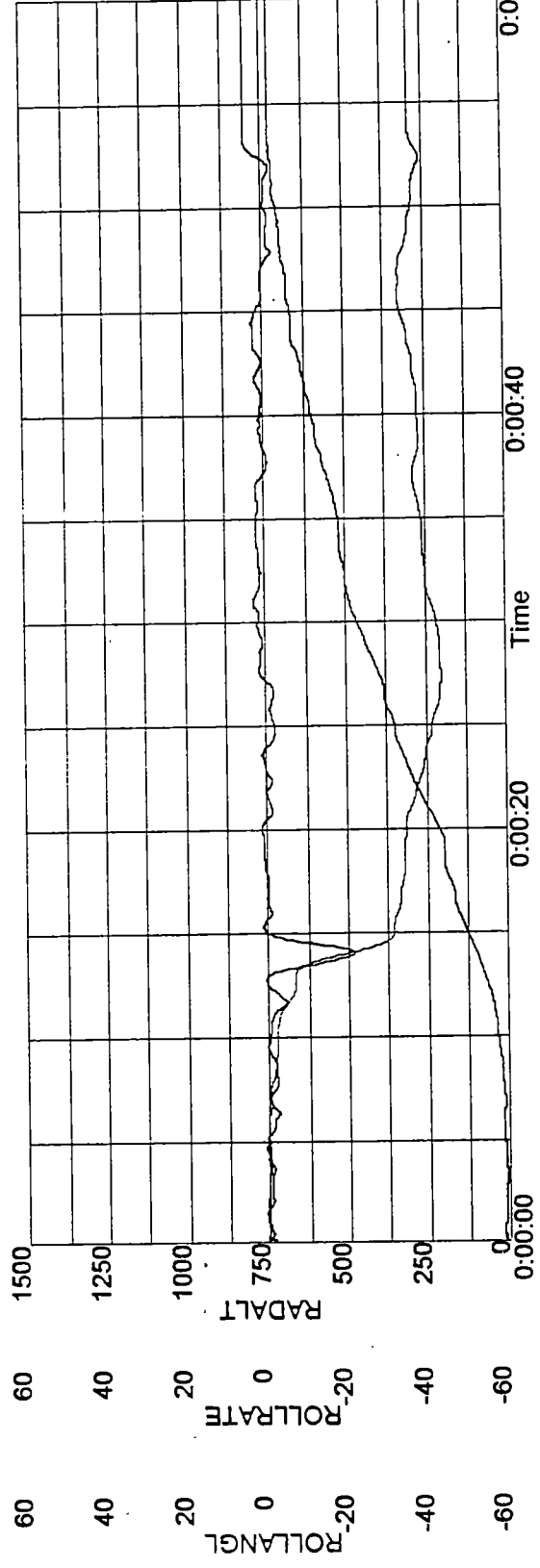
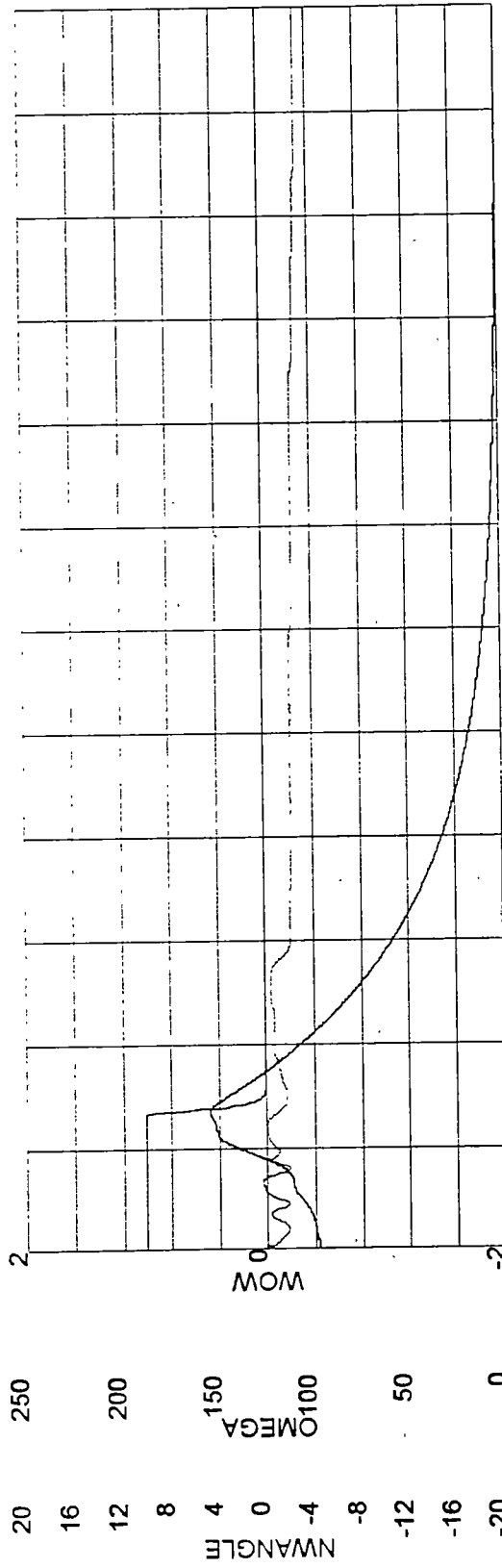




Flight 9 Event 5
page 2 of 2



Flight 9 Event 6
page 1 of 2



Flight 9 Event 6
page 2 of 2

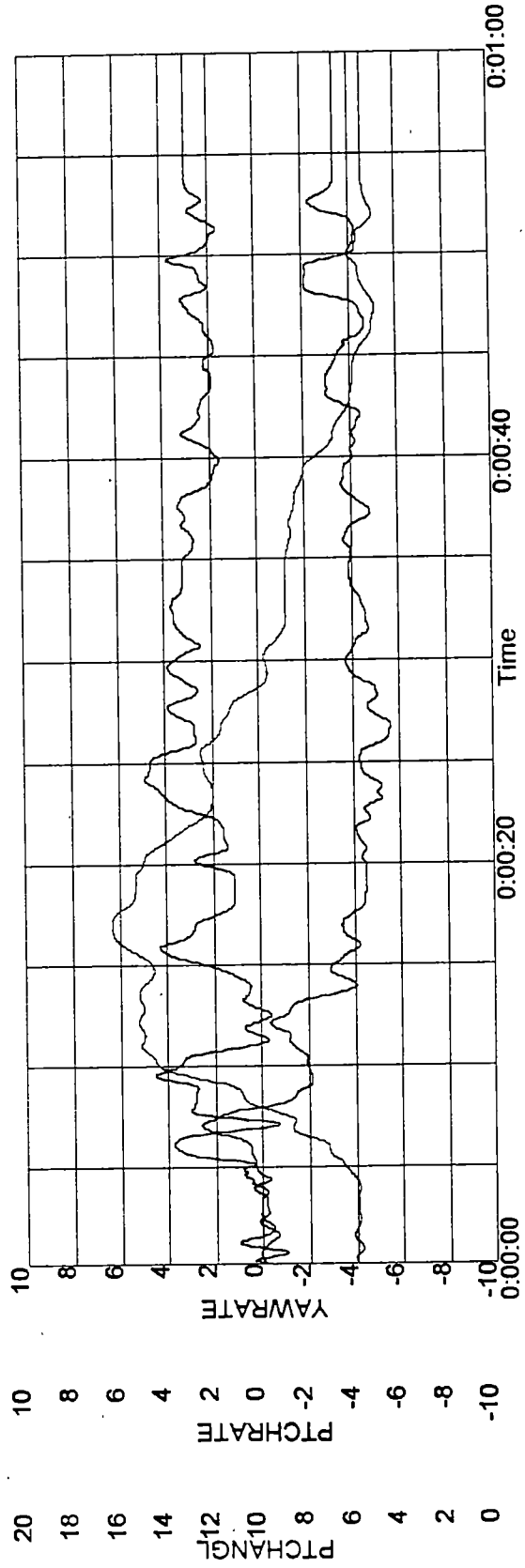
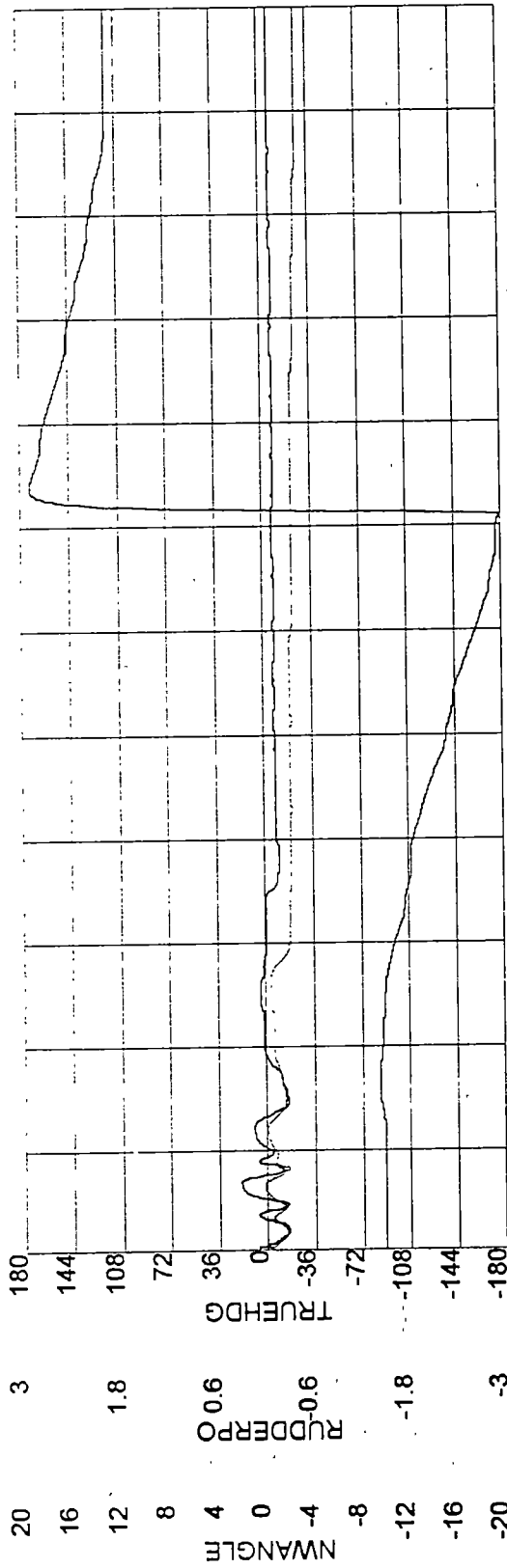


Table B-1: Tabular Computation of Nose Wheel Precession

Initial Values		Body Axes Reference		Nose Wheel Axes Reference		rad to deg conversion factor		Nose Wheel Vector					
ω_0 (rad/sec)	Ω_0 (deg)	Ω_n (deg)	E_n (deg)	Roll Rate p deg/sec	Pitch Rate q deg/sec	Yaw Rate r deg/sec	k	Roll Rate p deg/sec	Pitch Rate q deg/sec	Yaw Rate r deg/sec	ω_x deg/sec	ω_y deg/sec	ω_z deg/sec
Time t sec	NW Rot Ang Ω deg	NW Rate ω_{nw} deg/sec					57.3						
0.00	0.0	-3946		0.37	0.08	0.19		0.4	0.1	0.2	0.4	-3945.7	0.2
0.05	-195.5	-3910		0.37	0.10	0.21		-0.3	0.1	-0.3	-0.3	-3910.3	-0.3
0.10	-29.3	-3875		0.32	0.09	0.22		0.2	0.1	0.4	0.2	-3875.3	0.4
0.15	-221.3	-3841		0.27	0.09	0.24		0.0	0.1	-0.4	0.0	-3840.6	-0.3
0.20	-51.6	-3806		0.18	0.09	0.22		-0.1	0.1	0.3	-0.1	-3806.1	0.3
0.25	-240.2	-3772		0.07	0.08	0.18		0.1	0.1	-0.2	0.1	-3772.1	-0.1
0.30	-67.2	-3738		0.01	0.10	0.12		-0.1	0.1	0.1	-0.1	-3738.2	0.0
0.35	-252.4	-3705		-0.01	0.13	0.06		0.1	0.1	0.0	0.1	-3704.7	-0.1
0.40	-76.0	-3672		0.02	0.13	0.00		0.0	0.1	0.0	0.0	-3671.5	0.0
0.45	-257.9	-3639		0.10	0.12	-0.04		-0.1	0.1	-0.1	-0.1	-3638.6	-0.2
0.50	-78.2	-3606		0.21	0.09	-0.07		0.1	0.1	0.2	0.1	-3606.1	0.1
0.55	-256.9	-3574		0.28	0.03	-0.07		-0.1	0.0	-0.3	-0.1	-3573.8	-0.3
0.60	-74.0	-3542		0.17	-0.05	-0.09		0.1	0.0	0.1	0.1	-3541.9	0.1
0.65	-249.5	-3510		-0.01	-0.10	-0.12		-0.1	-0.1	0.0	-0.1	-3510.2	0.0
0.70	-63.4	-3479		-0.76	-0.17	-0.20		-0.2	-0.2	-0.8	-0.2	-3478.8	-0.8
0.75	-235.8	-3447		-1.61	-0.23	-0.29		0.7	-0.3	1.5	0.7	-3447.7	1.5
0.80	-46.7	-3417		-3.32	-0.26	-0.51		-1.9	-0.3	-2.8	-1.9	-3416.9	-2.9
0.85	-215.9	-3386		-5.02	-0.27	-0.73		3.6	-0.4	3.5	3.6	-3386.3	3.3
0.90	-23.7	-3356		-7.74	-0.18	-1.10		-6.6	-0.3	-4.1	-6.6	-3356.0	-4.6
0.95	-190.0	-3326		-10.16	-0.06	-1.46		9.7	-0.3	3.2	9.7	-3325.8	2.4
1.00	-354.8	-3296		-13.39	0.17	-1.94		-13.5	-0.1	-0.7	-13.5	-3295.9	-2.0
1.05	-158.1	-3266		-16.09	0.39	-2.34		15.8	0.0	-3.8	15.8	-3266.2	-5.6
1.10	-320.0	-3237		-19.59	0.71	-2.83		-16.8	0.2	10.4	-16.8	-3236.8	8.1
1.15	-120.4	-3208		-22.40	0.97	-3.22		14.1	0.4	-17.7	14.1	-3207.6	-20.6
1.20	-279.3	-3179		-25.63	1.30	-3.63		-7.7	0.5	24.7	-7.7	-3178.7	21.3
1.25	-76.9	-3151		-28.30	1.57	-3.95		-2.6	0.6	-28.5	-2.6	-3150.1	-32.4
1.30	-233.0	-3123		-31.32	1.87	-4.26		15.5	0.7	27.6	15.5	-3121.8	23.3
1.35	-3095	-3095		-33.67	2.11	-4.50		-27.8	0.7	-19.7	-27.8	-3093.8	-24.4
1.40	-181.1	-3067		-36.21	2.37	-4.71		36.2	0.7	5.4	36.2	-3066.1	0.4
1.45	-333.0	-3039		-38.30	2.57	-4.88		-36.4	0.6	13.1	-36.4	-3038.7	7.9
1.50	-123.6	-3012		-40.42	2.77	-5.02		26.6	0.5	-31.0	26.6	-3011.6	-36.4

Table B-1: Tabular Computation of Nose Wheel Precession

Time t sec	Nose Wheel Vector			Nose Wheel Reference Torquing Moment			Strut Axes Moment		Steering Angle			
	$d\omega_x/dt$ deg/s/s	$d\omega_y/dt$ deg/s/s	$d\omega_z/dt$ deg/s/s	M_x ft-lb/ft	M_y ft-lb/ft	M_z ft-lb/ft	M_x ft-lb/ft	M_y ft-lb/ft	E deg	E dot deg/sec	F dot deg/sec	F deg
0.00									-1.06			
0.05	-13.2	707.3	-9.4	-0.2	8.1	0.1	0.1	0.1	-1.06	0.02	0.00	-1.06
0.10	9.3	700.6	13.2	0.2	8.1	0.0	0.0	0.1	-1.06	0.03	0.00	-1.06
0.15	-4.4	694.4	-14.5	-0.2	8.0	-0.1	-0.1	0.1	-1.06	0.01	0.00	-1.06
0.20	-0.2	688.1	12.5	0.1	7.9	0.1	0.1	0.0	-1.06	0.00	0.00	-1.06
0.25	3.6	681.9	-8.5	0.0	7.9	-0.1	-0.1	0.0	-1.06	0.01	0.00	-1.06
0.30	-4.5	676.3	3.4	0.0	7.8	0.1	0.1	0.0	-1.06	0.00	0.00	-1.06
0.35	3.3	670.6	-1.7	0.0	7.7	0.0	0.0	0.0	-1.07	-0.06	0.00	-1.06
0.40	-1.0	663.8	1.0	0.0	7.6	0.0	0.0	0.0	-1.07	-0.03	0.00	-1.06
0.45	-1.3	657.7	-2.8	-0.1	7.6	0.0	0.0	0.1	-1.07	-0.06	0.00	-1.06
0.50	3.4	651.5	5.3	0.1	7.5	0.0	0.0	0.1	-1.07	-0.08	0.00	-1.06
0.55	-4.9	645.1	-8.2	-0.1	7.4	0.0	0.0	0.1	-1.08	-0.04	0.00	-1.06
0.60	5.4	638.8	8.2	0.1	7.4	0.0	0.0	0.1	-1.08	-0.02	0.00	-1.06
0.65	-4.9	633.6	-2.5	0.0	7.3	0.0	0.0	0.0	-1.08	-0.06	0.00	-1.06
0.70	-1.1	627.3	-15.0	-0.3	7.2	0.0	0.0	-0.2	-1.08	0.01	0.00	-1.06
0.75	16.5	621.8	44.7	0.6	7.2	0.0	0.0	-0.5	-1.08	-0.02	0.00	-1.06
0.80	-51.3	616.5	-86.7	-1.3	7.1	0.2	0.2	-1.0	-1.08	-0.10	0.00	-1.06
0.85	110.6	611.3	122.9	1.8	7.0	-0.5	-0.5	-1.5	-1.10	-0.25	0.00	-1.06
0.90	-205.3	607.4	-157.4	-2.7	7.0	1.3	1.3	-2.3	-1.12	-0.46	-1.62	-1.15
0.95	327.7	602.6	139.2	2.7	6.9	-2.5	-2.5	-2.9	-1.16	-0.83	-2.02	-1.25
1.00	-465.3	598.9	-87.5	-3.3	6.9	4.0	4.0	-3.7	-1.23	-1.29	-2.56	-1.37
1.05	586.5	593.4	-72.5	1.5	6.8	-5.6	-5.6	-4.6	-1.32	-1.80	-3.24	-1.54
1.10	-652.7	589.3	275.3	-1.1	6.8	7.1	7.1	-4.7	-1.43	-2.31	-3.28	-1.70
1.15	618.7	582.7	-574.8	-3.1	6.7	-7.9	-7.9	-6.6	-1.58	-2.89	-4.64	-1.93
1.20	-436.9	578.1	837.2	4.3	6.7	7.3	7.3	-5.4	-1.75	-3.48	-3.78	-2.12
1.25	102.8	571.4	-1073.1	-9.7	6.6	-5.4	-5.4	-8.2	-1.95	-3.91	-5.74	-2.41
1.30	361.6	566.2	1113.8	9.4	6.5	1.6	1.6	-6.6	-2.16	-4.33	-4.59	-2.64
1.35	-865.1	559.7	-954.0	-12.6	6.4	3.1	3.1	-8.6	-2.40	-4.74	-6.04	-2.94
1.40	1279.3	554.4	495.2	7.5	6.4	-8.3	-8.3	-8.4	-2.65	-5.02	-5.91	-3.24
1.45	-1452.2	548.2	150.2	-6.0	6.3	12.0	12.0	-8.0	-2.91	-5.21	-5.59	-3.51
1.50	1260.6	542.5	-885.2	-3.8	6.2	-13.2	-13.2	-10.4	-3.18	-5.44	-7.29	-3.88

Table B-1: Tabular Computation of Nose Wheel Precession

Time t sec	Body Axes Reference				Nose Wheel Axes Reference				Nose Wheel Vector			
	NW Rate ω_{nw} deg/sec	NW Rot Ang Ω deg	Roll Rate p deg/sec	Pitch Rate q deg/sec	Yaw Rate r deg/sec	Roll Rate p deg/sec	Pitch Rate q deg/sec	Yaw Rate r deg/sec	ω_x deg/sec	ω_y deg/sec	ω_z deg/sec	
1.55	-2985	-272.9	-42.07	2.92	-5.12	-7.2	0.4	41.9	-7.2	-2984.8	36.3	
1.60	-2958	-60.8	-43.49	3.06	-5.20	-16.7	0.2	-40.6	-16.7	-2958.2	-46.2	
1.65	-2932	-207.4	-44.51	3.17	-5.27	37.2	0.0	25.2	37.2	-2931.8	19.6	
1.70	-2906	-352.7	-44.93	3.25	-5.28	-45.4	-0.1	0.5	-45.4	-2905.7	-5.2	
1.75	-2880	-136.7	-45.04	3.33	-5.29	36.5	-0.3	-27.2	36.5	-2879.9	-32.7	
1.80	-2854	-279.3	-43.73	3.37	-5.20	-12.3	-0.3	42.4	-12.3	-2854.1	37.0	
1.85	-2828	-60.8	-42.23	3.39	-5.09	-16.3	-0.4	-39.4	-16.3	-2828.6	-44.7	
1.90	-2803	-200.9	-39.01	3.34	-4.82	34.9	-0.3	18.5	34.9	-2803.2	13.5	
1.95	-2778	-339.8	-34.96	3.28	-4.49	-34.5	-0.1	7.9	-34.5	-2777.9	3.4	
2.00	-2753	-117.4	-30.45	3.21	-4.12	17.8	0.1	-25.3	17.8	-2752.7	-29.4	
2.05	-2728	-253.8	-25.90	3.19	-3.77	3.6	0.5	26.1	3.6	-2727.7	22.4	
2.10	-2704	-29.0	-21.04	3.17	-3.39	-16.9	0.9	-13.3	-16.9	-2702.9	-16.5	
2.15	-2680	-163.0	-16.86	3.27	-3.15	17.3	1.4	-2.0	17.3	-2678.1	-4.8	
2.20	-2656	-295.8	-13.45	3.38	-2.98	-8.7	1.9	11.1	-8.7	-2653.7	8.6	
2.25	-2632	-67.4	-9.92	3.58	-2.88	-1.3	2.4	-10.6	-1.3	-2629.3	-12.8	
2.30	-2608	-197.8	-7.27	3.74	-2.84	6.4	2.9	5.0	6.4	-2605.3	3.2	
2.35	-2585	-327.0	-4.90	3.97	-2.96	-6.1	3.4	0.4	-6.1	-2581.4	-1.2	
2.40	-2562	-95.1	-3.18	4.15	-3.11	3.4	3.8	-3.4	3.4	-2557.9	-4.7	
2.45	-2539	-222.0	-1.75	4.38	-3.38	-0.6	4.1	4.0	-0.6	-2534.5	2.9	
2.50	-2516	-347.8	-0.73	4.55	-3.64	-2.0	4.4	-3.3	-2.0	-2511.5	-4.2	
2.55	-2493	-112.5	-0.03	4.79	-4.03	4.0	4.7	1.0	4.0	-2488.6	0.2	
2.60	-2471	-236.0	0.56	4.98	-4.33	-3.6	5.0	2.5	-3.6	-2466.0	1.8	
2.65	-2449	-358.5	0.97	5.19	-4.65	0.2	5.3	-4.7	0.2	-2443.6	-5.3	
2.70	-2427	-119.8	1.31	5.37	-4.91	3.9	5.5	3.0	3.9	-2421.5	2.4	
2.75	-2405	-240.1	1.51	5.55	-5.20	-4.9	5.7	1.9	-4.9	-2399.5	1.4	
2.80	-2384	-359.3	1.69	5.66	-5.41	0.9	5.8	-5.4	0.9	-2377.8	-5.8	
2.85	-2362	-117.4	1.89	5.82	-5.65	4.5	6.0	3.6	4.5	-2356.3	3.3	
2.90	-2341	-234.5	2.00	5.97	-5.87	-5.5	6.2	2.4	-5.5	-2335.0	2.2	
2.95	-2320	-350.5	2.09	6.10	-6.09	0.3	6.3	-6.2	0.3	-2313.9	-6.4	
3.00	-2299	-105.4	2.17	6.22	-6.24	5.6	6.4	3.0	5.6	-2292.9	2.9	
3.05	-2279	-219.4	2.25	6.33	-6.37	-5.2	6.6	4.0	-5.2	-2272.2	3.9	
3.10	-2258	-332.3	2.19	6.35	-6.41	-1.8	6.6	-6.3	-1.8	-2251.8	-6.4	
3.15	-2238	-84.2	2.15	6.36	-6.41	6.5	6.6	0.7	6.5	-2231.6	0.6	
3.20	-2218	-195.1	2.06	6.34	-6.35	-2.9	6.5	5.8	-2.9	-2211.5	5.7	
3.25	-2198	-305.0	1.96	6.32	-6.30	-4.5	6.5	-4.6	-4.5	-2191.7	-4.6	
3.30	-2179	-53.9	1.83	6.26	-6.19	5.6	6.4	-2.8	5.6	-2172.1	-2.8	
3.35	-2159	-161.9	1.74	6.21	-6.09	1.0	6.4	6.1	1.0	-2152.6	6.0	
3.40	-2140	-268.9	1.69	6.13	-5.94	-6.0	6.3	-0.8	-6.0	-2133.4	-0.8	
3.45	-2120	-14.9	1.68	6.06	-5.81	2.4	6.2	-5.4	2.4	-2114.3	-5.4	
3.50	-2101	-120.0	1.75	5.90	-5.62	4.4	6.1	3.7	4.4	-2095.4	3.6	

Table B-1: Tabular Computation of Nose Wheel Precession

Time t sec	Nose Wheel Vector			Nose Wheel Reference Torquing Moment			Strut Axes Moment		Fit Test Data		Steering Angle		Computed	
	$d\omega_x/dt$ deg/s/s	$d\omega_y/dt$ deg/s/s	$d\omega_z/dt$ deg/s/s	M_x ft-lb	M_y ft-lb	M_z ft-lb	M_x ft-lb	M_y ft-lb	E deg	F deg	E dot deg/sec	F dot deg/sec	F deg	F deg
1.55	-676.8	536.8	1453.8	7.0	6.2	10.5	10.5	-7.5	-3.46	-5.57	-5.26	-4.14	-4.52	
1.60	-190.0	531.8	-1650.7	-14.8	6.1	-4.5	-4.5	-10.7	-3.74	-5.65	-7.52	-4.52	-4.52	
1.65	1078.5	526.5	1316.2	12.0	6.1	-3.4	-3.4	-8.5	-4.03	-5.64	-5.96	-5.13	-5.13	
1.70	-1651.0	522.0	-494.5	-11.0	6.0	10.4	10.4	-8.9	-4.31	-5.66	-6.24	-5.13	-5.13	
1.75	1636.6	517.6	-551.1	0.0	6.0	-13.7	-13.7	-10.0	-4.59	-5.56	-7.01	-5.48	-5.48	
1.80	-974.5	514.8	1394.4	5.0	5.9	11.5	11.5	-6.8	-4.86	-5.43	-4.77	-5.72	-5.72	
1.85	-80.2	510.5	-1633.1	-13.2	5.9	-4.8	-4.8	-9.1	-5.12	-5.20	-6.04	-6.04	-6.04	
1.90	1022.4	508.2	1163.1	9.7	5.9	-3.1	-3.1	-6.4	-5.37	-4.97	-4.46	-6.26	-6.26	
1.95	-1387.2	505.8	-202.8	-7.1	5.8	8.5	8.5	-5.5	-5.59	-4.56	-3.85	-6.45	-6.45	
2.00	1045.2	502.9	654.8	-2.1	5.8	-8.7	-8.7	-5.9	-5.80	-4.10	-4.11	-6.66	-6.66	
2.05	-282.4	500.5	1036.5	4.5	5.8	5.0	5.0	-3.0	-5.98	-3.67	-2.08	-6.76	-6.76	
2.10	-411.7	497.4	-779.1	-6.9	5.7	0.1	0.1	-3.4	-6.14	-3.23	-2.40	-6.88	-6.88	
2.15	684.5	494.5	234.0	2.6	5.7	-3.3	-3.3	-2.4	-6.29	-2.82	-1.67	-6.97	-6.97	
2.20	-519.1	489.3	269.2	-0.7	5.6	3.9	3.9	-1.1	-6.41	-2.43	0.00	-6.97	-6.97	
2.25	147.5	487.2	-428.2	-2.5	5.6	-2.1	-2.1	-1.5	-6.52	-2.19	0.00	-6.97	-6.97	
2.30	154.2	480.6	318.3	1.7	5.5	0.2	0.2	-0.4	-6.61	-1.88	0.00	-6.97	-6.97	
2.35	-250.1	477.2	-87.0	-1.8	5.5	1.1	1.1	0.0	-6.69	-1.61	0.00	-6.97	-6.97	
2.40	190.1	470.8	-69.6	-0.1	5.4	-1.3	-1.3	-0.2	-6.76	-1.32	0.00	-6.97	-6.97	
2.45	-80.0	466.8	150.8	0.3	5.4	1.0	1.0	0.6	-6.82	-1.16	0.00	-6.97	-6.97	
2.50	-28.6	460.8	-141.5	-1.2	5.3	-0.3	-0.3	0.6	-6.86	-0.92	0.00	-6.97	-6.97	
2.55	119.4	457.2	88.0	0.7	5.3	-0.5	-0.5	0.6	-6.90	-0.79	0.00	-6.97	-6.97	
2.60	-150.5	452.1	-141.8	-0.4	5.2	1.1	1.1	1.0	-6.94	-0.68	0.00	-6.97	-6.97	
2.65	75.5	447.9	154.9	-0.9	5.2	-0.9	-0.9	0.9	-7.00	-0.58	0.00	-6.97	-6.97	
2.70	74.6	443.2	-177.2	1.0	5.1	-0.1	-0.1	0.9	-7.00	-0.52	0.00	-6.97	-6.97	
2.75	-177.2	438.9	-21.2	-0.7	5.1	1.1	1.1	1.1	-7.02	-0.52	0.00	-6.97	-6.97	
2.80	116.7	433.8	-144.0	-0.7	5.0	-1.0	-1.0	1.1	-7.04	-0.42	0.00	-6.97	-6.97	
2.85	71.2	430.8	182.4	1.2	5.0	0.0	0.0	1.0	-7.06	-0.34	0.00	-6.97	-6.97	
2.90	-199.8	426.5	-22.6	-0.6	4.9	1.2	1.2	1.2	-7.07	-0.24	0.00	-6.97	-6.97	
2.95	115.9	422.5	-171.0	-0.8	4.9	-1.1	-1.1	1.2	-7.08	-0.17	0.00	-6.97	-6.97	
3.00	107.1	418.2	185.2	1.3	4.8	-0.2	-0.2	1.2	-7.09	-0.13	0.00	-6.97	-6.97	
3.05	-216.2	414.4	-20.7	-0.4	4.8	1.3	1.3	1.2	-7.09	-0.11	0.00	-6.97	-6.97	
3.10	68.1	408.7	-206.0	-1.1	4.7	-0.8	-0.8	1.2	-7.10	-0.08	0.00	-6.97	-6.97	
3.15	165.5	404.8	140.5	1.1	4.7	-0.7	-0.7	1.2	-7.10	-0.07	0.00	-6.97	-6.97	
3.20	-187.8	400.4	102.3	0.2	4.6	1.2	1.2	1.1	-7.10	-0.06	0.00	-6.97	-6.97	
3.25	-32.4	396.8	-207.2	-1.2	4.6	-0.2	-0.2	1.1	-7.11	-0.05	0.00	-6.97	-6.97	
3.30	202.1	392.4	35.5	0.5	4.5	-1.0	-1.0	1.0	-7.11	-0.04	0.00	-6.97	-6.97	
3.35	-92.5	389.2	177.9	0.8	4.5	0.8	0.8	1.0	-7.11	-0.04	0.00	-6.97	-6.97	
3.40	-138.8	385.1	-137.8	-1.0	4.4	0.5	0.5	1.0	-7.11	-0.04	0.00	-6.97	-6.97	
3.45	166.6	381.9	-91.6	-0.2	4.4	-1.0	-1.0	0.9	-7.12	-0.04	0.00	-6.97	-6.97	
3.50	99.7	377.0	181.3	1.0	4.3	0.1	0.1	0.9	-7.12	-0.03	0.00	-6.97	-6.97	

Table B-1: Tabular Computation of Nose Wheel Precession

Time t	Body Axes Reference				Nose Wheel Axes Reference				Nose Wheel Vector			
	NW Rate ω_{nw} deg/sec	NW Rot Ang Ω deg	Roll Rate p deg/sec	Pitch Rate q deg/sec	Yaw Rate r deg/sec	Roll Rate p deg/sec	Pitch Rate q deg/sec	Yaw Rate r deg/sec	ω_x deg/sec	ω_y deg/sec	ω_z deg/sec	
3.55	-2083	-224.1	1.85	5.76	-5.45	-4.6	5.9	3.1	-4.6	-2076.7	3.0	
3.60	-2064	-327.3	2.06	5.56	-5.20	-1.7	5.8	-5.1	-1.7	-2058.2	-5.2	
3.65	-2045	-69.6	2.25	5.38	-4.99	5.2	5.6	-0.3	5.2	-2039.9	-0.4	
3.70	-2027	-170.9	2.45	5.12	-4.74	-1.0	5.4	5.0	-1.0	-2021.8	4.9	
3.75	-2009	-271.4	2.60	4.93	-4.54	-4.5	5.2	-2.1	-4.5	-2003.8	-2.2	
3.80	-1991	-10.9	2.72	4.72	-4.33	2.9	5.0	-3.9	2.9	-1986.0	-3.9	
3.85	-1973	-109.6	2.77	4.54	-4.19	3.2	4.9	3.5	3.2	-1968.3	3.4	
3.90	-1955	-207.4	2.75	4.36	-4.08	-3.8	4.7	2.6	-3.8	-1950.8	2.5	
3.95	-1938	-304.3	2.73	4.23	-4.01	-2.1	4.5	-4.1	-2.1	-1933.4	-4.1	
4.00	-1921	-40.3	2.72	4.09	-3.98	4.2	4.4	-1.6	4.2	-1916.2	-1.7	
4.05	-1903	-135.5	2.73	3.96	-3.97	1.2	4.3	4.4	1.2	-1899.1	4.4	
4.10	-1886	-229.8	2.62	3.83	-3.99	-4.4	4.1	1.0	-4.4	-1882.2	1.0	
4.15	-1869	-323.3	2.55	3.72	-4.00	-0.7	4.0	-4.4	-0.7	-1865.4	-4.4	
4.20	-1853	-55.9	2.47	3.63	-3.99	4.4	3.9	-0.6	4.4	-1848.8	-0.6	
4.25	-1836	-147.7	2.35	3.57	-3.98	0.5	3.8	4.4	0.5	-1832.3	4.4	
4.30	-1820	-238.7	2.24	3.50	-3.96	-4.3	3.8	0.3	-4.3	-1815.9	0.5	
4.35	-1803	-328.8	2.23	3.43	-3.93	-0.5	3.7	-4.3	-0.5	-1799.7	-4.3	
4.40	-1787	-58.2	2.24	3.37	-3.88	4.3	3.6	-0.5	4.3	-1783.6	-0.6	
4.45	-1771	-146.8	2.26	3.29	-3.86	0.6	3.6	4.2	0.6	-1767.6	4.3	
4.50	-1755	-234.5	2.32	3.24	-3.84	-4.2	3.5	0.7	-4.2	-1751.8	0.7	
4.55	-1740	-321.5	2.38	3.21	-3.83	-0.9	3.5	-4.2	-0.9	-1736.1	-4.2	
4.60	-1724	-47.7	2.45	3.20	-3.80	4.2	3.5	-1.1	4.2	-1720.5	-1.0	
4.65	-1709	-133.1	2.50	3.19	-3.77	1.3	3.5	4.1	1.3	-1705.1	4.1	
4.70	-1693	-217.8	2.65	3.19	-3.75	-4.1	3.5	1.6	-4.1	-1689.7	1.6	
4.75	-1678	-301.7	2.77	3.18	-3.72	-1.9	3.5	-4.0	-1.9	-1674.6	-4.0	
4.80	-1663	-24.8	2.83	3.17	-3.68	3.7	3.5	-2.3	3.7	-1659.5	-2.3	
4.85	-1648	-107.3	2.90	3.16	-3.66	2.8	3.5	3.5	2.8	-1644.6	3.5	
4.90	-1633	-188.9	2.97	3.14	-3.64	-3.1	3.5	3.2	-3.1	-1629.9	3.2	
4.95	-1619	-269.9	2.95	3.13	-3.61	-3.6	3.5	-2.5	-3.6	-1615.3	-2.5	
5.00	-1604	-350.1	2.92	3.12	-3.58	1.8	3.5	-4.0	1.8	-1600.8	-3.9	
5.05	-1590	-69.6	2.93	3.12	-3.57	4.2	3.5	1.1	4.2	-1586.4	1.2	
5.10	-1576	-148.3	2.94	3.11	-3.56	-0.3	3.5	4.4	-0.3	-1572.2	4.4	
5.15	-1561	-226.4	2.95	3.11	-3.55	4.3	3.5	0.6	4.3	-1558.0	0.6	
5.20	-1548	-303.8	2.94	3.10	-3.54	-1.5	3.4	-4.1	-1.5	-1544.1	-4.1	
5.25	-1534	-20.5	2.94	3.10	-3.53	3.6	3.4	-2.4	3.6	-1530.2	-2.5	
5.30	-1520	-96.5	2.95	3.10	-3.52	3.2	3.4	2.9	3.2	-1516.5	2.8	
5.35	-1506	-171.8	2.95	3.10	-3.52	-2.0	3.4	3.8	-2.0	-1502.8	3.8	
5.40	-1493	-246.4	2.95	3.10	-3.52	4.2	3.4	-0.9	4.2	-1489.3	-1.0	
5.45	-1479	-320.4	2.95	3.10	-3.51	-0.3	3.4	-4.3	-0.3	-1476.0	-4.3	
5.50	-1466	-33.7	2.95	3.09	-3.51	4.1	3.4	-1.5	4.1	-1462.7	-1.4	

Table B-1: Tabular Computation of Nose Wheel Precession

Time t	Nose Wheel Vector			Nose Wheel Reference Torquing Moment			Strut Axes Moment		Fit Test Data			Steering Angle			Computed	
	$d\omega_x/dt$ deg/s/s	$d\omega_y/dt$ deg/s/s	$d\omega_z/dt$ deg/s/s	M_x ft-lb	M_y ft-lb	M_z ft-lb	M_x ft-lb	M_y ft-lb	E deg	$E \cdot \dot{}$ deg/sec	$F \cdot \dot{}$ deg/sec	F deg	$F \cdot \dot{}$ deg/sec	F deg	$F \cdot \dot{}$ deg/sec	F deg
3.55	-179.2	373.9	-12.1	-0.4	4.3	0.9	0.9	-7.12	-0.09	0.00	-6.97	0.00	-6.97			
3.60	58.5	369.8	-165.1	-0.7	4.3	-0.6	0.9	-7.13	-0.10	0.00	-6.97	0.00	-6.97			
3.65	137.8	366.7	96.8	0.7	4.2	-0.5	0.9	-7.13	-0.10	0.00	-6.97	0.00	-6.97			
3.70	-124.9	362.0	104.7	0.3	4.2	0.8	0.8	-7.14	-0.10	0.00	-6.97	0.00	-6.97			
3.75	-69.4	359.8	-141.0	-0.8	4.1	0.1	0.8	-7.14	-0.11	0.00	-6.97	0.00	-6.97			
3.80	147.8	356.1	-35.0	0.1	4.1	-0.8	0.8	-7.15	-0.08	0.00	-6.97	0.00	-6.97			
3.85	6.3	353.4	146.6	0.7	4.1	0.2	0.7	-7.15	-0.06	0.00	-6.97	0.00	-6.97			
3.90	-140.6	349.9	-17.1	-0.3	4.0	0.6	0.7	-7.15	-0.08	0.00	-6.97	0.00	-6.97			
3.95	34.5	347.9	-133.6	-0.6	4.0	-0.4	0.7	-7.16	-0.08	0.00	-6.97	0.00	-6.97			
4.00	126.7	344.3	49.3	0.4	4.0	-0.5	0.7	-7.16	-0.05	0.00	-6.97	0.00	-6.97			
4.05	-60.8	341.6	121.2	0.5	3.9	0.5	0.7	-7.16	0.01	0.00	-6.97	0.00	-6.97			
4.10	-112.4	338.3	-68.3	-0.5	3.9	0.4	0.6	-7.16	0.03	0.00	-6.97	0.00	-6.97			
4.15	73.6	335.6	-107.3	-0.4	3.9	-0.5	0.6	-7.15	0.05	0.00	-6.97	0.00	-6.97			
4.20	103.4	333.0	76.5	0.5	3.8	0.5	0.6	-7.15	0.02	0.00	-6.97	0.00	-6.97			
4.25	-78.0	330.6	99.2	0.4	3.8	0.5	0.6	-7.15	0.02	0.00	-6.97	0.00	-6.97			
4.30	-96.9	327.3	-77.6	-0.5	3.8	0.3	0.6	-7.16	-0.04	0.00	-6.97	0.00	-6.97			
4.35	76.2	324.7	-96.9	-0.3	3.7	-0.5	0.6	-7.16	-0.04	0.00	-6.97	0.00	-6.97			
4.40	95.2	321.9	75.4	0.4	3.7	-0.3	0.6	-7.16	-0.05	0.00	-6.97	0.00	-6.97			
4.45	-73.3	318.8	96.2	0.3	3.7	0.5	0.6	-7.16	0.02	0.00	-6.97	0.00	-6.97			
4.50	-96.3	316.4	-71.1	-0.4	3.6	0.3	0.5	-7.16	0.01	0.00	-6.97	0.00	-6.97			
4.55	67.6	314.2	-98.6	-0.3	3.6	-0.4	0.5	-7.16	-0.01	0.00	-6.97	0.00	-6.97			
4.60	100.5	311.6	64.0	0.4	3.6	-0.4	0.5	-7.16	0.02	0.00	-6.97	0.00	-6.97			
4.65	-57.0	309.0	103.0	0.4	3.6	0.4	0.5	-7.15	0.02	0.00	-6.97	0.00	-6.97			
4.70	-107.6	306.5	-50.5	-0.3	3.5	0.4	0.5	-7.15	0.00	0.00	-6.97	0.00	-6.97			
4.75	42.5	303.5	-111.4	-0.4	3.5	-0.3	0.5	-7.15	-0.02	0.00	-6.97	0.00	-6.97			
4.80	113.4	300.7	33.2	0.3	3.5	-0.4	0.5	-7.15	0.01	0.00	-6.97	0.00	-6.97			
4.85	-19.6	297.9	115.6	0.5	3.4	0.2	0.5	-7.15	0.01	0.00	-6.97	0.00	-6.97			
4.90	-116.9	295.2	-5.0	-0.1	3.4	0.5	0.5	-7.15	0.01	0.00	-6.97	0.00	-6.97			
4.95	-10.7	292.4	-114.6	-0.5	3.4	-0.1	0.5	-7.15	0.01	0.00	-6.97	0.00	-6.97			
5.00	109.4	289.8	-27.6	0.0	3.3	-0.5	0.4	-7.15	0.06	0.00	-6.97	0.00	-6.97			
5.05	47.5	287.4	101.7	0.5	3.3	-0.1	0.5	-7.15	0.06	0.00	-6.97	0.00	-6.97			
5.10	-90.2	284.8	63.6	0.2	3.3	0.4	0.4	-7.15	0.01	0.00	-6.97	0.00	-6.97			
5.15	-80.6	282.3	-75.0	-0.4	3.3	0.2	0.4	-7.15	0.01	0.00	-6.97	0.00	-6.97			
5.20	55.7	279.7	-94.1	-0.3	3.2	-0.3	0.4	-7.15	-0.02	0.00	-6.97	0.00	-6.97			
5.25	102.8	277.2	32.4	0.2	3.2	-0.4	0.4	-7.15	-0.05	0.00	-6.97	0.00	-6.97			
5.30	-7.9	274.8	105.8	0.4	3.2	0.1	0.4	-7.16	-0.10	0.00	-6.97	0.00	-6.97			
5.35	-104.5	272.3	20.3	0.0	3.1	0.4	0.4	-7.16	-0.02	0.00	-6.97	0.00	-6.97			
5.40	-44.6	269.9	-95.6	-0.4	3.1	0.1	0.4	-7.16	-0.03	0.00	-6.97	0.00	-6.97			
5.45	79.1	267.5	-66.5	-0.2	3.1	-0.3	0.4	-7.16	0.05	0.00	-6.97	0.00	-6.97			
5.50	86.9	265.1	56.6	0.3	3.1	-0.3	0.4	-7.15	0.07	0.00	-6.97	0.00	-6.97			

Table B-1: Tabular Computation of Nose Wheel Precession

Time t sec	NW Rate ω_{nw} deg/sec	NW Rot Ang Ω deg	Body Axes Reference			Nose Wheel Axes Reference			Nose Wheel Vector		
			Roll Rate p deg/sec	Pitch Rate q deg/sec	Yaw Rate r deg/sec	Roll Rate p deg/sec	Pitch Rate q deg/sec	Yaw Rate r deg/sec	θ_x deg/sec	θ_y deg/sec	θ_z deg/sec
5.55	-1453	-106.4	2.95	3.09	-3.51	2.7	3.4	3.4	2.7	-1449.6	3.5
5.60	-1440	-178.4	2.95	3.09	-3.51	-2.4	3.4	3.6	-2.4	-1436.6	3.7
5.65	-1427	-249.7	2.95	3.09	-3.51	-4.2	3.4	-1.2	-4.2	-1423.7	-1.0
5.70	-1414	-320.4	2.95	3.09	-3.50	-3.0	3.4	-4.3	-3.0	-1410.9	-4.3
5.75	-1402	-30.5	2.95	3.09	-3.50	4.0	3.4	-1.7	4.0	-1398.2	-1.7
5.80	-1389	-100.0	2.95	3.09	-3.50	3.0	3.4	3.1	3.0	-1385.6	3.1
5.85	-1377	-168.8	2.95	3.09	-3.50	-1.8	3.4	3.9	-1.8	-1373.2	3.9
5.90	-1364	-237.0	2.95	3.09	-3.50	-4.3	3.4	-0.2	-4.3	-1360.9	-0.3
5.95	-1352	-304.6	2.95	3.09	-3.50	-1.4	3.4	-4.1	-1.4	-1348.6	-4.1
6.00	-1340	-11.6	2.95	3.09	-3.50	3.2	3.4	-2.9	3.2	-1336.5	-2.9
6.05	-1328	-78.0	2.95	3.09	-3.50	4.0	3.4	1.8	4.0	-1324.5	1.8
6.10	-1316	-143.8	2.95	3.09	-3.50	0.0	3.4	4.3	0.0	-1312.6	4.3
6.15	-1304	-209.0	2.95	3.09	-3.50	-3.0	3.4	1.8	-3.0	-1300.8	1.8
6.20	-1293	-273.6	2.95	3.09	-3.50	-3.3	3.4	-2.8	-3.3	-1289.1	-2.8
6.25	-1281	-337.7	2.95	3.09	-3.50	1.0	3.4	-4.2	1.0	-1277.6	-4.3
6.30	-1270	-41.2	2.95	3.09	-3.50	4.2	3.4	-1.0	4.2	-1266.1	-1.0
6.35	-1258	-104.1	2.94	3.09	-3.51	2.8	3.4	3.3	2.8	-1254.7	3.3
6.40	-1247	-166.4	2.96	3.11	-3.52	-1.6	3.5	4.0	-1.6	-1243.4	4.0
6.45	-1236	-228.2	2.97	3.13	-3.53	-4.3	3.5	0.4	-4.3	-1232.2	0.4
6.50	-1225	-289.4	2.94	3.12	-3.54	-2.5	3.5	-3.6	-2.5	-1221.2	-3.6
6.55	-1214	-350.1	2.91	3.12	-3.54	1.9	3.5	-3.9	1.9	-1210.2	-3.9
6.60	-1203	-50.3	2.89	3.12	-3.53	4.3	3.5	-0.3	4.3	-1199.3	-0.4
6.65	-1192	-109.9	2.85	3.10	-3.52	2.5	3.4	2.5	2.5	-1188.6	3.5
6.70	-1181	-168.9	2.85	3.06	-3.49	-1.7	3.4	3.9	-1.7	-1177.9	3.9
6.75	-1171	-227.5	2.89	3.04	-3.46	-4.2	3.4	0.5	-4.2	-1167.4	0.5
6.80	-1160	-285.5	2.87	3.00	-3.42	-2.6	3.3	-3.3	-2.6	-1156.9	-3.2
6.85	-1150	-343.0	2.86	2.97	-3.37	1.4	3.3	-3.9	1.4	-1146.6	-3.9
6.90	-1140	-40.0	2.88	2.89	-3.36	4.1	3.2	-1.0	4.1	-1136.3	-0.9
6.95	-1129	-96.4	2.87	2.82	-3.36	3.1	3.2	2.9	3.1	-1126.2	3.0
7.00	-1119	-152.4	2.88	2.76	-3.40	-0.7	3.1	4.2	-0.7	-1116.1	4.3
7.05	-1109	-207.8	2.94	2.70	-3.46	-3.9	3.0	1.9	-3.9	-1106.2	1.9
7.10	-1099	-262.8	3.02	2.65	-3.52	-3.8	3.0	-2.2	-3.8	-1096.3	-2.1
7.15	-1089	-317.3	3.07	2.64	-3.56	-0.4	3.0	-4.5	-0.4	-1086.4	-4.4
7.20	-1080	-11.3	3.06	2.61	-3.61	3.4	3.0	-3.0	3.4	-1076.7	-3.0
7.25	-1070	-64.8	3.04	2.57	-3.63	4.4	2.9	0.9	4.4	-1067.1	0.9
7.30	-1060	-117.8	2.97	2.53	-3.64	2.0	2.9	4.0	2.0	-1057.5	4.0
7.35	-1051	-170.3	2.88	2.48	-3.65	-1.9	2.8	4.0	-1.9	-1048.1	4.0
7.40	-1041	-222.4	2.76	2.45	-3.63	-4.2	2.8	1.0	-4.2	-1038.7	1.0
7.45	-1032	-274.0	2.68	2.42	-3.59	-3.4	2.7	-2.6	-3.4	-1029.4	-2.6
7.50	-1023	-325.1	2.63	2.42	-3.55	-0.1	2.7	-4.2	-0.1	-1020.2	-4.2

Table B-1: Tabular Computation of Nose Wheel Precession

Time t	Nose Wheel Vector			Nose Wheel Reference			Steering Angle			
	$d\omega_x/dt$ deg/s/s	$d\omega_y/dt$ deg/s/s	$d\omega_z/dt$ deg/s/s	M_x ft-lb	M_y ft-lb	M_z ft-lb	M_x ft-lb	M_y ft-lb	M_z ft-lb	Computed
5.55	-28.2	262.7	99.7	0.4	3.0	0.2	0.4	0.4	0.0	-6.97
5.60	-101.8	260.4	2.8	-0.1	3.0	0.2	-7.14	0.4	0.11	-6.97
5.65	-34.6	258.0	-94.0	-0.3	3.0	0.1	-7.13	0.3	0.15	-6.97
5.70	77.9	255.7	-65.2	-0.2	2.9	-0.3	-7.13	0.4	0.04	-6.97
5.75	84.8	253.4	51.7	0.2	2.9	-0.3	-7.13	0.4	0.03	-6.97
5.80	-19.2	251.2	96.8	0.3	2.9	0.1	-7.13	0.3	0.03	-6.97
5.85	-96.5	248.9	16.0	0.0	2.9	0.3	-7.13	0.3	0.01	-6.97
5.90	-50.2	246.7	-83.8	-0.3	2.8	0.1	-7.13	0.3	-0.03	-6.97
5.95	57.7	244.5	-76.1	-0.2	2.8	-0.2	-7.13	0.3	0.02	-6.97
6.00	92.7	242.3	23.4	0.1	2.8	-0.3	-7.13	0.3	0.03	-6.97
6.05	15.1	240.1	93.2	0.3	2.8	0.0	-7.13	0.3	0.01	-6.97
6.10	-78.8	238.0	50.8	0.1	2.7	0.3	-7.13	0.3	-0.01	-6.97
6.15	-78.7	235.8	-49.8	-0.2	2.7	0.2	-7.13	0.3	-0.01	-6.97
6.20	11.8	233.7	-92.0	-0.3	2.7	-0.1	-7.13	0.3	-0.02	-6.97
6.25	87.1	231.6	-29.7	0.0	2.7	-0.3	-7.13	0.3	-0.06	-6.97
6.30	63.9	229.5	64.5	0.2	2.6	-0.2	-7.13	0.3	-0.07	-6.97
6.35	-28.6	227.5	86.3	0.2	2.6	0.1	-7.14	0.3	-0.03	-6.97
6.40	-88.8	225.8	14.1	0.0	2.6	0.3	-7.14	0.3	-0.03	-6.97
6.45	-53.8	223.9	-71.9	-0.3	2.6	0.1	-7.14	0.3	-0.05	-6.97
6.50	37.0	221.3	-79.5	-0.2	2.5	-0.2	-7.14	0.3	-0.02	-6.97
6.55	86.9	219.3	-6.6	0.0	2.5	-0.3	-7.14	0.3	0.00	-6.97
6.60	48.8	217.4	71.1	0.2	2.5	0.1	-7.14	0.2	-0.01	-6.97
6.65	-36.4	215.0	76.6	0.2	2.5	0.1	-7.14	0.2	-0.02	-6.97
6.70	-84.1	212.8	8.1	0.0	2.5	0.3	-7.14	0.2	-0.01	-6.97
6.75	-50.0	211.4	-66.8	-0.2	2.4	0.1	-7.14	0.2	0.03	-6.97
6.80	32.0	209.1	-75.3	-0.2	2.4	-0.1	-7.14	0.2	0.07	-6.97
6.85	80.0	207.1	-13.0	0.0	2.4	-0.2	-7.13	0.2	0.07	-6.97
6.90	54.1	204.6	60.1	0.2	2.4	-0.1	-7.13	0.2	0.09	-6.97
6.95	-20.3	202.8	77.9	0.2	2.3	0.1	-7.12	0.2	0.16	-6.97
7.00	-74.2	201.2	25.4	0.1	2.3	0.2	-7.12	0.2	0.12	-6.97
7.05	-64.9	199.7	-47.4	-0.2	2.3	0.2	-7.11	0.2	0.07	-6.97
7.10	1.4	197.9	-80.8	-0.2	2.3	0.0	-7.11	0.2	0.09	-6.97
7.15	68.1	196.8	-45.3	-0.1	2.2	-0.2	-7.10	0.2	0.08	-6.97
7.20	75.8	194.6	27.3	0.1	2.2	-0.2	-7.10	0.2	-0.01	-6.97
7.25	21.3	192.7	78.3	0.2	2.2	0.0	-7.10	0.2	0.00	-6.97
7.30	-48.8	190.7	62.6	0.1	2.2	0.1	-7.10	0.2	-0.01	-6.97
7.35	-77.9	188.9	-0.2	0.0	2.2	0.2	-7.11	0.2	-0.02	-6.97
7.40	-46.8	187.2	-60.1	-0.2	2.2	0.1	-7.11	0.2	-0.02	-6.97
7.45	16.5	186.0	-72.6	-0.2	2.1	-0.1	-7.11	0.2	-0.02	-6.97
7.50	65.8	184.7	-32.6	-0.1	2.1	-0.2	-7.11	0.2	-0.02	-6.97

Table B-1: Tabular Computation of Nose Wheel Precession

Time t	NW Rate ω_{nw} deg/sec	NW Rot Ang Ω deg	Body Axes Reference			Nose Wheel Axes Reference			Nose Wheel Vector		
			Roll Rate p deg/sec	Pitch Rate q deg/sec	Yaw Rate r deg/sec	Roll Rate p deg/sec	Pitch Rate q deg/sec	Yaw Rate r deg/sec	ω_x deg/sec	ω_y deg/sec	ω_z deg/sec
7.55	-1014	-15.8	2.62	2.42	-3.50	3.2	2.7	-2.7	3.2	-1011.0	-2.8
7.60	-1005	-66.1	2.71	2.44	-3.43	4.1	2.8	0.8	4.1	-1001.9	0.7
7.65	-996	-115.9	2.83	2.45	-3.39	2.0	2.8	3.7	2.0	-992.9	3.7
7.70	-987	-165.2	2.99	2.49	-3.34	-1.7	2.8	3.9	-1.7	-983.9	3.9
7.75	-978	-214.1	3.12	2.51	-3.30	-4.2	2.9	1.2	-4.2	-975.0	1.2
7.80	-969	-262.5	3.23	2.56	-3.23	-3.6	2.9	-2.4	-3.6	-966.2	-2.4
7.85	-960	-310.6	3.27	2.61	-3.18	-0.5	3.0	-4.3	-0.5	-957.5	-4.2
7.90	-952	-358.2	3.31	2.67	-3.10	2.8	3.1	-3.2	2.8	-948.8	-3.1
7.95	-943	-45.3	3.33	2.73	-3.03	4.2	3.1	0.0	4.2	-940.2	0.0
8.00	-935	-92.1	3.27	2.75	-2.95	2.8	3.1	3.0	2.8	-931.7	3.1
8.05	-926	-136.4	3.23	2.75	-2.90	-0.2	3.1	4.1	-0.2	-923.4	4.1
8.10	-918	-184.3	3.11	2.78	-2.85	-2.9	3.1	2.6	-2.9	-915.0	2.6
8.15	-910	-229.8	2.97	2.79	-2.82	-3.8	3.1	-0.2	-3.8	-906.8	-0.2
8.20	-902	-274.9	2.81	2.79	-2.80	-2.6	3.1	-2.7	-2.6	-898.7	-2.7
8.25	-894	-319.6	2.70	2.81	-2.78	0.0	3.1	-3.6	0.0	-890.6	-3.7
8.30	-886	-3.9	2.59	2.85	-2.79	2.4	3.1	-2.6	2.4	-882.6	-2.8
8.35	-878	-47.7	2.52	2.86	-2.81	3.5	3.1	-0.3	3.5	-874.6	-0.3
8.40	-870	-91.2	2.41	2.85	-2.84	2.8	3.1	2.8	2.8	-866.8	2.1
8.45	-862	-134.3	2.31	2.85	-2.87	0.7	3.1	3.4	0.7	-859.0	3.4
8.50	-854	-177.1	2.18	2.88	-2.93	-1.7	3.1	3.0	-1.7	-851.3	3.0
8.55	-847	-219.4	2.06	2.89	-2.98	-3.2	3.1	1.2	-3.2	-843.6	1.3
8.60	-839	-261.4	1.88	2.91	-3.04	-3.2	3.1	-1.0	-3.2	-836.0	-1.0
8.65	-832	-302.9	1.74	2.93	-3.10	-1.9	3.1	-2.8	-1.9	-828.5	-2.8
8.70	-824	-344.2	1.55	2.92	-3.19	0.3	3.1	-3.4	0.3	-821.1	-3.3
8.75	-817	-25.0	1.38	2.88	-3.26	2.3	3.0	-2.5	2.3	-813.8	-2.5
8.80	-809	-65.5	1.16	2.84	-3.33	3.4	3.0	-0.7	3.4	-806.5	-0.6
8.85	-802	-105.6	0.99	2.78	-3.39	3.1	2.9	1.5	3.1	-799.3	1.6
8.90	-795	-145.3	0.85	2.71	-3.47	1.6	2.8	3.1	1.6	-792.3	3.1
8.95	-788	-184.7	0.75	2.67	-3.52	-0.7	2.7	3.5	-0.7	-785.2	3.5
9.00	-781	-223.8	0.66	2.62	-3.59	-2.7	2.7	2.4	-2.7	-778.2	2.4
9.05	-774	-262.5	0.63	2.58	-3.65	-3.7	2.6	0.2	-3.7	-771.2	0.1
9.10	-767	-300.8	0.60	2.53	-3.71	-3.0	2.6	-2.1	-3.0	-764.3	-2.2
9.15	-760	-338.8	0.56	2.48	-3.76	-1.1	2.5	-3.6	-1.1	-757.5	-3.6
9.20	-753	-16.5	0.48	2.43	-3.80	1.2	2.5	-3.6	1.2	-750.8	-3.7
9.25	-747	-53.8	0.41	2.39	-3.83	3.2	2.4	-2.2	3.2	-744.1	-2.3
9.30	-740	-90.8	0.27	2.32	-3.84	3.8	2.3	0.0	3.8	-737.5	0.0
9.35	-733	-127.4	0.13	2.26	-3.82	3.1	2.3	2.2	3.1	-730.9	2.1
9.40	-727	-163.8	-0.03	2.19	-3.79	-0.03	2.2	3.6	1.4	-724.4	3.5
9.45	-720	-199.8	-0.12	2.12	-3.72	-0.9	2.1	3.6	-0.9	-718.0	3.6
9.50	-714	-235.5	-0.21	2.05	-3.63	-2.7	2.0	2.4	-2.7	-711.6	2.5

Table B-1: Tabular Computation of Nose Wheel Precession

Time t	Nose Wheel Vector		Nose Wheel Reference Torquing Moment			Strut Axes Moment		Steering Angle		Computed F
	$d\omega_x/dt$ deg/s/s	$d\omega_y/dt$ deg/s/s	M_x ft-lb	M_y ft-lb	M_z ft-lb	M_x ft-lb	M_y ft-lb	E deg	E dot deg/sec	
7.55	65.9	183.3	0.1	2.1	-0.2	0.2	-7.11	-0.04	0.00	-6.97
7.60	18.7	182.2	0.2	2.1	0.0	0.2	-7.11	-0.05	0.00	-6.97
7.65	-43.0	180.7	0.1	2.1	0.1	0.2	-7.12	-0.05	0.00	-6.97
7.70	-73.3	179.4	0.0	2.1	0.2	0.2	-7.12	0.00	0.00	-6.97
7.75	-48.8	177.6	-0.2	2.0	0.1	0.2	-7.12	-0.01	0.00	-6.97
7.80	11.5	176.5	-0.2	2.0	-0.1	0.2	-7.11	0.02	0.00	-6.97
7.85	61.3	174.7	-0.1	2.0	-0.2	0.1	-7.11	0.06	0.00	-6.97
7.90	67.2	173.4	0.1	2.0	-0.1	0.1	-7.11	0.07	0.00	-6.97
7.95	27.8	171.7	0.2	2.0	0.0	0.1	-7.11	0.03	0.00	-6.97
8.00	-27.8	169.4	0.1	2.0	0.1	0.1	-7.10	0.04	0.00	-6.97
8.05	-61.2	167.4	0.0	1.9	0.1	0.1	-7.10	0.04	0.00	-6.97
8.10	-54.7	166.3	-0.1	1.9	0.0	0.1	-7.11	-0.05	0.00	-6.97
8.15	-17.7	164.4	-0.1	1.9	0.0	0.1	-7.11	-0.07	0.00	-6.97
8.20	25.0	162.6	-0.1	1.9	-0.1	0.1	-7.11	-0.06	0.00	-6.97
8.25	51.1	161.9	0.0	1.9	-0.1	0.1	-7.12	-0.09	0.00	-6.97
8.30	48.5	160.6	0.0	1.8	-0.1	0.1	-7.12	-0.12	0.00	-6.97
8.35	22.4	158.7	0.1	1.8	0.0	0.1	-7.13	-0.05	0.00	-6.97
8.40	-14.5	156.9	0.1	1.8	0.0	0.1	-7.13	-0.02	0.00	-6.97
8.45	-41.9	155.7	0.0	1.8	0.1	0.1	-7.13	-0.03	0.00	-6.97
8.50	-47.0	154.6	0.0	1.8	0.1	0.1	-7.13	0.02	0.00	-6.97
8.55	-30.7	153.1	-0.1	1.8	0.1	0.1	-7.12	0.07	0.00	-6.97
8.60	-0.9	151.6	-0.1	1.7	0.0	0.1	-7.12	0.03	0.00	-6.97
8.65	27.4	150.6	-0.1	1.7	-0.1	0.1	-7.12	0.03	0.00	-6.97
8.70	42.4	148.3	0.0	1.7	-0.1	0.1	-7.12	0.05	0.00	-6.97
8.75	40.7	146.5	0.0	1.7	-0.1	0.1	-7.12	0.02	0.00	-6.97
8.80	21.4	144.9	0.1	1.7	-0.1	0.1	-7.12	0.02	0.00	-6.97
8.85	-5.3	143.5	0.1	1.7	0.0	0.1	-7.11	0.03	0.00	-6.97
8.90	-30.8	141.9	0.1	1.6	0.1	0.1	-7.11	0.00	0.00	-6.97
8.95	-45.2	141.5	0.0	1.6	0.1	0.1	-7.11	0.00	0.00	-6.97
9.00	-40.4	140.1	0.0	1.6	0.1	0.1	-7.11	0.00	0.00	-6.97
9.05	-18.7	139.0	-0.1	1.6	0.0	0.1	-7.12	-0.05	0.00	-6.97
9.10	12.3	137.5	-0.1	1.6	0.0	0.1	-7.12	-0.05	0.00	-6.97
9.15	38.3	136.4	-0.1	1.6	-0.1	0.1	-7.12	-0.04	0.00	-6.97
9.20	47.6	135.0	0.0	1.6	-0.1	0.1	-7.13	-0.08	0.00	-6.97
9.25	38.2	133.9	0.1	1.5	-0.1	0.1	-7.13	-0.09	0.00	-6.97
9.30	13.7	132.1	0.1	1.5	0.0	0.1	-7.13	-0.06	0.00	-6.97
9.35	-14.3	131.0	0.1	1.5	0.0	0.1	-7.14	-0.06	0.00	-6.97
9.40	-35.5	129.7	0.1	1.5	0.1	0.1	-7.14	-0.05	0.00	-6.97
9.45	-45.0	128.6	0.0	1.5	0.1	0.1	-7.14	-0.01	0.00	-6.97
9.50	-36.6	127.3	0.0	1.5	0.1	0.1	-7.14	0.02	0.00	-6.97

Table B-1: Tabular Computation of Nose Wheel Precession

Time t sec	NW Rate			NW Rot Ang			Body Axes Reference			Nose Wheel Axes Reference			Nose Wheel Vector		
	ω_{yw} deg/sec	Ω deg	Roll Rate p deg/sec	Pitch Rate q deg/sec	Yaw Rate r deg/sec	Roll Rate p deg/sec	Pitch Rate q deg/sec	Yaw Rate r deg/sec	Roll Rate p deg/sec	Pitch Rate q deg/sec	Yaw Rate r deg/sec	ω_x deg/sec	ω_y deg/sec	ω_z deg/sec	
9.55	-707	-270.8	-0.21	1.97	-3.54	-3.6	1.9	0.4	-3.6	-705.3	0.4				
9.60	-701	-305.9	-0.18	1.90	-3.47	-3.1	1.9	-1.7	-3.1	-699.1	-1.7				
9.65	-695	-340.6	-0.11	1.82	-3.39	-1.4	1.8	-3.1	-1.4	-692.9	-3.0				
9.70	-688	-15.0	-0.06	1.75	-3.35	0.6	1.7	-3.3	0.6	-686.7	-3.3				
9.75	-682	-49.1	0.06	1.68	-3.30	2.4	1.7	-2.3	2.4	-680.6	-2.3				
9.80	-676	-82.9	0.15	1.64	-3.27	3.2	1.6	-0.5	3.2	-674.5	-0.4				
9.85	-670	-116.5	0.28	1.60	-3.23	2.9	1.6	1.5	2.9	-668.5	1.5				
9.90	-664	-149.7	0.39	1.58	-3.19	1.4	1.6	2.8	1.4	-662.5	2.8				
9.95	-658	-182.6	0.50	1.58	-3.19	0.4	1.6	3.2	0.4	-656.5	3.2				
10.00	-652	-215.2	0.57	1.58	-3.21	-2.1	1.6	2.4	-2.1	-650.6	2.4				
10.05	-646	-247.5	0.63	1.58	-3.24	-3.2	1.6	0.8	-3.2	-644.7	0.8				
10.10	-641	-279.5	0.67	1.58	-3.28	-3.2	1.6	-1.0	-3.2	-638.9	-1.0				
10.15	-635	-311.3	0.73	1.61	-3.35	-2.2	1.7	-2.6	-2.2	-633.2	-2.6				
10.20	-629	-342.7	0.81	1.63	-3.39	-0.4	1.7	-3.4	-0.4	-627.4	-3.4				
10.25	-624	-13.9	0.94	1.69	-3.42	1.5	1.8	-3.2	1.5	-621.7	-3.1				
10.30	-618	-44.8	1.06	1.74	-3.45	3.0	1.9	-1.9	3.0	-616.1	-1.9				
10.35	-612	-75.4	1.24	1.80	-3.48	3.6	1.9	0.1	3.6	-610.5	0.1				
10.40	-607	-105.8	1.40	1.84	-3.50	3.1	2.0	2.1	3.1	-604.9	2.0				
10.45	-601	-135.8	1.52	1.87	-3.54	1.6	2.0	3.4	1.6	-599.4	3.4				
10.50	-596	-165.6	1.58	1.88	-3.58	-0.4	2.1	3.8	-0.4	-594.0	3.8				
10.55	-591	-195.2	1.61	1.89	-3.65	-2.3	2.1	3.2	-2.3	-588.7	3.2				
10.60	-585	-224.5	1.59	1.91	-3.72	-3.6	2.1	1.7	-3.6	-583.4	1.7				
10.65	-580	-253.5	1.51	1.93	-3.81	-4.0	2.1	-0.1	-4.0	-578.1	-0.1				
10.70	-575	-282.2	1.44	1.96	-3.88	-3.5	2.1	-2.0	-3.5	-572.9	-1.9				
10.75	-570	-310.7	1.36	2.00	-3.95	-2.3	2.2	-3.4	-2.3	-567.7	-3.4				
10.80	-565	-338.9	1.28	2.04	-4.00	-0.5	2.2	-4.1	-0.5	-562.6	-4.1				
10.85	-560	-6.9	1.16	2.07	-4.05	1.4	2.2	-3.9	1.4	-557.5	-4.0				
10.90	-555	-34.7	1.07	2.09	-4.08	3.0	2.2	-2.9	3.0	-552.5	-3.0				
10.95	-550	-62.2	0.99	2.12	-4.06	3.9	2.2	-1.3	3.9	-547.5	-1.2				
11.00	-545	-89.4	0.90	2.13	-4.03	4.0	2.2	0.6	4.0	-542.6	0.6				
11.05	-540	-116.4	0.88	2.15	-3.98	3.3	2.2	2.3	3.3	-537.7	2.3				
11.10	-535	-143.1	0.89	2.19	-3.90	1.8	2.3	3.5	1.8	-532.8	3.5				
11.15	-530	-169.7	0.91	2.22	-3.82	0.1	2.3	3.9	0.1	-528.0	3.9				
11.20	-526	-195.9	0.93	2.23	-3.78	-1.7	2.3	3.5	-1.7	-523.2	3.5				
11.25	-521	-222.0	0.97	2.22	-3.71	-3.0	2.3	3.0	-3.0	-518.5	2.3				
11.30	-516	-247.8	0.96	2.21	-3.66	-3.6	2.3	0.8	-3.6	-513.8	0.7				
11.35	-512	-273.4	0.95	2.18	-3.61	-3.6	2.3	-0.9	-3.6	-509.2	-0.9				
11.40	-507	-298.7	0.96	2.17	-3.55	-2.8	2.3	-2.3	-2.8	-504.7	-2.3				
11.45	-502	-323.8	0.96	2.15	-3.50	-1.5	2.2	-3.2	-1.5	-500.2	-3.2				
11.50	-498	-348.7	0.96	2.14	-3.47	0.0	2.2	-3.5	0.0	-495.7	-3.6				

Table B-1: Tabular Computation of Nose Wheel Precession

Time t	Nose Wheel Vector			Nose Wheel Reference Torquing Moment			Strut Axes Moment		Fill Test Data			Steering Angle		Computed F dot deg/sec
	$d\omega_x/dt$ deg/s/s	$d\omega_y/dt$ deg/s/s	$d\omega_z/dt$ deg/s/s	M_x ft-lb	M_y ft-lb	M_z ft-lb	M_x ft-lb	M_z ft-lb	E deg	E dot deg/sec	F dot deg/sec	F deg		
9.55	-16.5	126.4	-40.9	-0.1	1.5	0.0	0.0	0.1	-7.14	0.01	0.00	-6.97		
9.60	9.9	125.5	-41.7	-0.1	1.4	0.0	0.0	0.1	-7.14	0.03	0.00	-6.97		
9.65	32.2	124.1	-27.5	0.0	1.4	-0.1	-0.1	0.1	-7.13	0.05	0.00	-6.97		
9.70	40.9	123.2	-4.6	0.0	1.4	0.0	0.0	0.1	-7.13	0.03	0.00	-6.97		
9.75	35.9	122.4	20.2	0.1	1.4	0.0	0.0	0.1	-7.13	0.01	0.00	-6.97		
9.80	16.8	121.6	37.0	0.1	1.4	0.0	0.0	0.1	-7.13	0.04	0.00	-6.97		
9.85	-7.6	120.7	38.7	0.1	1.4	0.0	0.0	0.1	-7.13	0.02	0.00	-6.97		
9.90	-28.2	120.0	26.5	0.0	1.4	0.1	0.1	0.1	-7.13	0.00	0.00	-6.97		
9.95	-37.8	119.2	6.6	0.0	1.4	0.1	0.1	0.1	-7.13	0.00	0.00	-6.97		
10.00	-34.0	118.0	-15.1	0.0	1.4	0.1	0.1	0.1	-7.13	0.01	0.00	-6.97		
10.05	-20.1	117.0	-31.6	-0.1	1.3	0.0	0.0	0.1	-7.13	-0.01	0.00	-6.97		
10.10	-0.2	115.9	-36.7	-0.1	1.3	0.0	0.1	0.1	-7.13	0.01	0.00	-6.97		
10.15	19.8	115.5	-31.7	-0.1	1.3	0.0	0.0	0.1	-7.13	0.02	0.00	-6.97		
10.20	34.7	114.4	-16.4	0.0	1.3	-0.1	-0.1	0.1	-7.13	0.01	0.00	-6.97		
10.25	39.1	114.1	5.2	0.0	1.3	0.0	0.0	0.1	-7.13	0.01	0.00	-6.97		
10.30	30.2	113.2	25.7	0.1	1.3	0.0	0.0	0.1	-7.13	0.00	0.00	-6.97		
10.35	10.35	112.3	38.8	0.1	1.3	0.0	0.0	0.1	-7.13	-0.02	0.00	-6.97		
10.40	-11.4	110.9	39.0	0.1	1.3	0.0	0.0	0.1	-7.13	-0.04	0.00	-6.97		
10.45	-30.0	109.8	27.5	0.0	1.3	0.1	0.1	0.1	-7.13	-0.02	0.00	-6.97		
10.50	-39.1	108.1	7.2	0.0	1.2	0.1	0.1	0.1	-7.13	-0.04	0.00	-6.97		
10.55	-37.4	107.1	-12.0	0.0	1.2	0.1	0.1	0.1	-7.13	0.00	0.00	-6.97		
10.60	-25.8	106.1	-28.1	0.0	1.2	0.0	0.0	0.1	-7.13	0.04	0.00	-6.97		
10.65	-8.9	105.2	-35.5	-0.1	1.2	0.0	0.0	0.1	-7.13	0.10	0.00	-6.97		
10.70	9.3	104.3	-38.5	-0.1	1.2	0.0	0.0	0.1	-7.12	0.04	0.00	-6.97		
10.75	25.3	103.7	-28.1	0.0	1.2	0.0	0.0	0.1	-7.12	0.06	0.00	-6.97		
10.80	35.8	102.8	-14.7	0.0	1.2	-0.1	-0.1	0.1	-7.12	0.01	0.00	-6.97		
10.85	37.3	101.5	2.6	0.0	1.2	-0.1	-0.1	0.1	-7.12	-0.04	0.00	-6.97		
10.90	32.2	100.4	19.9	0.0	1.2	-0.1	-0.1	0.1	-7.13	-0.07	0.00	-6.97		
10.95	18.8	99.8	34.3	0.0	1.1	0.0	0.0	0.0	-7.13	0.01	0.00	-6.97		
11.00	2.4	98.6	37.2	0.0	1.1	0.0	0.0	0.0	-7.12	0.02	0.00	-6.97		
11.05	-15.0	98.0	34.7	0.0	1.1	0.0	0.0	0.0	-7.12	0.04	0.00	-6.97		
11.10	-28.9	97.5	24.2	0.0	1.1	0.0	0.0	0.0	-7.12	0.07	0.00	-6.97		
11.15	-35.5	96.4	6.6	0.0	1.1	0.0	0.0	0.0	-7.12	0.01	0.00	-6.97		
11.20	-34.7	95.3	-8.7	0.0	1.1	0.0	0.0	0.0	-7.12	0.00	0.00	-6.97		
11.25	-26.6	94.2	-23.8	0.0	1.1	0.0	0.0	0.0	-7.12	-0.04	0.00	-6.97		
11.30	-13.0	92.9	-30.9	0.0	1.1	0.0	0.0	0.0	-7.12	-0.04	0.00	-6.97		
11.35	1.6	92.0	-33.2	0.0	1.1	0.0	0.0	0.0	-7.13	-0.06	0.00	-6.97		
11.40	15.4	91.3	-27.3	0.0	1.1	0.0	0.0	0.0	-7.13	-0.01	0.00	-6.97		
11.45	25.5	90.4	-19.5	0.0	1.0	0.0	0.0	0.0	-7.13	-0.05	0.00	-6.97		
11.50	30.2	89.9	-6.4	0.0	1.0	0.0	0.0	0.0	-7.13	-0.06	0.00	-6.97		

VITA

Major Werth is a 1996 distinguished graduate of the United States Naval Test Pilot School and is currently employed as an AV8B test pilot for the United States Marine Corps. With an accumulated 1700+ flight hours in over twenty different fixed wing and rotary wing aircraft, his test experience includes both aircraft and weapons system developmental test. In his current role, he is the lead military officer for the Tri-National (US, Italy, Spain) AV8B Test Team. Major Werth's technical background with a Bachelor of Aerospace Engineering and Mechanics (BAEM) degree from the University of Minnesota and his test pilot experience give him the requisite knowledge to discuss the design and use of nose wheel steering systems.

In 1997, Major Werth planned, tested, and reported on a new system designed to replace the existing AV8B nose wheel steering system. Several deficiencies had been noted on the old system which led to the design of the Harrier's new nose wheel steering system. The propensity for gyroscopic precession of the AV8B's castering nose strut was inadvertently discovered by Major Werth and his test team during this test flight program.